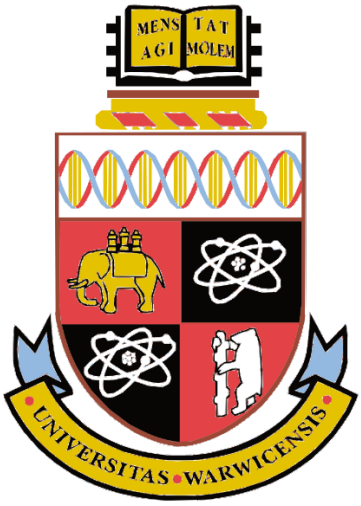

Post-mortem analysis of lithium-ion cells after accelerated lifetime testing

by

Limhi Somerville

An innovation report submitted in partial fulfilment of

requirements for the degree of

Doctor of Engineering (EngD)

August 2017

The University of Warwick

Abstract

Lithium-ion cells are the most commonly used method of energy storage for portable electronics. However, the capacity and power reduces with time and is dependent on usage conditions. This is a challenge for electric vehicle battery packs that are expected to last for up to eight years. Vehicle manufacturers need to understand the causes of this phenomena to accurately predict the vehicles achievable range over its entire lifetime. For automotive manufacturers to tackle this challenge they must know what operating conditions impact cell capacity and power. And, once this has been established, how these operating conditions impact cell capacity and power. Answers to these questions would provide critical information for manufactures; allowing them to mitigate or plan for their impact.

In this work, electrical testing was performed across seven cell conditions for between six and thirty months to determine changes in capacity and resistance. Due to the different facility requirements at least one of the following cell chemistries were used for each test, Nickel manganese cobalt (NMC), Nickel Cobalt Aluminium (NCA) and lithium cobalt dioxide ($LiCoO_2$) / all with graphite negative electrodes. State of charge, temperature, current rate during charge, the quantity of the state of charge window utilised and vibration all impacted electrical performance. Cell orientation and external pressure had no effect on cell lifetime.

Cell capacity and resistance change over its lifetime is a function of the parasitic chemical reactions occurring within the cell. Understanding how these operating conditions impact cell performance requires a study of the fundamental materials that are at fault. Therefore, materials characterisation of the negative electrode surface film (identified as the primary source of changes to cell capacity and resistance) was performed.

Consistency of analytical methods to study this surface film is dependent on the processes of preparation. Those used within literature to open cells, and process the internal cell electrodes led to erroneous results through modification of the surface films chemical properties. A new method is introduced of opening 18650-type cells that is simpler, costs less and stops surface film damage and contamination. In addition, washing electrode surfaces with solvents, which is routinely done within literature, was found to affect the surface film. This work shows that washing can remove surface film and selectively solvate parts of it. It is therefore recommended that washing is not performed.

After cell opening, samples were then analysed to determine material changes. A method is introduced to determine the relative surface film thickness (which relates to cell resistance) with x-ray photoelectron spectroscopy that is an improvement on the current method within literature. A wet chemistry method is also shown to selectively remove $LiPF_6$ salt. This makes it possible to use high performance liquid chromatography to study the polymeric species without it reacting with hydrofluoric acid.

Using these methods, a relationship is identified between current rate during charge and surface film thickness at the negative electrode up to rates of 4-C. At rates of 6-C and greater the surface film altered chemically. Cell vibration was found to cause the selectively formed film to be replaced with electrolyte reduction products, increasing cell resistance. Subjecting cells to different temperatures and states of charge (SoC) caused different films to form at each temperature. Coupled with electrical performance data, this could be reduced to two. One at 10^{o}C and one at 45^{o}C. SoC was also found to accelerate film formation but not chemically alter it at these two temperatures. Problems with the USABC test for a percentage change in state of charge for lithium-ion cells was identified, but these problems stopped surface film analysis.

This work identifies what conditions impact cell performance and their effect on the negative electrode surface film. Changes in the surface film have significant implications on the users of electric-vehicles, most especially the range of the vehicle battery and how that reduces over its lifetime. Such information may directly impact the vehicle warranty, battery size and type of accelerated testing performed to predict cell lifetime. All of these factors represent considerable costs to manufacturers of electric-vehicles. Accuracy is therefore of critical importance.

Acknowledgements

Any project that is as vast as this requires the acknowledgement of so many people. It goes without saying that doctoral work is the collaboration of a student with their supervisors. I am grateful to Paul Jennings for supervising and facilitating both my ideas and everything that was done in this work. Andrew McGordon for supervising and especially reading, then editing and providing feedback on everything, again and again. I am also grateful to Christopher Lyness who gave a lot of technical electrochemistry instruction and helped me to get a running start as well as supporting my work throughout. These three have listened and prompted for many years and have made all the difference to my confidence and the work.

A lot of this work, and much of its quality, would not have been possible without Argonne National Laboratory (ANL) but especially Ira Bloom who never (appeared) tired of my many questions, Javier Bareño with whom I spent many days receiving instruction, asking numerous questions and receiving detailed responses, and Nancy Dietz-Rago for many technical and non-technical discussion, microscopy help and surface science information. These three taught me a great deal during my time there for which I cannot repay. My thanks also go to Dr Bloom's entire team but especially Panos and John for their help with electrical characterisation and walking me through test methods and procedures. The ANL placement and subsequent collaboration would not have been possible without Nick Mallinson, who spent many hours orchestrating and working behind the scenes. In addition to Nigel Taylor and Nick Green from Jaguar Land Rover who not only organised money but also legalities.

I am also grateful to the entire team at The University of Warwick and Jaguar Land Rover. James T, Anup, James M, James H, Mark, Dhammika, Kotub, Gael, Julie, Ravi, Shane, Paul B, Yue and others who performed testing, purchased equipment, helped me to learn something or told me when to be quiet. This would not have been possible or as much fun without so many people who worked hard and put in a lot of time and talent.

Finally, having saved the best till last, I am grateful to my wife Rebecca who has spent hours listening to me give mock presentations, discuss my research and putting up with me not being around. Thank you for making the last years' fun, exciting and of course for raising Theodore, Elijah, Rupert and Wilbur while their dad wasn't around as much.

Declaration

I declare that the work described in this report was undertaken by myself (unless otherwise acknowledged in the text) and that none of the work has been previously submitted for any other academic degree.

Contents

List of symbols and units

%	Percentage
% Δ SoC	Percentage change in State of charge
£	Great British Pound Sterling
Δ	Delta (change)
©	Copyright
µm	Micron
Ah	Ampere-hour
Ar^+	Argon ion
B.P.	Boiling point
C	Carbon
C	Concentration
C=C	Alkene bond
C=O	Carbonyl functional group
Ca	Calcium
$CaCO_3$	Calcium carbonate
CaF_2	Calcium difluoride
Ccell	Cell terminal voltage
C-H	Alkane bond
C-Li	Lithium carbide
CO_2	Carbon dioxide
D	Diffusion coefficient
Da	Dalton
E	Represented by state of charge
e^-	Electron
eV	Electron volt
F	Fluorine
F^-	Fluoride ion
$g.km^{-1}$	Grams per kilometre

I	Current
J	Diffusion flux
K	Kelvin
kPa	Kilopascal
Li^{+}	Lithium ion
$LiCoO_2$	Lithium cobalt dioxide
$LiPF_6$	Lithium hexafluorophosphate
$Mg.l^{-1}$	Milligrams per litre
$Min.ml^{-1}$	Minutes per millilitre
$mol.cm^{-2}.s^{-1}$	Mols per centimetre squared per second
mV	Millivolt
Ni	Nickel
nm	Nanometre
^{o}C	Degrees celsius
O-C=O	Ester functional group
P	Phosphorous
p.s.i	Pounds per square inch
R	Resistance
R^2	Coefficient of determination
s.d.	Standard deviation
Si	Silicon
Si-O	Silicon oxide
T	Temperature
V	‘Voltage’, ‘potential of the electrode’ or ‘vanadium’
Vocv	Open circuit voltage
x	Distance
Ω	Ohm

List of abbreviations

18650	Cylindrical cell format (18mm in circumference and 65.0mm in length)
ANL	Argonne National Laboratory
BMS	Battery management system
CC	Current collector
DCM	Dichloromethane
DMC	Dimethyl carbonate
EC	Ethlyene carbonate
EDAX	Energy dispersive x-ray microanalysis
EIS	Electrochemical impedance spectroscopy
EngD	Engineering doctorate
EOL	End of life
GBP	Great British Pound
GC-MS	Gas chromatography – mass spectrometry
GPC	Gel permeation chromatography
HF	Hydrofluoric acid
HPLC	High performance liquid chromatography
IC	Ion chromatography
ICS	Ion chromatography system
IR	Infra-red
JLR	Jaguar Land Rover
LiF	Lithium fluoride
MCMB	Mesocarbon microbeads
NASA	National Aeronautics and Space Administration
NIST	National institute of standards and technology
NMC	Nickel manganese cobalt
NMR	Nuclear magnetic resonance
OEM	Original equipment manufacturer
PW	Published work

RTP	Room temperature and pressure
S#	Submission number
SBR	Styrene butadiene rubber
SEI	Solid electrolyte interphase
SEM	Scanning electron microscope
SoC	State of charge
UK	United Kingdom
USABC	United States Advance Battery Consortium
VC	Vinylene carbonate
WMG	WMG – department at The University of Warwick
XPS	X-ray photoelectron spectroscopy

List of figures

List of tables

1. Introduction

European regulation 443/2009 states that the fleet average exhaust emissions of carbon dioxide (CO_2) for all passenger vehicles sold within the European union must be 95g.km^{-1} by 2021 [1]. The fleet average exhaust emissions of CO_2 for Jaguar Land Rover (JLR) in 2015 was 182g.km^{-1} [2], if unchanged, companies with CO_2 emissions like JLR will be subject to fines on their vehicles and therefore they need to reduce their exhaust CO_2 emissions.

JLR and other automotive manufacturers have chosen to reduce CO_2 emissions by introducing a range of hybrid and all-electric vehicles [3]. The JLR programme uses lithium-ion cells [4]. These cells are identical in operating principles to those used in most hand-held electronic systems and laptop computers [5].

Lithium-ion technology is used for energy storage in laptop computers and mobile phones, however these are only expected to last for two to three years [6]. During this time, the capacity and power that the cells provide diminishes and the device requires more frequent charging or uses more energy to perform the same tasks [7]. Most mobile phone users replace their handsets within this two-year period. However, automotive manufacturers are expected to have vehicle batteries that last for up to eight years [8]. Please note that battery end of life (EOL) is when it equals 80% of initial capacity or a 50% increase in internal resistance – this is an internal standard from JLR (sponsoring company).

If electric vehicles do not meet this lifetime then original equipment manufacturers (OEM), like JLR, may have to replace them at cost. The price of a battery pack (consisting of multiple lithium-ion cells) for an all-electric vehicle may be as high as £10,000 each [9] so replacement is not a sound business strategy. This means that vehicle manufacturers need to find a way of accurately predicting the battery's predicted lifetime.

When JLR initially commissioned this doctoral study, they had no documentation of whether a vehicle containing a lithium-ion battery pack could reach this lifetime requirement. The initial aim of this doctorate was to determine how long a battery would last and provide some evidence in the form of real-world testing and mathematical modelling to predict the expected lifetime.

Lifetime performance decline of lithium-ion cells is affected by the conditions of its use [6]. It is possible to use a battery management system (BMS) to control the operating conditions of the battery (e.g. temperature). This would mean that those conditions which prolong cell lifetime are preferentially chosen over those that degrade it [10]. Ultimately, it may be possible to militate against the detrimental conditions that reduce cell capacity and power if it is understood what causes it to happen. To make this calculation, manufacturers need to know which conditions impact cell performance and by how much.

The most accurate method of predicting lithium-ion cell lifetime is to take the cell from a supplier and then use it in real-world conditions for the warranty period of eight years. However, when considered within the constraints of a company's supplier sourcing, vehicle production, and manufacturing processes this type of testing is not practical due to the infinite number of potential driving conditions. For example, the protocol for driving in Hong Kong [11] contains different operating conditions to those for UK urban areas [12]. And this is before we have considered the impact of driver style and usage. Lithium-ion cells also come in many shapes and sizes, the same cell chemistry made by two different manufacturers may give markedly different lifetime performance [13]. If an automotive company wishes to change suppliers, use new cells from the same supplier or use a new type of cell chemistry the cell lifetime may have to be predicted again, requiring additional testing before implementation in a vehicle [14]. Vehicle manufacturers cannot wait this long and therefore need to predict lifetime much sooner.

Currently, accelerated lifetime prediction is performed by increasing the frequency and / or intensity of laboratory tests [15]. Spotnitz refers to accelerated testing for simulating capacity fade of commercial lithium-ion cells [16]. The example they introduce is 'time temperature superposition' where doubling the temperature can halve the testing time. Bloom et al. performed this type of testing for accelerated calendar and cycle life ageing and found an Arrhenius relationship $(\text{time})^{1/2}$ for temperature between cells stored at different states of charge [17] they intimate that it may be due to electrolyte interface layer growth (a surface film that forms on the negative electrode). Bloom et al. then relate that this relationship is not consistent for cells cycled at 3% of the state of charge (SoC) window compared to 6% – as shown by a non-linear change in cell capacity. Suggesting that a change in the operating condition induces a different internal mechanism of degradation to occur.

Ultimately, capacity and resistance measured through the cell terminals are external representations of multiple internal reactions. The conclusions of Bloom et al. [17] work are based on the assumption that no chemical changes occurred to the surface films composition for SoC reactions sped up by temperature. Accelerated ageing hinges on the concept that the acceleration can be performed without changing the chemical reactions that occur [16]. However, Bloom et al. [17] electrical work alone does not provide sufficient evidence that this is true. It is possible that different reactions still occur as temperature increases but performance decline still follows a $(\text{time})^{1/2}$ kinetic rate. This becomes more complicated at more extreme conditions, or if multiple different conditions and cell materials are included.

Automotive companies stake reputation and considerable money on determining how long their battery pack lasts. There is a business case for accurately accelerating the ageing for lithium-ion cells by ensuring that the conditions which accelerate ageing do so by increasing surface film thickness and not chemically altering its composition. This is because if additional

chemical reactions do occur then the lifetime of the cell may diverge from the predicted values. This type of divergence has the potential to be very costly to OEM's in the long term due to warranty costs.

It is possible to use post-mortem analysis to study what chemical changes occur within the lithium-ion cell. This works by studying specific components of the cell for changes in the material properties [18-21]. It may be possible to use post-mortem type analysis to lithium-ion cells to determine the chemical reaction mechanisms with a decline in capacity and increase in resistance [22]. Such results may validate or refute accelerated ageing methods, identify the causes of cell ageing, and suggest those conditions that require further investigation.

The aim of this work is to investigate how post-mortem analysis can be used to detect material changes in commercial lithium-ion cells after accelerated lifetime testing.

Figure 1 show the outline of this work, and shows the general flow of the document and portfolio. The majority of the work within this portfolio deals with the process of post-mortem analysis and is highlighted within the 'Innovations' section. However, the majority of the work that is of interest to a commercial entity is contained in 'Background' and 'results / impact'. In reality, the 'Results / impact' section are affected by the improvements made within the 'innovations' section. This is reflected by the majority of submissions to the portfolio being within the 'Innovations' section but the majority of published work being in the 'results / impact' section. Specific portfolio submissions are referred to within the portfolio when their contents become significant - all such points are referred to by a note in standard font size and

italicised script within the main body of the text. It is advisable to read these chapters as they are mentioned in the text.

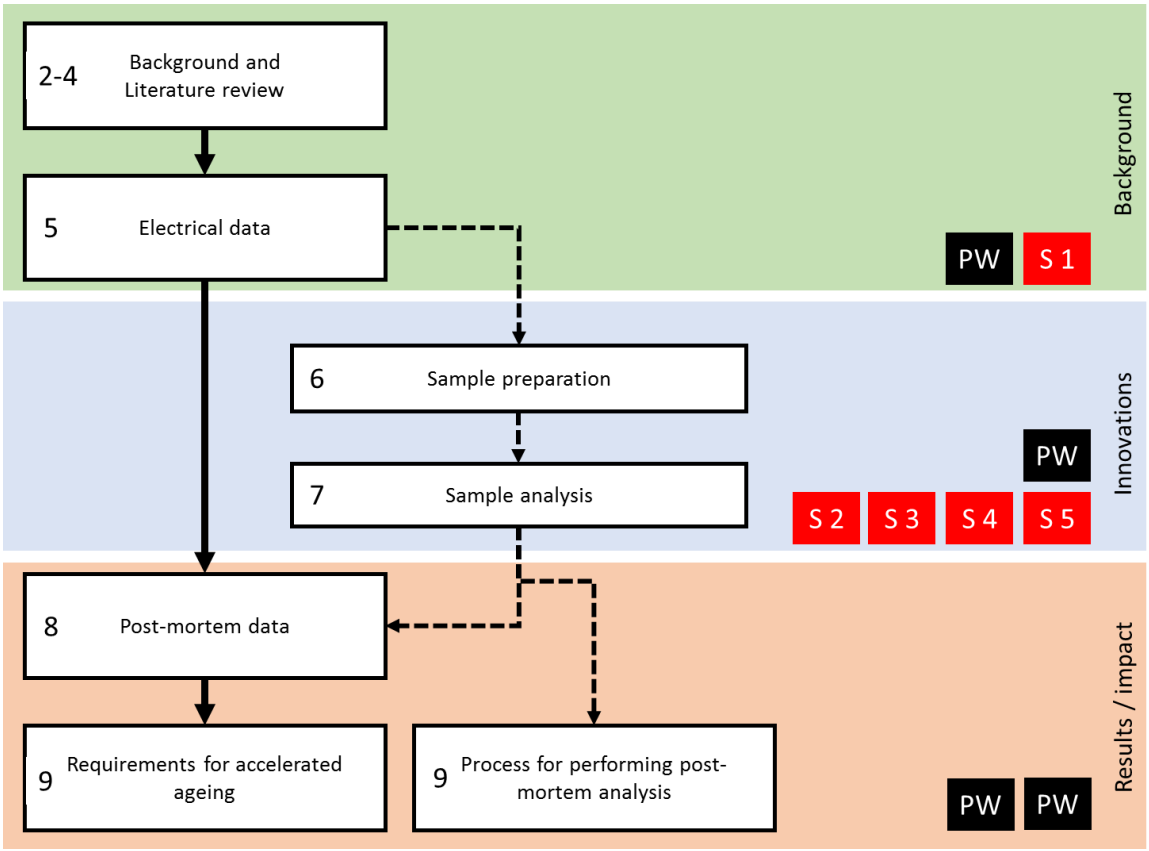

Figure 1. Outline of the engineering doctorate portfolio, numbers to the left of white topic boxes represent chapters within this innovation report. Red boxes labelled S1-5 represent the five portfolio submissions; the black PW boxes represent published work.

2. Ageing of lithium-ion cells

This chapter addresses the causes of ageing (reduction in capacity, increase in resistance) within lithium-ion cells and the induced chemical reactions. In order to understand ageing it is important to comprehend some fundamental aspects of what lithium-ion cells are and how they work. Therefore, this chapter begins with principles of lithium-ion cells and then presents the current literature into what conditions cause a reduction in capacity and an increase in resistance. Figure 2 shows this chapter's position within the context of the wider portfolio.

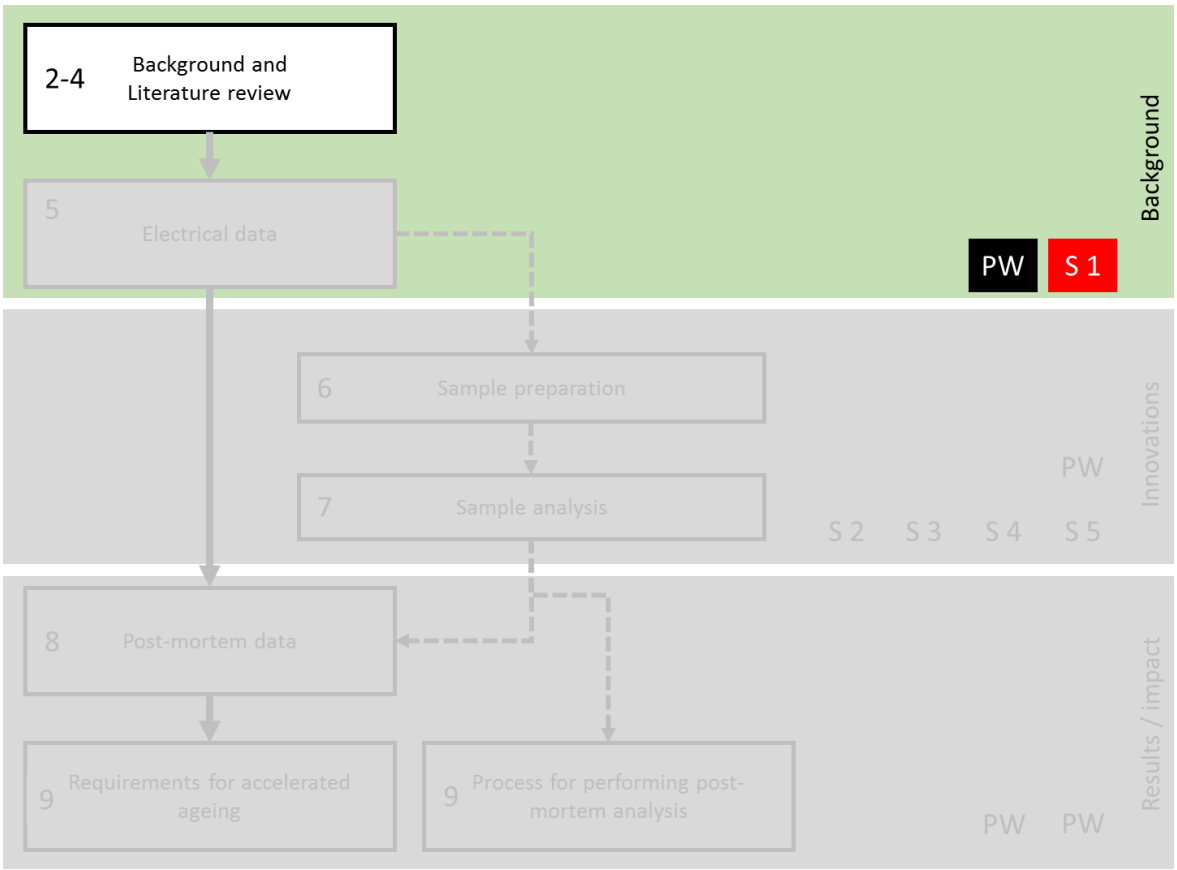

Figure 2. Outline of the engineering doctorate portfolio, highlighted for Chapters 2-4. Red box labelled S1 represent the first portfolio submission; the black PW box represents published work.

2.1. Lithium-ion cells

Lithium-ion cells are secondary (rechargeable) cells that store energy chemically. Each cell is comprised of many different chemicals with many interchangeable possibilities [23]. Commercially available cells from different manufacturers use varied and complex compositions of materials that can be slightly or significantly different from one another [24]. These differences and variety of compositions introduce complications to understanding what chemical mechanisms are occurring within the cell to cause resistance to increase and capacity to decline.

N.B. Chapter Two of Submission One from this Portfolio covers the general composition of lithium-ion cells and their chemistry in more detail.

Figure 3 is a graphic of a lithium-ion cell and shows the eight basic steps to release and store energy. These steps are:

- Transferring Li^+ ions out of the negative electrode active material
- Solvating Li^+ into the electrolyte
- Diffusing Li^+/Li through the surface film of the negative electrode
- Li^+ Migrating through the electrolyte and separator
- Li^+ Diffusing through the positive electrode surface film
- Li^+ De-solvating out of the electrolyte
- Intercalating (process of Li^+ movement into the unit cell of the host lattice) into the positive electrode active material
- Transfer of electrons through the external circuit, providing power

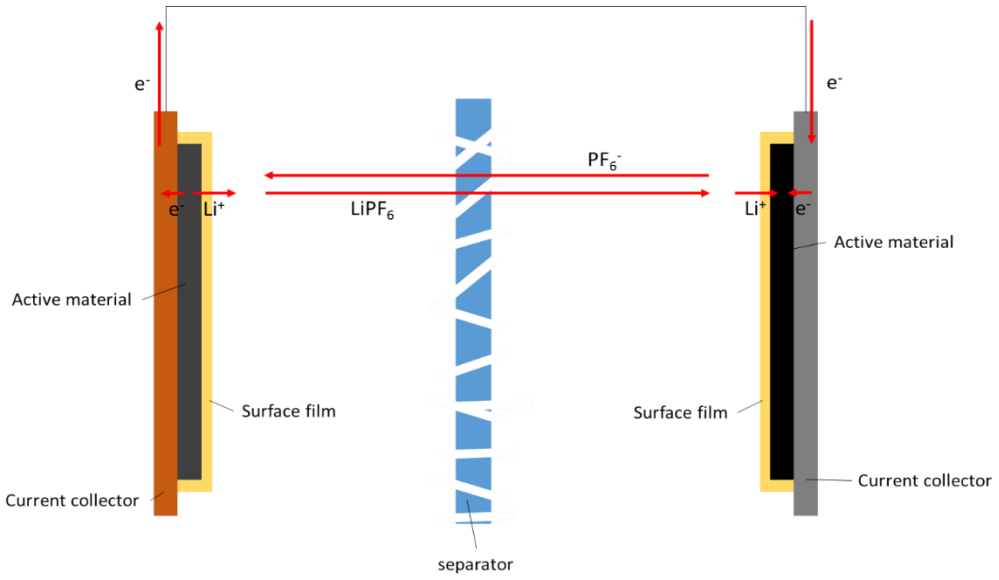

Figure 3. Graphic showing the main components and processes of a lithium-ion cell during release of energy. Electrons are represented by e^- whereas lithium cations are presented by Li+; all processes for normal cell operation are represented by red arrows.

Movement of charge governs lithium-ion cells, whether by electrons (e^-) or ions (Li^+). Electrical current is produced when there is a potential difference between two bodies that are electrically and ionically connected [25]. Figure 3 shows that the individual cell electrodes are connected ionically through the electrolyte and electrically through the external circuit. More details on the charge transfer phenomenon and electrical current can be found here [26].

An electrochemical cell has two electrodes; one positive and one negative. These are spatially separated but ionically connected by a salt bridge, which is the electrolyte mixture containing lithium salt [27]. Lithium-ion cells work by transferring lithium ions (Li^+) between the two electrodes through the electrolyte. This movement allows the cell to store / release energy. When lithium intercalates into the negative electrode the voltage of the cell increases. Intercalation can be defined as the insertion of atoms into the crystal lattice of another material. The voltage is a measure of the reserved energy per unit charge from redox (oxidation / reduction) reactions that occur at the electrode surfaces. Two different redox reactions occur,

one at each electrode, but can be represented by a single reaction (1) that is commonly broken down into two half-cell reactions. During discharge these are oxidation at the anode (2) and reduction at the cathode (3). C represents carbon, Li represents lithium and MO represents transition metal oxides; the letters w, x, y and z represent varied stoichiometric quantities. When a cell is charged, Li^+ migrate to the negative electrode; a potential difference is required to force the movement of Li^+ out of the cathode, because it is the lowest available energy state. Once the Li^+ are in the negative electrode the difference in electrode potential means they still want to migrate to the positive electrode (lower energy).

$$C_x + Li_wMO_y \leftrightarrow Li_zC_x + LizMOy \quad (1)$$

$$Li_{w-z}\,C_x \leftrightarrow ZLi^+ + XC + e^- \quad (2)$$

$$Li_{w-z}MO_y + e^- + ZLi^+ \leftrightarrow Li_wMO_y \quad (3)$$

This entire process is possible because once the Li^+ reaches the electrode it gains an electron from the electrode active material, and reduces to lithium (3). After this reduction, the lithium must diffuse through the bulk of the material and intercalate into the active material. Fick's first law, which is simplified for no changes in concentration, shows two key parameters that impact this. These are the chemical composition of the material being diffused through and the path length (4). Equation 4 holds where J is the diffusion flux ($mol.cm^{-2}\ s^{-1}$), D is the diffusion coefficient, C is the concentration and x is the distance travelled by the ion. D is proportional to the velocity squared of the material particles and is dependent on temperature, material viscosity and particle size.

$$J = -D\,\frac{dC}{dx} \quad (4)$$

2.2. Causes of lifetime reduction

The work contained in this section focuses on the causes of lifetime reduction (ageing) within a lithium-ion cell as reported by academic literature. It connects the manner in which a cell is treated with the internal chemical mechanisms it induces.

N.B. An earlier edition of this literature review is presented in submission one of this doctoral portfolio. The application of this work and proof of its use to modelling of lithium-ion cells is shown in the work of Uddin et al. [28].

2.2.1. Definition of ageing

For the purposes of this work 'ageing' is a permanent reduction in capacity, or an increase in the resistance, of lithium-ion cells.

Capacity is a measure of the available lithium and the available sites in the active material that lithium can be stored in. The second is resistance (6), because the cell (V_{cell}) (cell terminal voltage under load) assuming the current (I) is a constant, is dependent on the resistance (R) and the voltage of the cell under no load (V_{ocv}), which relates to the potential difference between electrodes.

$$V_{cell} = V_{ocv} - (I \bullet R) \qquad (5)$$

2.2.2. Causes of cell ageing

The causes of ageing reported within literature are:

- Temperature [10,29-34]
- State of charge [35-38,34,39,40]
- Percentage change in state of charge [41,42]
- Number of cycles [34]
- Rate of intercalation (current rate) [43,44,41,45,36,46,30,47-49]
- Charge procedure [48]
- Time [40]
- Depth of discharge [50] (% Δ SoC)
- External mechanical conditions [51,52]
- Choice of materials [50]

Not all of these are relevant to the vehicle user case for this work because the requirements of an automotive manufacturer are different. Whilst correct choice of materials for cells is crucial it is beyond the scope of this work. This is because this work assumes that manufacturers of lithium-ion cells have addressed this issue. This assumption and its validity is a major advantage over using laboratory cells. Although laboratory cells provide more information on specific chemical mechanism interpretation, because the chemistry parameters are better known, they are open to significant error through poor manufacturing processes – it is difficult to create repeatable results from laboratory made cells. This is the reason that Dahn et al. use small commercial pouch cells for their tests [53,54].

Time and number of cycles is commonly cited as a cause of cell ageing. However, accelerated ageing is potentially able to reduce the time taken to age by replicating conditions more frequently or increasing its intensity, as shown by Bloom et al [17]. Therefore, if replication or

intensity of a different factor in the same period of time or number of cycles is able to age a cell at a faster rate; then the measurement medium itself (time, number of cycles) cannot be the origin of the failure. A study of anything but the origin of failure may lead to incorrect interpretation of results. Therefore the number of cycles is excluded as a cause of cell ageing.

From a commercial point of view, vehicle manufacturers cannot apply a limit on the time a battery is stored for or how many times a vehicle can be used in a day. Because few people would buy a vehicle with such limitations. This also applies to current rate during discharge; vehicle manufacturers use supplier imposed limits on discharge for cells. However, the precise frequency and type of acceleration during discharge over a cell lifetime, within this supplier imposed limit, is beyond the control of vehicle manufacturers and therefore it has also not been studied.

Charge procedure is also an example of a cause that is easy to misinterpret. It is reported as a cause of capacity fade [48,55,56]. Zhang [48] changed the charging protocol from constant current or voltage during charge to a multi-stage variation. They reduced the current initially (<10% SoC) and at the end of charging, (>90% SoC); this reduced capacity fade. Nevertheless, 'charging protocol' is the amalgamation of a specific current rate and SoC of the cell. It is possible that current, SoC or total coulombs alone caused the ageing. This is because 'charge procedure' as a term is not the root cause of the problem but rather an amalgamation of specific cell usage conditions. Without investigating them separately it is not possible to de-convolute the capacity and power values to determine a root cause and therefore, this work only investigates the isolated causes of cell ageing.

There are also some conditions that need to be investigated as requirements from JLR. Vehicles, are subject to vibration during use [57], and the cells are also held within a vehicle pack [58] so may be subject to pressure to save on weight and space. In addition, the batteries

will be held at a specific orientation and the question has been raised by JLR whether this would impact performance due to cell design – because no other root cause sufficiently addresses these problems they are also being investigated.

The following have been identified as possible independent variables that do not depend on any other factors:

- State of charge
- Percentage change in state of charge
- Temperature
- Current rate
- Vibration
- External pressure
- Orientation

Therefore, one or more of these seven conditions outlined above is responsible for reducing capacity or increasing resistance of the cells within a vehicle battery pack. The innovation within this work is on connecting these causes with material changes within the cell; to determine their impact on cell lifetime.

3. Internal chemical mechanisms responsible for ageing

The purpose of this chapter is to determine from literature what internal mechanisms are occurring under each of the seven conditions. And, how they can be studied using post-mortem analysis.

3.1. Definitions within this work

3.1.1. State of charge (SoC)

SoC can be defined as the percentage of available stored energy compared to total possible energy [59]. Electrically, it can be defined by a standard capacity test [60]. For commercial lithium-ion cells 100% SoC is approximately 4.2V whilst 0% SoC is approximately 2.5V. Variations can occur with differing chemistries so the actual value should be tailored for each individual cell. Electrochemically, SoC can be defined by the percentage of the negative electrode that has been intercalated with lithium ions. At 100% SoC the negative electrode is theoretically fully intercalated.

3.1.2. Percentage change in state of charge (% Δ SoC)

A % Δ SoC can also be referred to as ‘change in depth of discharge’ or ‘SoC swing’[61]. Occurring within the SoC window, % Δ SoC defines how much of the SoC window is used irrespective of the SoC. This concept is illustrated in Figure 4, A, has a different % Δ SoC to B and C, but B has the same % Δ SoC as C.

Electrically % Δ SoC is the total number of coulombs for a charge-discharge cycle and may occur at any voltage. Electrochemically it defines the total number of lithium ions that intercalate into the electrode and is also a measure of the total work done on a system.

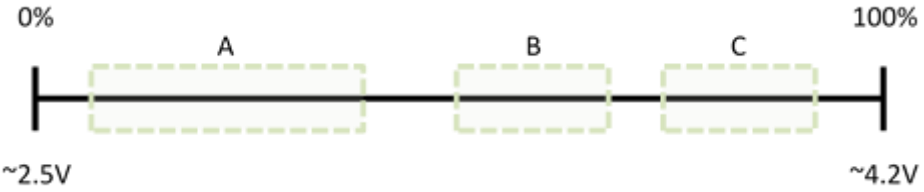

Figure 4. The difference between SoC and %ΔSoC is shown through three different boxes on a state of charge scale bar. A has a greater %ΔSoC than B whilst B and C are equal in %ΔSoC values but the SoC values differ.

3.1.3. Temperature (T)

Temperature is also a root cause of cell ageing. As far back as 1889 Arrhenius kinetics showed the dependence of chemical reactions on T [62]. Nernst Heat Theorem states, 'in a perfectly crystalline substance, exchange of entropy accompanying transformations [chemical reactions] approaches zero asymptotically as temperature approaches zero [Kelvin]'[63]. Therefore, temperature is essential for any reaction to occur and is also a determining factor in its rate.

3.1.4. Current (I) rate

Although % Δ SoC defines the total number of coulombs in a charge-discharge cycle, the current rate determines how fast the lithium ions and electrons move. The rate of e^- movement

in the external circuit and subsequent Li^+ ion intercalation may affect ageing of li-ion cells. For this reason, the current rate is separate from T, % Δ SoC and SoC.

3.1.5. Pressure, orientation and vibration

Irrespective of chemically induced ageing or test conditions, external mechanical stresses including vibration [51] orientation [64] and external pressure [52] may cause ageing within lithium ion cells. Because none of these are dependent on I, SoC, % Δ SoC or T and are all experienced within a vehicle. they will also be investigated for their impact on cell capacity and resistance.

3.2. Chemical mechanisms responsible for cell ageing

This section describes the dominant ageing mechanisms responsible for a reduction in capacity and power, according to literature. Each of the seven causes is investigated individually and possible mechanisms for degradation are highlighted within their own sub-sections. In some cases the same mechanism can be accelerated by different causes, in these instances the mechanisms are mentioned under each cause. The mechanistic pathway covered for each cause is the one that literature has associated with it.

3.2.1. State of charge

As a cell is charged lithium-ions intercalate into the negative electrode from the positive electrode via the electrolyte. This moves the negative electrode potential closer to zero at the same time as the positive electrode's potential increases. The actual value depends on potential differences in materials and is the open circuit voltage of the cell. This voltage relates to the cells 'state of charge' value [65]. Therefore, a high state of charge relates to a higher quantity of lithium in the negative electrode.

3.2.1.1. Lithium plating

As the negative electrode approaches 0V, i.e. 100% SoC, it is closer to the potential at which lithium deposits from the electrolyte onto the surface of the negative electrode (lithium plating) [66]. For normal cell function, lithium intercalates from the salt in the electrolyte ($LiPF_6$) to the negative electrode. At lower electrode potentials intercalation is no longer the thermodynamically favourable reaction and is replaced by Li^+ reduction, forming lithium metal which plates at the surface of the electrode. This decreases the amount of available lithium and increases resistance through formation of a surface film [67]. This film then reduces available

pathways for intercalation, as shown in part b. of Figure 5. The simplified schematic does not show the complex nature of path blocking. It is often not just a sterically hindered phenomenon, in many instances paths can be extended in length and not blocked. Capacity is reduced by loss of lithium inventory through being used up by reactions [68]. Resistance increases from an increased path length for the Li^+ ions and blocked pores on the electrode surface.

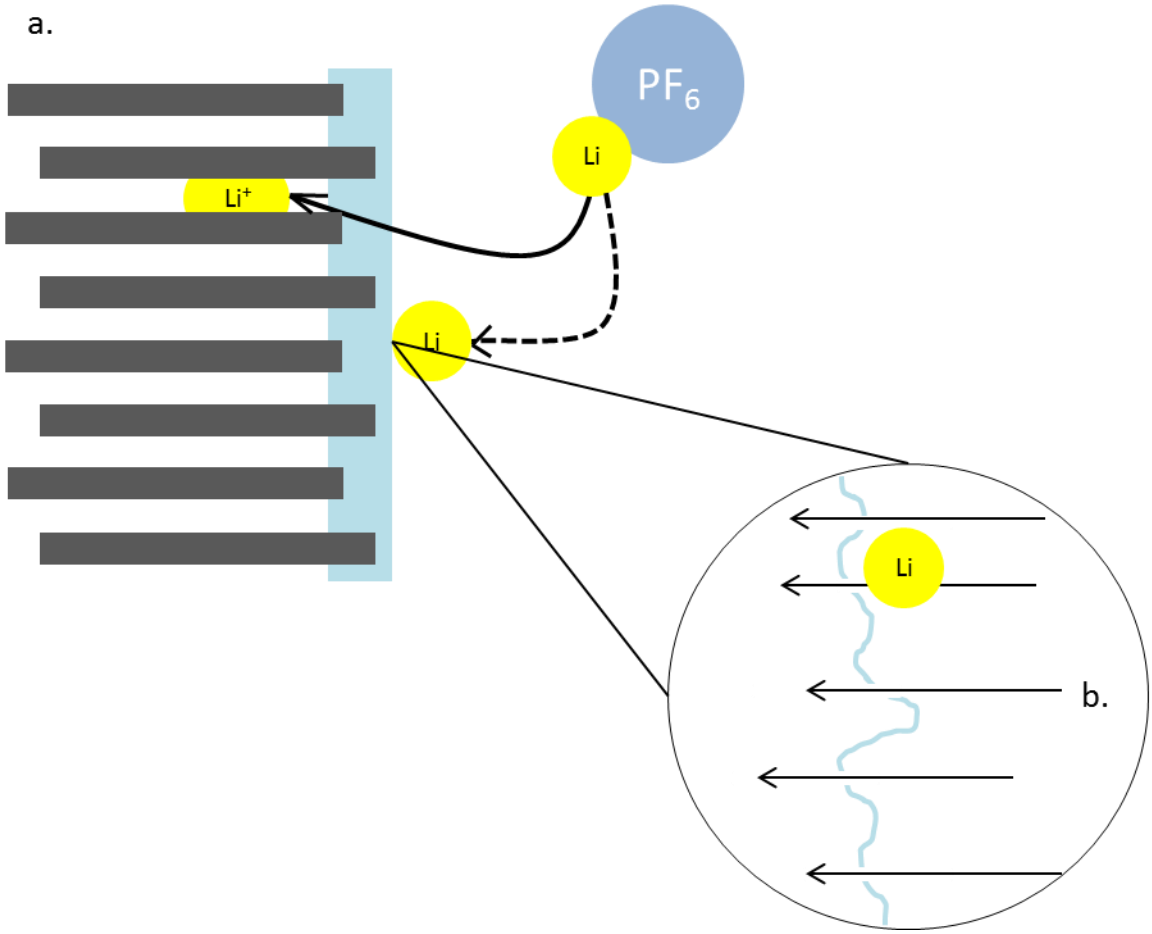

Figure 5. Part a. Schematic showing the traditional intercalation of Li into the negative electrode (solid black arrow) and the alternate path that occurs during lithium plating (dotted arrow). The light blue rectangle represents lithium plating whilst the dark grey rectangles represent a carbon or graphite negative electrode particle. Part b. This is a schematic showing possible intercalation paths blocked by Lithium plating.

Lithium plating is shown in the work of Burns et al. [69]. Their work detects the impact of lithium plating on electrical performance with high precision coulometry and uses photographs to prove lithium plating occurs. However, this is not quantitative so would introduce problems

in comparing how much lithium is present if anything but a binary test is performed. Harris et al. [66] detect lithium-plating by creating a custom cell and cycling it. However, this is also not quantitative and it would be simpler to just open the cell and look at it. Klamor et al. have shown detection of lithium plating with ^{7}Li nuclear magnetic resonance (NMR) [70] which is able to quantify lithium plating.

However, quantification of the lithium on the surface may not tell the entire story. Agubra et al. performed testing on cells with lithium plating and showed that the plated lithium can re-oxidise at 100mV [71] and re-intercalate into the electrodes. This means that lithium plating is reversible and may not necessarily always lead to capacity loss. In addition, Zhang et al. propose that lithium plating can form at the interface between the graphite and the surface film [48]. These complications make determining how to detect lithium through the surface film less useful. A possible solution to this predicament is shown by Sinha et al. who propose that plated lithium reacts with electrolyte to thicken a resistive film at the negative electrode surface [67]. Therefore, if plated lithium detection with NMR is unlikely to be able to be connected back to a change in electrical performance. However, once the lithium reacts to form surface film, then it is not reversible. Therefore, the mechanism of lithium plating that permanently impacts cell performance could be analysed by a change in the surface film that forms on the negative electrode.

3.2.1.2. Electrolyte reduction

Increased SoC increases the likelihood of electrolyte reduction at the negative electrode [72] which then forms a film. The rate of surface film formation is increased by higher SoC (lower potential of the negative electrode) of the cell [73].

3.2.2. Increased Temperature (T)

3.2.2.1. Surface film formation

Amatucci *et al*. [74] report that lithium-ion cells cycled at high temperatures see a decrease in capacity and an increase in internal resistance. Their study focused on carbon negative and transition metal oxide positive electrodes. This general composition makes up the majority of lithium-ion cell chemistries commercially so it is especially relevant to this work [72]. Surface film formation (electrolyte reduction) at the negative electrode is cited as the primary cause of capacity fade and resistance increase within their work. This was found to decrease capacity by consumption of Li^+ cations but also to increase resistance through reduction in surface area available for intercalation and an increase in path length for the Li^+ ions [75].

Although the initial surface film formation at the negative electrode occurs during cycling, Andersson *et al*. [76] report that irreversible reactions thickening the surface film occurs at higher temperatures.

3.2.2.2. Surface film dissolution

Amatucci *et al.* noted that at higher temperatures (70^{o}C) the surface film dissolves and decomposes. Decomposed surface film of the form LiOH, ROLi and LiF would not be useable lithium inventory and would become a precipitate in the electrolyte solvent or else comprise surface film [77]. This decomposition then allows for electron tunnelling through a, now, thinner surface film layer and further reduction of the electrolyte happens. The result is further capacity loss through re-forming of the surface film layer. However, because 70^{o}C is a higher temperature than expected during normal cell use it should not occur during normal cell lifetime. Spotnitz infers that the upper temperature limit before such reactions may occur is

around 55°C. The temperature chosen within these studies should be lower than this to allow for such nuances.

3.2.3. Low Temperature

3.2.3.1. Lithium plating

Lin et al. [78] and Smart and Ratnakumar [68] tested MCMB-$LiCoO_2$ cells at low temperatures, -40 to 25 °C. Using a Li reference electrode placed between the anode and cathode they determined that interfacial resistance and thus lithium plating was the primary cause of capacity fade. The mechanism they propose is that Li concentration increases at the negative electrode due to intercalation not being energetically favourable at low temperatures (e.g. -20 °C) during charge. Because the concentration of Li has increased at the surface of the electrode, reaction of lithium with the electrolyte, which is thermodynamically favourable at these temperatures then occurs and thickens the surface film.

3.2.4. Current rate during charge

3.2.4.1. Lithium plating

Lithium plating has been discussed previously with respect to SoC in section 3.2.1.1 and with respect to low temperature in section 3.2.3.1. In addition to both SoC and low temperature multiple sources [65,68,48] have shown that increased current during charge speeds up the rate of lithium plating at the negative electrode. It is likely that each of these causes will have a contributory impact to the rate of lithium plating and the mechanisms induced are likely to combine. For example, Figure 5 shows a pore blocking mechanism that lithium plating induces. This could be accelerated even further at low temperatures and increased current rates. The reason that lithium plating occurs at high currents is due to its electrochemical potential and the kinetics of intercalation, as shown by Smart and Ratnakumar [68]. The reason the potential

of the cell is affected by current rate is shown by equation (6), which is ohms law for a cell. Where V (potential of the electrode) is determined by E, which is represented by SoC, the current rate (I) and the cells internal resistance. As the current rate increases the potential of the electrode reduces. Therefore, as current rate increases the potential of the electrode will reach the potential at which lithium begins plating at a lower SoC.

$$V = E - IR \quad (6)$$

3.2.5. Vibration

Vibration has been referred to as a possible cause of ageing [79]. These authors have only referred to it in passing. For example, Svens *et al*. [80] refer to it as a factor of ageing in performing laboratory tests that replicate real life but no further information is given or implied. Testing for the possible ageing associated with vibration is a niche market because consumers throw away cells after only a few years use. They are often disposed of before vibration has an effect. For this reason, some authors have referred to the expensive and costly nature of creating reproducible data on ageing mechanisms associated with vibration [80]. Therefore, vibration remains essentially untouched in terms of its impact on lifetime of lithium-ion cells. The author has been unable to find any examples of the impact of vibration on the negative electrode, or any electrode for that matter. However, electric-vehicles may be subjected to harsh vibration profiles and the impact of vibration on materials in general is well established [81].

3.2.5.1. Electrode flaking

The only literature on electrical performance was a five minute vibration test using a varied frequency shaker table that showed no effect on cell lifetime [51]. Further work is therefore

needed to conclusively determine whether vibration has an impact on the lifetime of lithium-ion cells.

Research has been done into impact of vibration on lead –acid batteries and this mechanism may extrapolate to lithium-ion cells. For lead-acid batteries as the electrode flakes and erodes due to temperature, vibration can increase the rate at which these flakes then break off [82], presumably through mechanical damage or interaction of the flakes with the separator. For lithium-ion cells this would increase the rate of subsequent surface film formation and thus reduce capacity.

3.2.6. Orientation

NASA performed an orientation test on a single seven amp hour cell with 100% ΔSoC at room temperature [83]. It prematurely failed after 630 cycles, although with destructive analysis no ageing mechanism was discernible. Further tests on different cells showed no ageing associated with 100% %ΔSoC at 398 and 413 K after 1000 cycles. Whereas, for cells float charged (maintained at the same voltage) at 4.1 V, orientation made no difference at 25ºC but failed after 115 days at 45ºC. All four of the vertical cells were kept in inverted orientation but with no control cells [64]. Essentially, no useful information was obtainable from their test because of premature cell failures that did not align with a specific orientation. Three years later the supplier of the cells for the Mars Rover missions 'YARDNEY' stated in its data sheets that its cells can operate in any orientation including zero gravity [84]. There has not been much investigation into the impact of orientation on cell capacity or resistance. Further work is needed to conclusively evidence its effect on electrical performance.

3.2.7. External pressure

High external pressure such as when a cell is placed within a module or pack caused consistent capacity fade when compared to unconstrained or lightly constrained cells [85]. Loss of cycleable lithium was shown by localised deformation in the separator and surface film of the anode with post-test analysis of the cells using scanning electron microscopy (SEM). No other studies have been performed to investigate external pressure affects ageing so further work is required.

3.2.8. Discussion

The chemical changes that each of the seven mechanisms induce are summarised in Figure 6. Joining the results of primary and secondary mechanisms shows that creation of surface film at the negative electrode is the ultimate cause of ageing within the cell under these conditions – and is even a product of increased lithium plating.

It is not clear whether vibration, orientation or pressure impact cell performance at all, although in keeping with the other lifetime impacting factors if vibration does impact the cells, it may impact the negative electrode surface film.

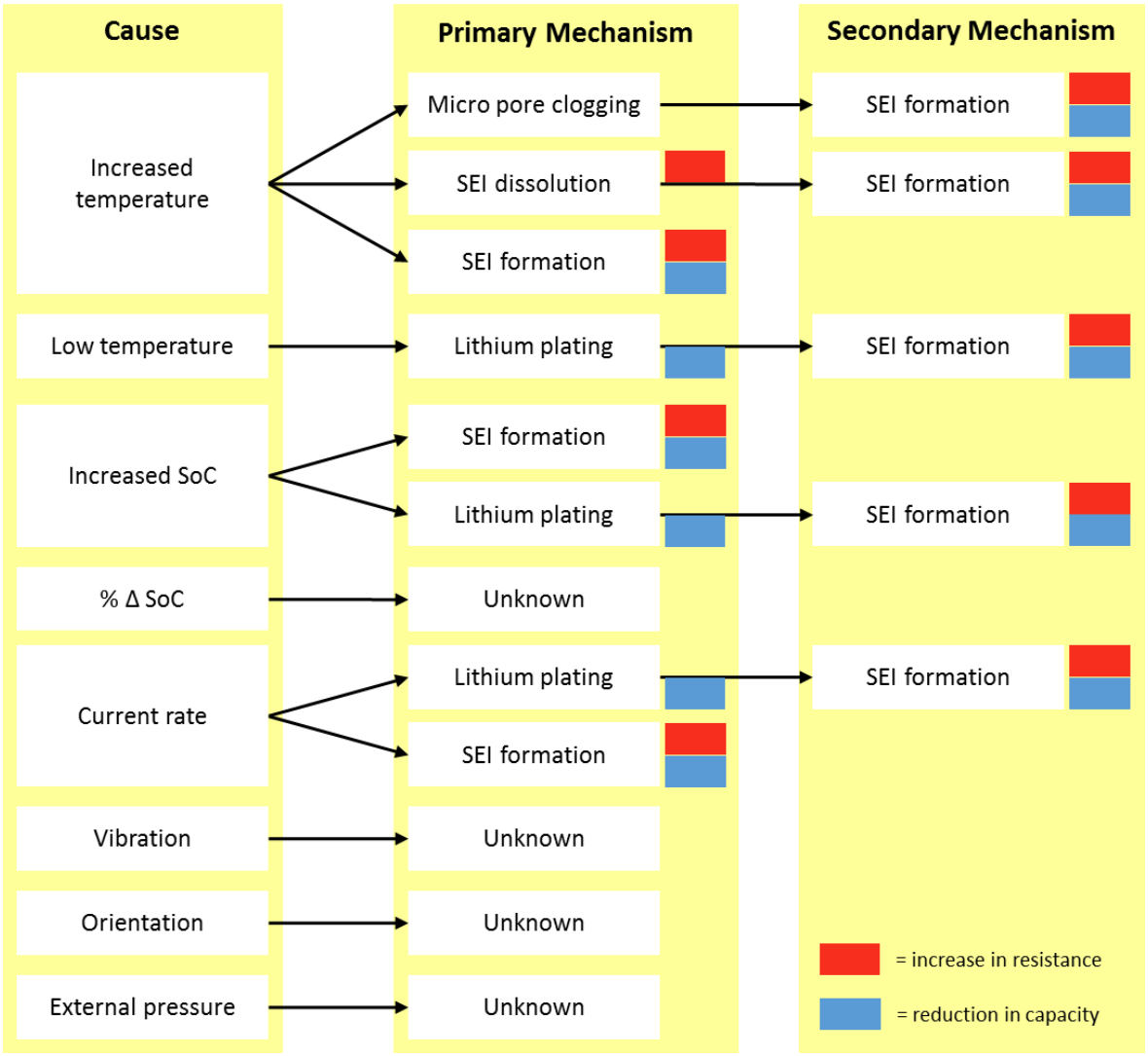

Figure 6. The seven (+1 for low temperature, as a subset of temperature) possible causes of lithium-ion cell ageing related to the internal mechanisms responsible for increase in cell resistance and a reduction in capacity

This literature review shows that post-mortem analysis should be centred on investigation of the negative electrode surface films composition. If this assumption is accurate, then accelerating the condition will impact cell performance without chemically altering the surface film. If this is the case and the chemical nature of the surface film does not change, then it is crucial that analysis be performed to determine the surface film's thickness. This is because, as Fick's law shows (4), diffusion into the bulk of the material is dependent on temperature, path

length (thickness) and the diffusion coefficient (chemical structure of the surface film). Therefore, the chemical structure of the surface film and its thickness are key parameters in connecting the post-mortem results to electrical performance.

Surface film at the negative electrode is cited as the primary mechanism of cell ageing by multiple authors [86-90]. This conclusion is supported in a highly cited review of degradation mechanisms for lithium-ion cells by Vetter et al. that ageing is caused by reactions at the electrode surface [6].

However, the positive electrode has been shown to contribute to the ageing of lithium-ion cells. Wright et al. performed a study on over 300 commercial cells tested at three different national laboratories within the United States of America. They concluded that oxidation of the electrolyte at high SoC at the positive electrode was the cause of decreased cell performance [91]. However, this assertion appears to be based purely on a paper by Guyomard and Tarascon [92] that studied the electrical performance of cells with voltages that exceed the 4.2V reached in commercial cells. The majority of the work that Wright et al. perform is also on cells at greater than 40^{o}C. This suggests a potential maximum temperature that the cells can be stored at, within this study, of around 40-50^{o}C, because the change in resistance occurs within this juncture.

This work is seeking to understand, measure and predict ageing of commercial lithium-ion cells. The majority of literature focuses on a surface film that forms at the negative electrode and assumes that the positive electrode contribution is negligible. This assumption is also made for this work, which is especially appropriate considering the temperatures that will be experienced in real-world conditions are not routinely greater than 40-50^{o}C.

3.3. The negative electrode Surface film

This section begins by investigating the origins and current understanding about the negative electrode surface film and concludes with which analytical techniques can be used to study it.

3.3.1. Introduction to the negative electrode surface film

In 1979 Peled proposed that whilst the transfer of Li^+ ions was occurring parasitic reactions also occur. The product of these parasitic reactions, forms at the interface of the electrolyte and active material [93]. His work was performed on alkali and alkaline based earth metals in non-aqueous battery systems; he called this surface film a solid electrolyte interphase (SEI). There is some confusion in using this term because some surface films do not form an interphase between the electrolyte and the surface film. These terms are used interchangeably within this work. Fong et al. showed this mechanism was also true for lithiated graphite within lithium-ion cells [94]. And that formation of this film was coupled with a sharp reduction in capacity and increase in resistance within the first few cycles of the cell's life. This occurs because the abundant electrons that provide current to the external electrical circuit are freely available to the electrolyte. As the Li^+ intercalate into the active material the electrodes are at the correct potential for reaction with the electrolyte. These electrons migrate through the electrically conducting active material from the site of lithium de-intercalation and react with the solvent. However, this performance decline is not as severe after the first few formation cycles [95]. The reason is that the formation of this surface film passivates the electrode to further similar parasitic reactions [96]. Therefore, this passivating film must be at least partly electrically insulating, because the cell does not continue to lose capacity and increase in resistance at the same rate. But it is also ionically conductive, to allow intercalation to still take place. This indicates that the surface film forms on the electrode active material particles and thus reduces

the rate of Li^+ diffusion into (or out of) the active material. As shown by (5), with an increase in parameter x (path length) this causes a reduction in the rate of diffusion. Therefore, this parasitic reaction to form surface film would cause the cell resistance to increase and, if lithium was used in its formation, lose capacity. This is directly noticeable by the user of the car as a reduction in available driving range.

3.3.2. Chemical composition of the surface film

The negative electrode active material in commercial cells is consistently carbon based, normally graphite or hard carbon. The particles are approximately 5-20 μm in diameter – as seen in the micrographs of Markervich et al. work [97]. These particles are bound together with a binder material, this is typically a styrene butadiene rubber (SBR) type compound or something similar [98]. In addition to the intercalating carbon and binder, commercial electrodes are coated or mixed with additives to improve performance – there are likely to be many additives all performing different roles, as explained by Zhang [99].

Lithium-ion cells also require a salt for the transfer of cations within solution, for commercial cells this is normally $LiPF_6$, within a solvent [24]. This solvent will invariably contain ethylene carbonate (EC) due to its preferential reaction at the electrode surface for passivation [100]. However, like $LiPF_6$ it is a solid at room temperature and pressure (RTP). Electrolyte liquid is created by solvating these compounds in lower boiling point alkyl carbonate solvents such as dimethyl carbonate (DMC) and diethyl carbonate (DEC) [24]. It is not possible to know the precise chemical composition of the materials present within commercial cells [99]. However, Table 1 shows the chemical structure of commonly used electrolyte solvents, the $LiPF_6$ salt and some additives.

Table 1. Common components likely to be present in electrolyte using skeletal bond formula representation with solid lines representing bonds in the plane of the paper, wedged lines representing bonds that are behind the paper and dashed lines for those moving out from the paper.

Salt	Low boiling point solvents	High boiling point solvents	Additives
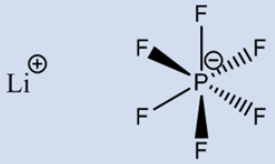 $LiPF_6$	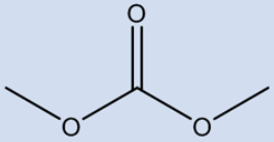 Dimethyl carbonate	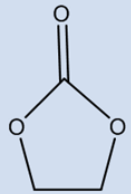 Ethylene carbonate	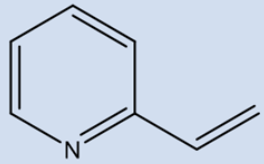 2-vinyl pyridine
	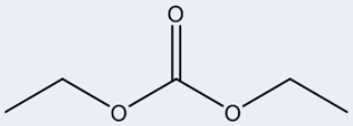 Diethyl carbonate	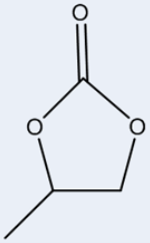 Propylene carbonate	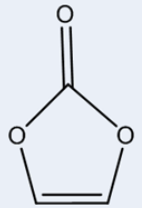 Vinylene carbonate
	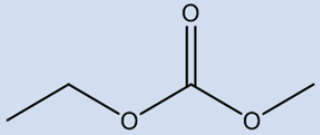 Ethyl methyl carbonate		

Some of the first studies into the chemical composition of the surface film suggest that its formation follows a mechanism like that shown in Figure 7 to form various alkyl carbonates [101]. This general mechanism of ring opening, although not with propylene carbonate (PC) due to its formation of unstable surface films with $LiPF_6$ [102], is held to be generally accurate for other similar solvents. The surface film is comprised of small hydrocarbons (product 1) and more specifically alkyl carbonates (products 2 and 3) at the electrode surface [103].

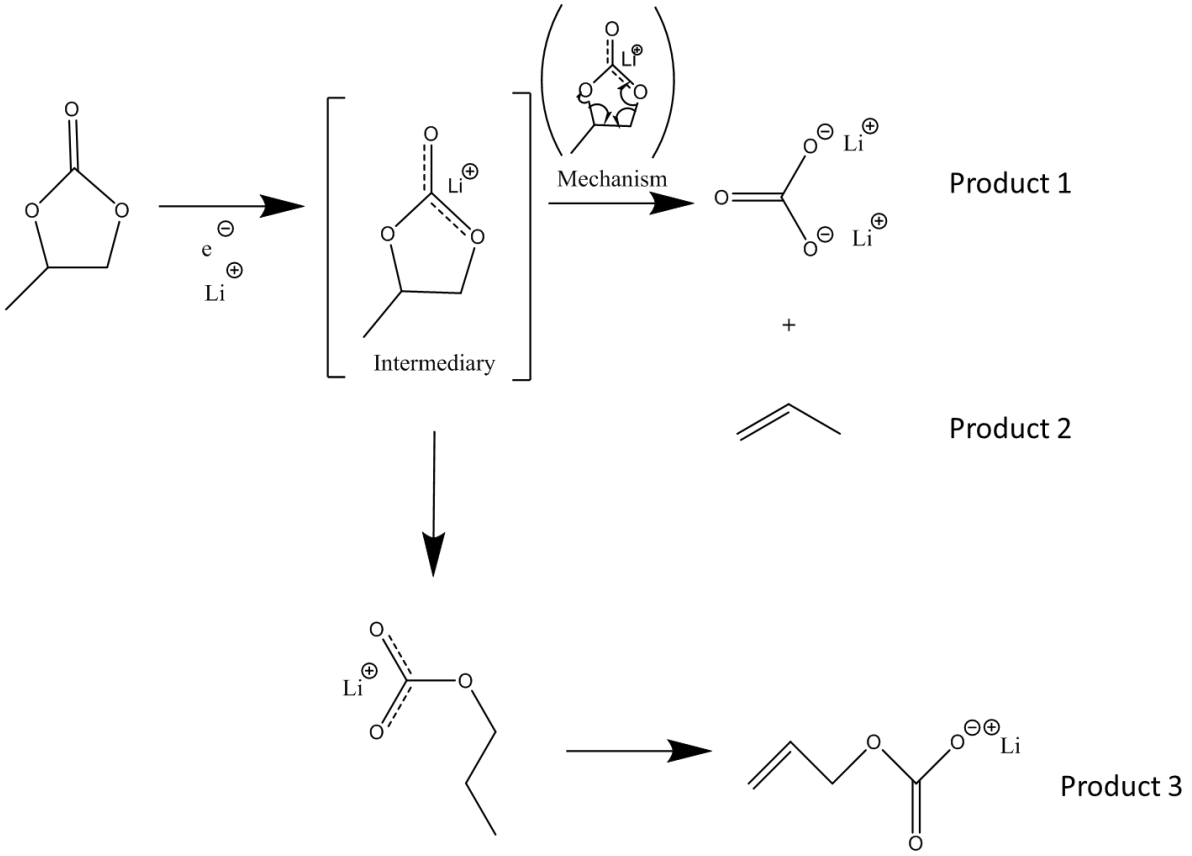

Figure 7. Two possible reduction mechanisms when propylene carbonate is the reagent, as proposed by Aurbach et al. [104]

Additives such as vinylene carbonate (VC) have been shown to preferentially polymerise on the surface of the electrode initially and stabilise it to further reaction with electrolyte solvents [105]. This polymerisation forms polyvinylene dicarbonate plus a myriad of other polymerised chains containing R-OCO_2Li groups [106], where R- represents a varied residual hydrocarbon

species of unknown specific composition. The polymerisation suggested in their work involves acetylene. Reaction with this molecule, although preferential due to it being an alkyne, is not the only one possible. With the addition of other chemicals and additives, such as the many possibilities in commercial cells, it is likely that other polymerised products are also formed. In fact, it is the polymerisation of these organic additives that is often attributed with the increased cycle life and other beneficial properties [107-109].

Figure 7 that shows the proposed reduction and ring opening of propylene carbonate to form two different products. One of these products (product 3) contains only a single Li^+ whereas the other contains two (product 1). There are no papers that predict the stoichiometric quantities of products one or two; and due to the complexity of reagents present such predictions would be even more complex for commercial cells. However, hypothetically as an illustration, if this ring opening mechanism were to be the main cause of capacity loss (loss of lithium) within the cell and if product 1 and 2 is stoichiometrically more prevalent than Product 3. The capacity of the cells under these conditions would reduce at a rate of twice of that compared to if product 3 was the stoichiometric preference. This is because Product 1 contains twice as many lithium atoms. Therefore, it may not be possible to know the precise cause of capacity fade within lithium-ion cells without knowing the stoichiometric quantities and all of the internal mechanisms occurring. However, a study of the surface film chemical composition should be identical if the cells have been treated in the same way and therefore, chemical changes to this film should still provide details of changes in chemical mechanisms that have occurred.

Examples of molecules present in the surface film are shown in Figure 8. Although this figure is not intended to be exhaustive it is indicative of the type of materials being studied. The typical composition of the gases shown in Figure 8 are from [110], whilst the typical composition of surface film components and electrolyte deposits is taken from [111,112].

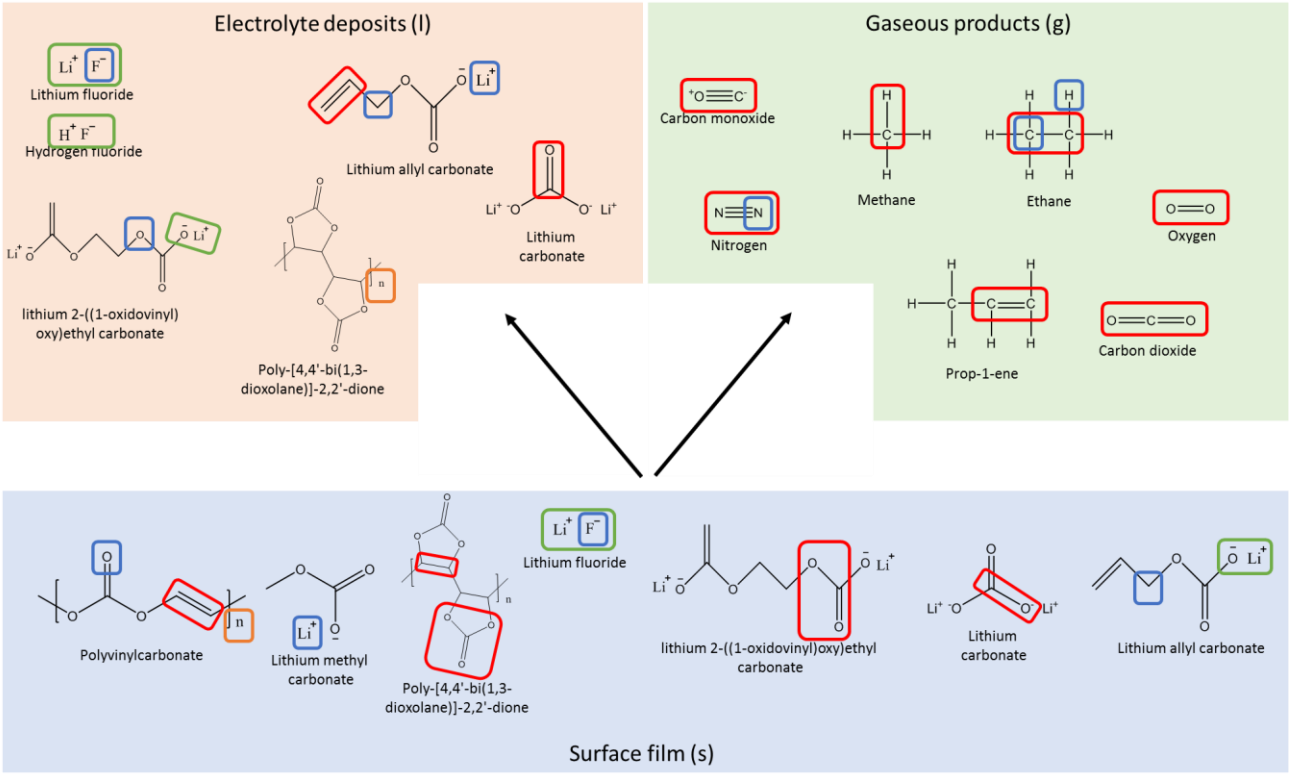

Figure 8. Chemical composition of the typical classes of materials within the surface film, electrolyte and gas. Red rectangular outlined boxes indicate organic functional groups. Green boxes indicate inorganic containing compounds, blue boxes indicate the individual elements being studied and orange boxes indicate polymeric species by circling the 'n' annotation of the molecule. The symbols (l), (g) and (s) refer to the phases of liquid, gas and solid respectively.

Figure 8 shows possible chemical components of the surface and in the electrolyte are oligomers, small inorganic molecules, carbonates and other small organic molecules (e.g. propane).

3.4. Techniques to study the chemical composition of the surface film

The negative electrode surface film may be as thin as a few nanometres [107,113,114] and is stochastically and in-homogeneously ordered with significant relative surface roughness (active material particles that protrude from the surface are microns in diameter but the surface film is only nanometres) [115,116]. This means that the surface film surrounds each particle, the particles themselves are 1000 times larger. This makes analysis of this film complicated. However, it is more complicated than this, Figure 9 shows the typical composition of the electrode during use. It shows that the surface film situated on the graphite particles is covered by electrolyte that contains solvents, deposits, and other materials. Once the cell is opened the low boiling point (B.P.) solvents (B.P. < 20^{o}C) evaporate leaving the other products deposited onto the electrode surface. These products can block or saturate analysis of the thin surface film and it may be difficult to differentiate the surface film from the deposits.

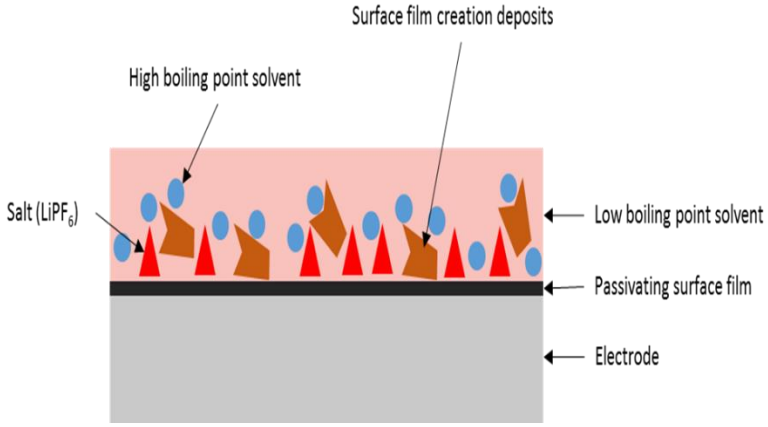

Figure 9. Graphic of the electrode surface during cell use

The gaseous products are exclusively small organic hydrocarbons, mainly saturated but with some alkene groups (C=C). All of these molecules can be detected and quantified with GC-MS

[117]. Raman or IR spectroscopy can also be used for confirmation of the GC-MS results, as shown in the work of Stoicheff for CO_2 gas analysis with Raman spectroscopy [118].

Analysis of the surface film and electrolyte deposits is more difficult. This is due to problems associated with separation of the two. As shown in Figure 9, once the cell is opened the low boiling point solvents evaporate and leave high boiling point solvents, electrolyte deposits and salts. In addition, many of the inorganic chemicals in both the surface film and the deposits are the same (Figure 9). Some molecules may impact resistance of the cell when contained within the surface film [119] but will not have the same effect within the electrolyte. In order to overcome this a method is required that can differentiate between the surface film, electrolyte deposits and the bulk.

Figure 9 shows that the surface film and deposits contain a mixture of longer chain organic hydrocarbons, inorganic compounds and polymers. X-ray photoelectron spectroscopy (XPS) is capable of studying these elements, and can also differentiate between molecules (chemical functional group). XPS is uniquely placed as a technique which can offer the combination of chemical state specificity and the high degree of surface sensitivity (< 10 nm) [120] needed to identify the compounds found in the surface films of lithium-ion cells. This is proven by its universal use for post-mortem analysis of lithium-ion surface films by leading scientists in the field, such as Peled who discovered SEI [113]; Aurbach, Peleds successor and one of the principle authorities on surface film chemical composition [121]; and Dahn, who identified SEI formation on graphite particles [122]. XPS is one of, if not the most, commonly used method for quantitative analysis of the surface films chemical composition [19,123-125,104,126-132]; this is likely due to five reasons:

- Sampling depth (analyses at a depth of 1-10nm so can potentially isolate surface film from bulk materials)

- Sensitivity of detection up to 1%
- Can detect lithium
- Detection and quantification of organic species and their chemical environment (functional group)
- Detection and quantification of inorganic species and their chemical environment

Information obtained through XPS can be supported by IR and Raman spectroscopy. Work by Aurbach et al. exhibited this when they studied the surface film / deposits of the electrode using XPS, IR and Raman [133]. However, they then propose a mechanism involving polymerisation of VC, but state that none of the methods they used (IR, Raman, XPS) were capable of verifying this conclusion because they could not detect the polymeric species.

A common method for studying polymers is size exclusion high performance liquid chromatography (HPLC). The problem with this method is that it exposes the $LiPF_6$ salt, which is also removed during washing [134], to moisture which then forms HF [135]. This acid corrodes the equipment and contaminates the sample.

Although XPS can study the number and type of functional groups present it cannot determine changes in the length or type of polymers present as reliably, to do this, HPLC can be used [136].

3.5. Determining surface film thickness with XPS

Diffusion through the surface film has long been established as a rate limiting factor for lithium-ion cells based on changes to the diffusion coefficient (chemical composition of the film) and the path length (surface film thickness) [137]. If the chemical structure of the surface film remains identical, and temperature remains the same, then the only other contributing factor of a resistance rise from the surface film must be due to the surface films thickness. Pinson et al. show that the electrode resistance of a film that does not alter in chemical composition can be attributed to its diffusion length [138]

The cell thickness has been calculated using sputter-depth profiling with XPS as shown in these previous studies [139,140]. Sputter-depth profiling is where the surface is removed by accelerating particles at the sample to remove the top layer. This type of sputtering, which is different to sputter-deposition, is used to remove surface material, rather than add it. This sputtering interleaved with analysis provides information on the chemical composition at each layer. In both studies, they use a standard to act as a depth gauge of sputter rate. This type of analysis is routinely performed on homogeneously oriented structures with well-established chemical configurations, such as Si / Si-O [141]. This is because the rate of sputtering is dependent on the orientation of particles [142] and on the material being sputtered [143]. Sputter depth profiling can be used for high quality Si/Si-O because they meet these criteria. However, for inhomogeneous samples with an unknown chemical composition this is not possible. In addition, any depth profiling study would also sputter through other deposits on the surface and salt. This means that any time based value is dependent on the time taken to sputter through these additional components and the thickness of these is not known either. Therefore the method used by Lu et al. [139] and Ma et al. [140] to determine an absolute thickness of the surface film is not likely to work.

3.6. Study of the polymeric species present in the surface film with HPLC

Aurbach et al. state that they were not able to study the polymeric structure and nature of the surface film with IR, XPS or EDAX [133]. A commonly used method for analysis of polymeric materials that are less than 10,000Da is HPLC using a gel permeation column (GPC) [144]. The surface film is removed by a solvent and then processed by HPLC. However, $LiPF_6$ is known to decompose to lithium fluoride and phosphorous pentafluoride (11). In the presence of moisture, phosphorous pentafluoride forms hydrofluoric acid (HF_{aq}), as shown in (12). HF is classed in the highest groups for both corrosiveness and toxicity under European Union legislation [145]. When HF forms inside the chromatography system it corrodes internal components causing leaks. It also corrodes the column itself, this in turn increases the total counts and changes the chemical composition of the sample being studied. This means that the results are not consistent because they contain varied quantities of the column and system lining as well as other parts of the equipment. This means chromatography cannot be used for electrode washings containing $LiPF_6$ because it taints the sample; nor would a laboratory wish to cause damage to expensive equipment.

$$LiPF_6 \rightarrow LiF + PF_5 \quad (7)$$

$$PF_5 + H_2O \rightarrow POF_3 + 2HF \quad (8)$$

This problem of HF formation from $LiPF_6$ reaction in lithium-ion cell samples damaging equipment is highlighted by Petibon et al. [146]. They suggest a liquid-liquid extraction method to circumvent the problem and process samples prior to analysis with gas chromatography [146]. Their method hydrolyses the $LiPF_6$ from the sample prior to analysis with GC but during

the period of HF formation the sample is in contact with the $LiPF_6$. This means that HF may react with the sample prior to analysis. Whilst their method is useful in not damaging equipment, because HF then reacts further, there is no guarantee that the short term creation of HF has not contaminated the sample itself. Analysis of that sample with GC could not have guaranteed that the sample was not contaminated, only that HF was no longer present to damage the equipment.

Therefore, a method is required to improve on Petibon et al. [146] process by stopping HF's reaction with the sample.

3.8. Obtaining access to the negative electrode surface film

3.8.1. Cell opening

Cell opening is the process of removing electrode active material from the outer casing and other components. For pouch cells this outer casing is made of aluminium lined with a polymer. For 18650-type cylindrical cells it is a stainless steel casing.

3.8.2. Pouch cells

Commercial pouch cells are comprised of alternate positive and negative electrodes with a separator between them. This can be either a folded single electrode or multiple sheets stacked on top of each other. The opening and removal of internal materials for pouch cells is relatively simple and intuitive. It involves the use of ceramic scissors and plastic or plastic tipped tweezers. The process described by Williard et al. appears consistent with the approaches in literature and there are no apparent reasons for the surface film to be affected by the process [147].

3.8.3. Cylindrical (18650) cells

Commercial 18650-type cells are comprised of alternately wound electrodes and separator rolled into a 'jelly roll' and placed into a steel cylinder with a small mandrel hole approximately 3-5mm in diameter down the centre.

The methods in literature suggest opening 18650-type cells by cutting the top or bottom and then along the length of the cell and removing the inner roll. This has been done with hand-held Dremel© saws [148] automated onto stages [149] or just with hacksaws [150]. The use of a Dremel© tool with a ceramic cutting disc is the most common method (Figure 10, A) [147].

Using this method, it is difficult to not also cut into active material and thus short the cell by electrode layers touching around the edges (Figure 10, B & C). It also creates black soot and sparks from the stainless steel as it is cut. The soot covers everything in the glove box – including the electrode roll. Williard et al. point out that this is likely to taint further analysis of the active material [147]. They also support the suggestion that short circuits and friction from the disc cutting the steel causes cell temperatures to increase. The work of Broussely et al. draws definitive conclusions which show that temperature is a critical component in inducing other aging mechanisms [50]. Therefore, using this method is likely to make changes to the surface film. Thirty 18650-type cells were opened using a combination of Dremel©, hacksaws and files; it was not possible to remove the inner roll without cutting into active material, creating short circuits and creating dust.

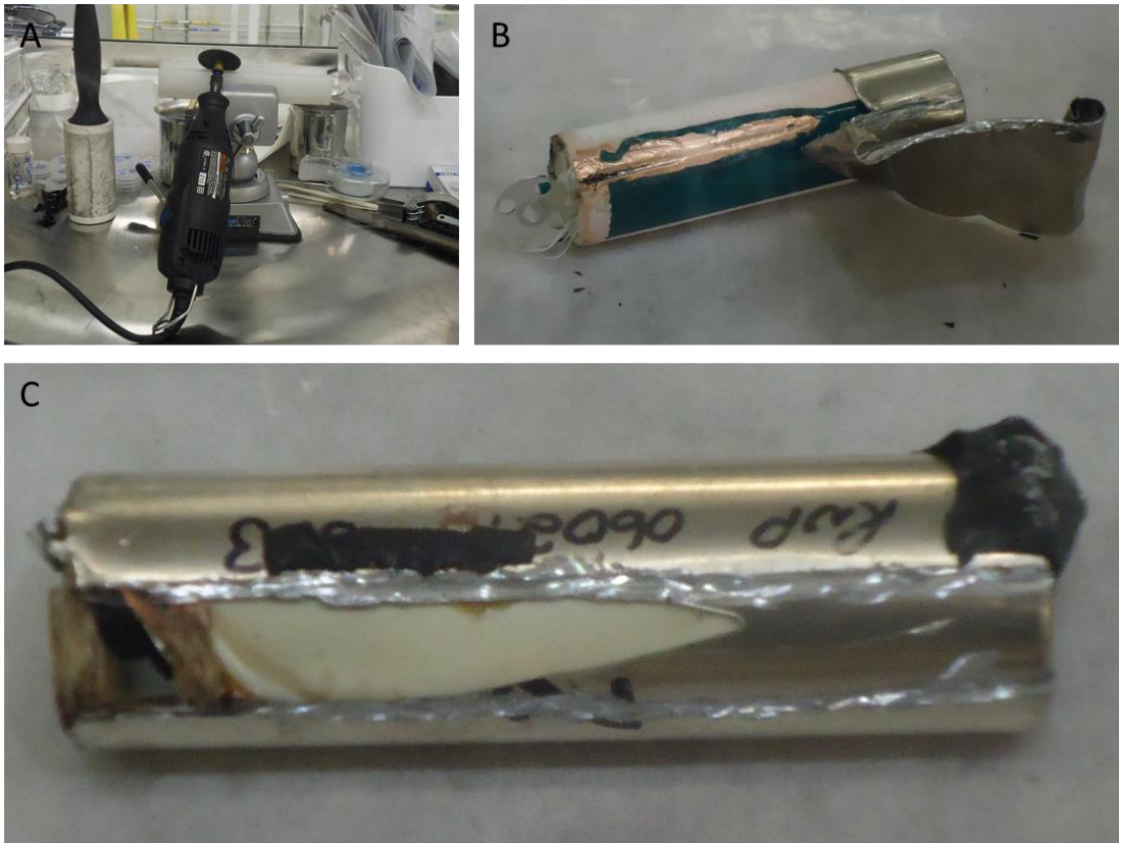

Figure 10. Image of a Dremel multi-tool with ceramic cutting blade attached (A). Images of failed attempts to open 18650 lithium-ion cells without short circuit. B is the best attempt with a hacksaw blade. C is the best attempt with a Dremel multi-tool using a stand to control cutting depth.

Therefore, it can be concluded that dust creation, temperature increases and short circuits always occur when these cutting methods are used. In addition, dust and particulates also spread onto nearby samples and can be moved around by air flow [151]. These could then land on, imbed in, or react with samples which are later analysed.

The problem is that techniques used to analyse these samples can be sensitive to the top 10 nm of a material surface. The impact of this type of contamination using techniques that are this sensitive mean that analysis may detect compounds that are not present in the cell during use but were added during cell opening. This could then lead to conclusions that are inaccurate.

3.9. Preparing samples for analysis

Previous works have highlighted the need of careful, clean and repeatable processing of samples prior to surface analysis within fields not specific to lithium-ion [152].

The vast majority of post-mortem type research rinses electrodes with solvents prior to analysis [153-157]. The reason often given for doing this is to remove the salts and solvents present on the surface film that saturate analysis. The most commonly used solvent for electrode washing is dimethyl carbonate (DMC). Malmgren et al. rinsed graphite electrodes with DMC and found that reactivity when exposed to air increased if the electrode was rinsed; they conclude that rinsing likely removes the passivating film [18]. Whilst Orsini et al state that washing electrodes may remove surface film [158], no one has systematically studied its impact to determine if this is true. A study is required to systematically investigate whether washing impacts the negative electrode surface film.

3.10. Conclusion

The initial aim of this work, proposed by JLR, was to determine how long a vehicle's battery would last and create a mathematical model predicting this lifetime supported by real-world testing. The literature showed that most of the lifetime reducing factors caused the formation of a surface film at the negative electrode. The negative electrode surface film is comprised of inorganic, organic and polymeric species; It also contain salts and electrolyte solvents. Some of these products can also be found deposited within the electrolyte. XPS can be used to detect and study changes in the chemical composition of these products, except for oligomers. The oligomers can be detected and studied with HPLC. However, to validate any lifetime performance model based on this surface film would require improvements in the methods of collecting, processing and analysing these material changes. Therefore, the aim of this work has refocused on ensuring the validation data collected is representative by investigating the following areas that have been identified as problematic:

1. A method of opening 18650-type cylindrical cells without affecting the surface film
2. Understand the impact of rinsing electrodes on the surface film
3. A process of studying the surface film composition separate from the electrolyte deposits
4. A process is required to determine the thickness of the electrode surface film
5. A process is required to stop $LiPF_6$ from affecting the chemical composition of the surface film in preparation for HPLC analysis

The reason for this shift away from the initial aim is because there would be no benefit in creating a technically complex model that is then populated with un-validated data.

4. Research methodology

The aim of this work is to investigate how post-mortem analysis can be used to detect material changes in commercial lithium-ion cells after accelerated lifetime testing. This will validate whether post-mortem analysis can provide more information than electrical testing alone. This information is required to improve current accelerated testing profiles, mitigate future damage and improve knowledge on the causes of lifetime reduction within lithium-ion cells.

Therefore, as explained throughout the review of the literature, the four main objectives of this work are now:

1. Determine the conditions of use that impact cell lifetime and how that lifetime reduces with respect to cell capacity and resistance after an accelerated testing period
2. Determine the post-mortem methods that allows connection between electrical performance data and material changes at the negative electrode
3. Perform post-mortem analysis on the negative electrode surface film of cells at each of the lifetime affecting conditions to determine viability of the method and investigate the causes of lifetime reduction within lithium-ion cells
4. Determine whether material changes to the surface film at the negative electrode can be correlated to the cells electrical performance

Objective one is especially applicable to automotive use, and the utilisation of resistance and capacity is chosen because it impacts automotive performance, lifetime and heat generation. These are important metrics for any automotive application with respect to cell lifetime performance.

Objective two is required because, as shown in the review of the literature, electrochemical models that are used in predicting the lifetime of lithium-ion cells are dependent on

assumptions made with respect to material changes. In many instances these assumptions remain unproven and therefore require further investigation. When such models are used to predict lifetime for automotive use, if the assumptions are incorrect then warranty and other costs could bankrupt even large automotive companies – because battery packs make up a considerable cost of electric-vehicles.

Objective three ensures that robustness in the process of cell opening and mechanism validation is considered throughout the process. There would be no value in performing analysis if the analysis itself changes the chemical composition of the sample.

Objective four is where the underlying science and materials analysis of the former objectives is applied to an automotive application. At this point it will be possible to determine whether the materials analysis has provided important information in elucidating internal chemical mechanisms responsible for performance decline and the point at which mitigation can be considered at a whole-vehicle level.

The research will be split into four stages, one to address each objective. Objective one will be investigated by testing cells at seven different conditions of in-vehicle use for changes in capacity and resistance.

Objective two will be investigated by resolving five problems identified from literature with the current process of post-mortem analysis, these five challenges are:

1. A method of opening 18650-type cylindrical cells without affecting the surface film
2. Understand the impact of rinsing electrodes on the negative electrode surface film
3. A process for studying the surface film composition separate from the electrolyte deposits
4. A process is required to determine the thickness of the electrode surface film

5. A process is required to stop $LiPF_6$ from affecting the chemical composition of the surface film in preparation for HPLC analysis

Objective three will be investigated by studying chemical changes in the surface film of cells that have undergone accelerated lifetime testing with XPS, IR, SEM and HPLC.

Objective four will be investigated by comparison of the electrical data with the post-mortem results.

Achieving these four objectives in this order comprises the methodology followed within this work. It will investigate how post-mortem analysis can be used to detect material changes in commercial lithium-ion cells after accelerated lifetime testing.

To meet these four objectives, it is necessary to utilise facilities and expertise that are world-leading in terms of both research output and scientific method. To do this in a short time a placement was organised at Argonne National Laboratory (ANL) based in the USA for 12 months. This was based in the newly built post-test facility under the direction of world renowned scientist Ira Bloom. Many of the advancements made in understanding the process of post-mortem analysis were created by the author under the direction and guidance of Ira and his team. Argonne was chosen because it is the largest non-commercial research facility for post-mortem type work in the world with access to cutting-edge technology and multiple world-renowned faculty members. It was decided that such a placement would provide the most in terms of learning and progression for the project.

Because of the placement and restrictions placed on this specific engineering doctorate, some of the choices with respect to cell selection, methodological choice (i.e. electrical characterisation) and the use of solvents was subject to decisions and protocols made at senior management levels. One example is the choice of cells that underwent fast charge at ANL, in

some cases a reason was not provided by the sponsoring company or ANL for such choices but each instance of this is highlighted in the text.

5. Electrical data

This chapter aims to meet the requirements of objective one for this work. This is to determine the conditions of use that impact cell lifetime and how that lifetime reduces with respect to cell capacity and resistance after an accelerated testing period

This chapter characterises the capacity and resistance of lithium-ion cells from seven different conditions, these are temperature, SoC, % Δ SoC, current rate during charge, vibration, external pressure and orientation. Each of these are presented in individual chapters. This chapter's work, within the context of the innovation report and portfolio, is outlined in Figure 11.

Figure 11. Outline of the engineering doctorate portfolio, chapters within this innovation report are shown as numbers to the left of white topic boxes. The green coloured box refers to the section of the portfolio that this chapter relates to 'Background'.

5.1. Cell selection and electrical performance bench-marking

The cells used in this study are commercially available 18650-type cells; except for the 'impact of external pressure' study, which uses commercially available large format pouch cells. These details are shown in Table 2. All cells were purchased directly from the manufacturers. The cells from each manufacturer came from the same batch and all had approximately the same nominal voltage and general chemistry. However, the B cells used $LiCoO_2$ as the positive electrode, this was based on other requirements at Argonne National Laboratory (ANL).

Manufacturers B and C have a reduced capacity compared to A and D. Cell E has a capacity of 8.0Ah, this is because this is a larger format pouch cell, required to apply equal pressure across the cell surface.

The choice to use 'cell D' for vibration was due to logistical requirements. The vibration tests were performed on two different types of cells to determine the impact of different accelerated vibration profiles (the other was A cells). Post-mortem analysis and electrical characterisation within the time frame required for this work meant that the A cells also being tested would not have completed in time to have post-mortem analysis performed and results written up.

N.B. choice of which cells to buy sits within an entire stream of other work at both institutions and within Jaguar Land Rover; based on non-disclosure agreements, previous experience and relationship with suppliers.

Table 2. Material type, nominal capacity and voltage for cells used in these tests, NMC represents $Ni_xMn_yCo_z$. The table is populated with information from cell supplier data sheets.

Cell	*Positive electrode*	*Negative electrode*	*Nominal capacity*	*Nominal voltage*	*Misc.*
A	NMC	Graphite	3.1	3.7	
B	$LiCoO_2$	Graphite	1.8	3.6	High power
C	NMC	Graphite	2.8	3.7	High power
D	NMC	Graphite	3.2	3.7	
E	NMC	Graphite	8.0	3.7	(pouch)

Electrical tests and the subsequent results obtained were requested and partly or substantially designed by the author but mainly performed by technicians at two different institutions. These were Argonne National Laboratory and WMG. Capacity was calculated with a 1C discharge current between 100% and 0% SoC. The voltage limits set for these SoC were according to manufacturer data sheets, and the total number of amps extracted during this discharge constituted the cell capacity. Resistance was calculated with a pulse power test at 50% SoC. This pulse power test constitutes a single discharge pulse that was 10 seconds long, at a rate equal to the maximum discharge pulse allowed by cell manufacturers (Imax / ΔI). The resistance was calculated by taking the change in voltage between the rest period prior to the discharge pulse and the voltage at the end of the 10s discharge pulse (ΔV / ΔI), this means it comprises the ohmic, charge transfer and diffusion resistances. The data contained in this work is from raw cell data and the processing, investigation and conclusions reached are all by the author.

All cell testing was performed on three duplicate cells for each condition. The total number of cells characterised in this work was 87, encompassing total electrical characterisation testing time of more than 900,000 hours. Considering this type of testing requires expensive equipment for long periods of time, this is a high population sample size. Many ageing tests are performed on a single cell or a small selection of cells [159]. Previous work has been performed on up to 300 cells but this is exceptionally rare [61] and these did not include commercially available

cells. A conservative estimate of what this testing cost the institutions is £825,984 GBP, as shown in table 3, using a value of £0.81 for each cell per hour, which is the cost at WMG.

Table 3. Table showing number of cells, manufacturers, time and cost to perform electrical testing of commercial lithium-ion cells, the location relates to the location of testing performed; being either Warwick University (WMG) or Argonne National Laboratory (ANL).

Test condition	***Manufacturer***	***Location***	***Total cells***	***Testing time (months)***	***Total cost (£)***
Temp. / SoC	A	WMG	27	30	466,560
Current rate	B/C	ANL	24	6	82,944
% Δ SoC	C	ANL	12	6	41,472
Vibration	D	WMG	9	12	62,208
Pressure	E	WMG	9	20	103,680
Orientation	A	WMG	6	20	69,120
Total			**87**	**94**	**825,984**

All cells were tested on commercial grade cycling equipment. All tests were performed within temperature controlled chambers at 25ºC. Except for the vibration tests, because the vibration table could not fit inside a temperature chamber. However, the room temperature (climate controlled to ~20ºC) was kept constant. This means that the cells undergoing vibration and the control cells were kept at the same temperature. The room temperature of ~20ºC is consistent with conditions required by cell suppliers for cell storage and therefore because both the vibrated cells and control samples were at the same temperature the vibration test results should not be affected by not being in temperature controlled chambers. It is assumed that this difference in temperature will be identical for those cells being vibrated and the control samples that remained within the same room, but not vibrated, so should not introduce additional error.

The error bars shown in the electrical data are calculated as one standard deviation (s.d.) from the mean based on the cell condition with the result population of a single condition as arguments. It is expected that 68% of the population falls within the standard error of the mean presented [160]. Where a data point has no error bar value, this is because the error is too small

and is consumed by the data point itself, is too large (this single instance is identified within the text) or it is not possible to calculate the error. In some cases, two-standard deviations in error for a single usage condition is greater than the difference between usage conditions. This is because, even though commercial lithium-ion cells were used in these tests, manufacturer tolerances mean that individual cells from an identical batch can have a range of resistances and capacities. Over a prolonged period of electrical testing these differences can cause significant deviations between otherwise identical usage conditions. This observation is consistent with electrical data from similar studies that contained a large number of cells [17].

The study uses two different locations to perform the tests and this introduces potential error through equipment, machine and user variables. However, for all tests end of life electrical data was collected in the same location as initial testing.

This section describes the results of the electrical testing and performance with respect to capacity and resistance changes. An in-depth discussion on what each of these results mean with respect both lifetime and material changes within the cell is discussed in their respective sections of chapter eight.

5.2. Temperature

Three different temperatures (10^{o}C, 25^{o}C and 45^{o}C) were investigated at three different SoC (80%, 50% and 20%) over two and a half years. The highest temperature is set at 45^{o}C so that additional chemical mechanisms of oxidation at the cathode are not induced, as highlighted within the literature. The temperatures were ultimately chosen by JLR with the author's guidance.

Impact of storage temperature on cell capacity and resistance is shown in Figures 12 and 13 respectively. In general, the best temperature for cells to be stored at to limit capacity loss is 25^{o}C followed by 10^{o}C. Cells stored at 45^{o}C had the highest capacity fade and resistance increase. The one exception was for 20% SoC where the worst condition was 10^{o}C. The cell is ideally suited to being at 25^{o}C to reduce capacity loss.

The impact of temperature on cell resistance is linear at all SoC, with the exception of 80% SoC that had a slightly higher impact at the highest temperature. The cell resistance increased more than three-fold from the lowest temperature to the highest temperature at the highest SoC.

These results are consistent with other publications that have recorded a similar level of degradation with temperature [91].

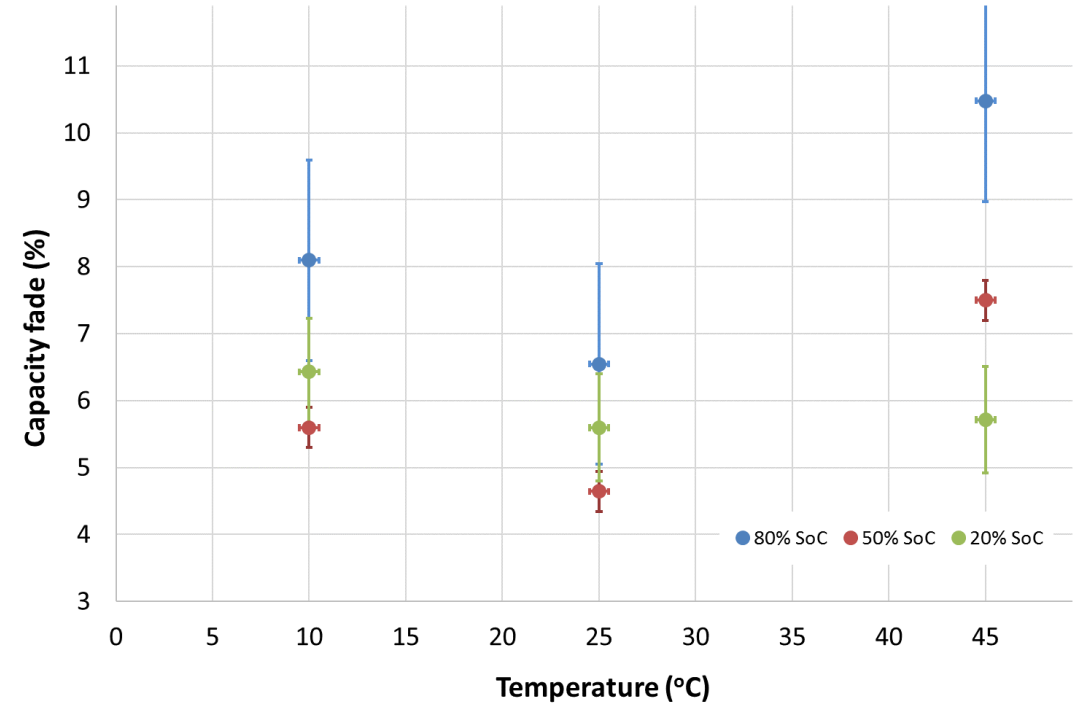

Figure 12. Impact of temperature on cell capacity

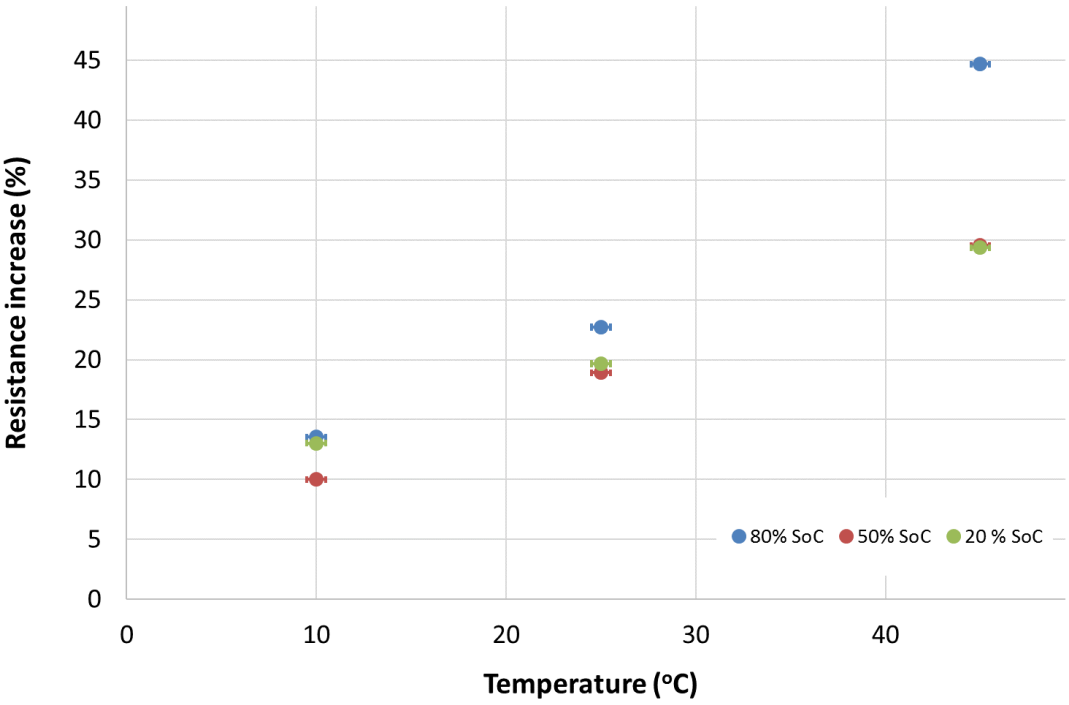

Figure 13. Impact of temperature on cell resistance

5.3. State of charge

Three different states of charge (20%, 50% and 80%) were studied at three different temperatures (10^{o}C, 25^{o}C and 45^{o}C). The SoC were used to represent the SoC window but were chosen by JLR. The impact of state of charge during storage on cell capacity and resistance is shown in Figures 14 and 15 respectively.

With the exception of high temperature (45^{o}C) the best SoC for both resistance and capacity is 50%. At every temperature the highest SoC causes the greatest decline in both capacity and resistance. With the exception of the highest SoC / temperature combination, the impact of SoC on cell resistance is less than 3% in total. Coupling this information with that of temperature suggests that the majority of cell resistance increase comes from difference in temperature, however, at the highest temperature its impact is magnified by the SoC; this is not true for capacity. As SoC increases from 50% to 80% the capacity fade also increases. For capacity better cell lifetime is achieved at 50% SoC, with the exception of 45^{o}C, which maintains an almost linear increase with SoC.

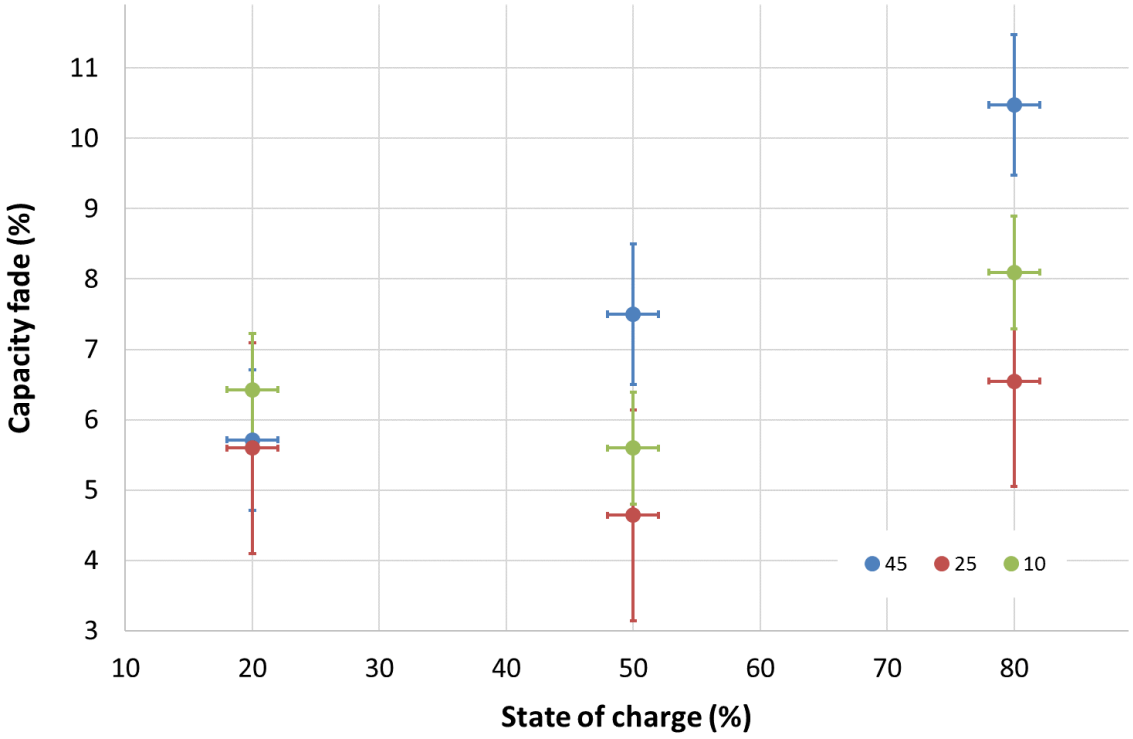

Figure 14. Impact of 'State of charge' on cell capacity at three different temperatures (45ºC, 25ºC and 10ºC)

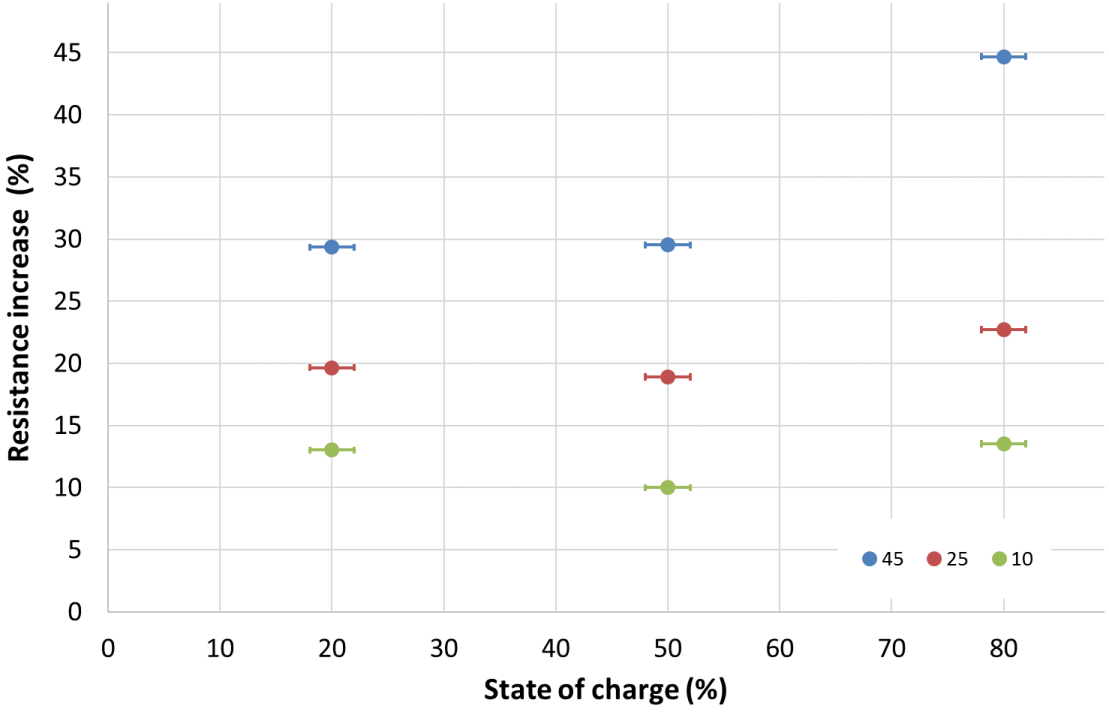

Figure 15. Impact of State of charge on cell resistance at three different temperatures (45ºC, 25ºC and 10ºC)

5.4. Increased current rate during charge

Cells were cycled between 0 and 100% SoC at different C-rates. The impact of charge rate on capacity and resistance is shown in Figures 16 and 17 respectively.

As C-rate during charge increases the rate of capacity fade also increases and follows a linear trend. The mean error is 0.9% of an average capacity fade of 10.1%, which is large, but it covers two different cell chemistries. Suggesting that the trend noted is representative of commercial cells generally. Lower -rates of charge are better for cell lifetime, this conclusion is consistent with literature and current practice of charging at C-rates of less than one [161].

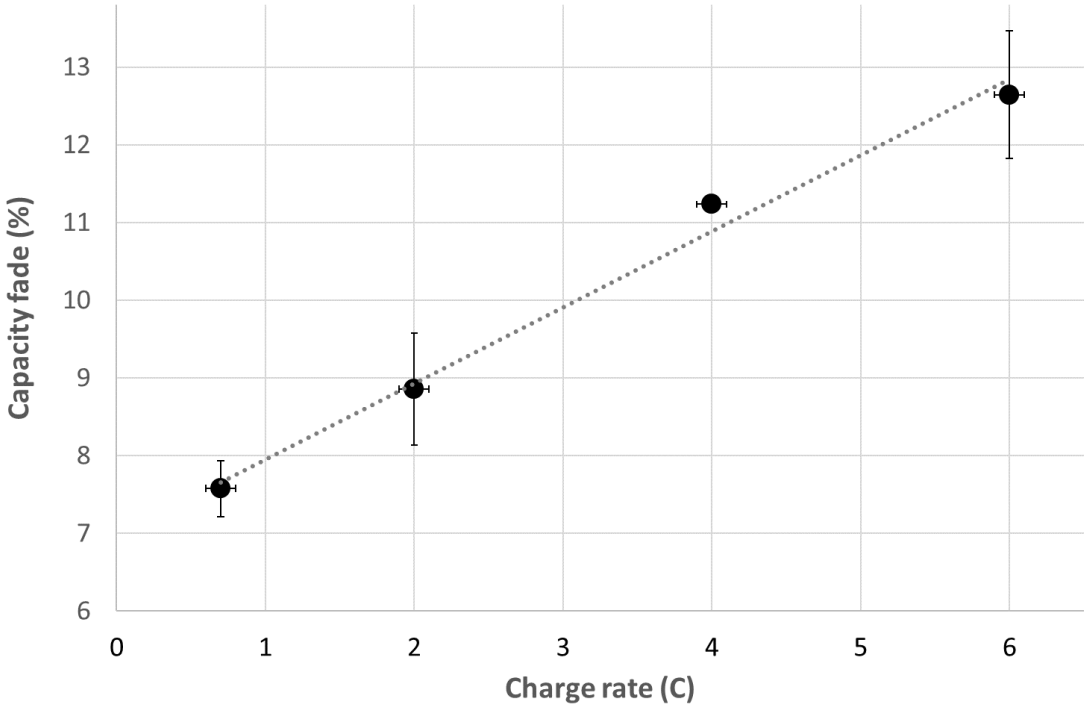

Figure 16. Impact of charging rate on cell capacity, a linear trend line has been applied to the data points with an R^2 value of 99.6%

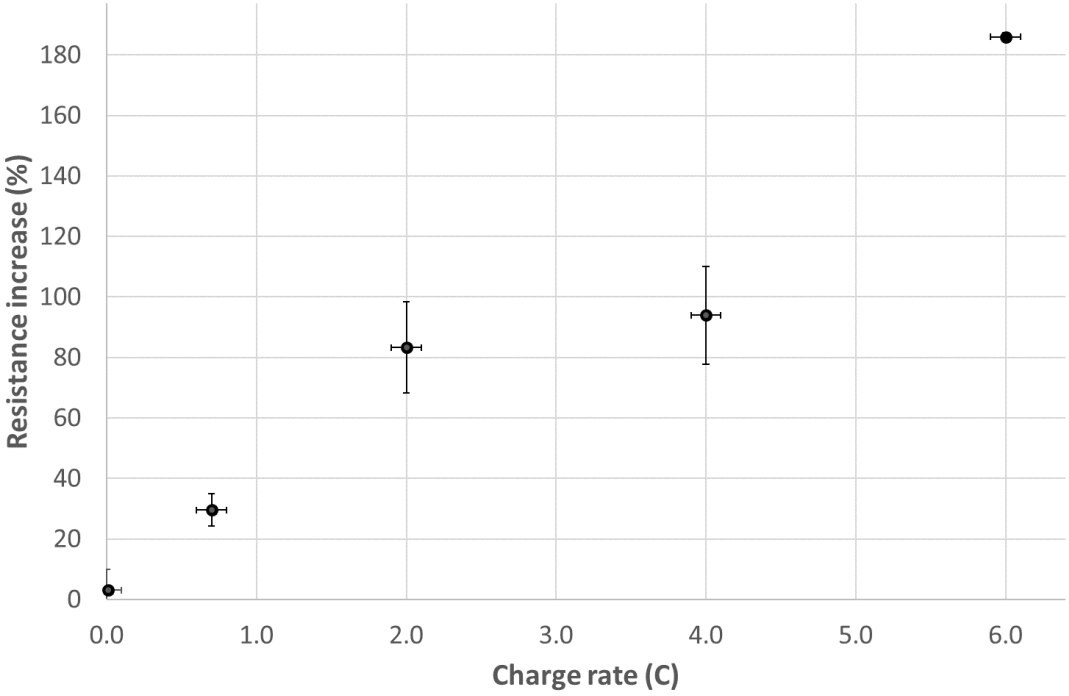

Figure 17. Impact of charging rate on cell resistance

Resistance does not follow the same trend as capacity. There is an initial resistance increase from 0-2C, which appears linear. A plateau from 2-4C, and then a sharp increase from 4-6C. This trend suggests that at least two competing mechanisms are occurring; one from 0-2C and one from 4-6C, however from electrical data alone this is not conclusive.

5.5. Percentage change in State of charge

Using the USABC testing profile, originally generated for testing Ni-MH chemistries, for comparison of a percentage change in state of charge, cells were charged from 0 to 40% SoC at C/3 and then between 40 and 80% SoC at different fast-charge rates, and then from 80-100% SoC at C/3. Cells were then discharged at C/3 to 2.5V at which point the cycle began again. These results were then compared to the cells cycled between 0 and 100% SoC at different C-rates from the previous section. The impact of percentage change in SoC on cell capacity and resistance is shown in Figures 18 and 19 respectively. More information on the charge cycle used and further interpretation of this data is also included in the work of Prezas *et al.* [162].

An increase in the % Δ SoC increases the capacity fade from just over 1% when cycled between 40 and 80% SoC to almost 13% at 100% SoC. Lower C-rates of charge are better for cell lifetime irrespective of the % Δ SoC. This conclusion is consistent with literature and current practice of charging at faster rates within less of the cell voltage window [161].

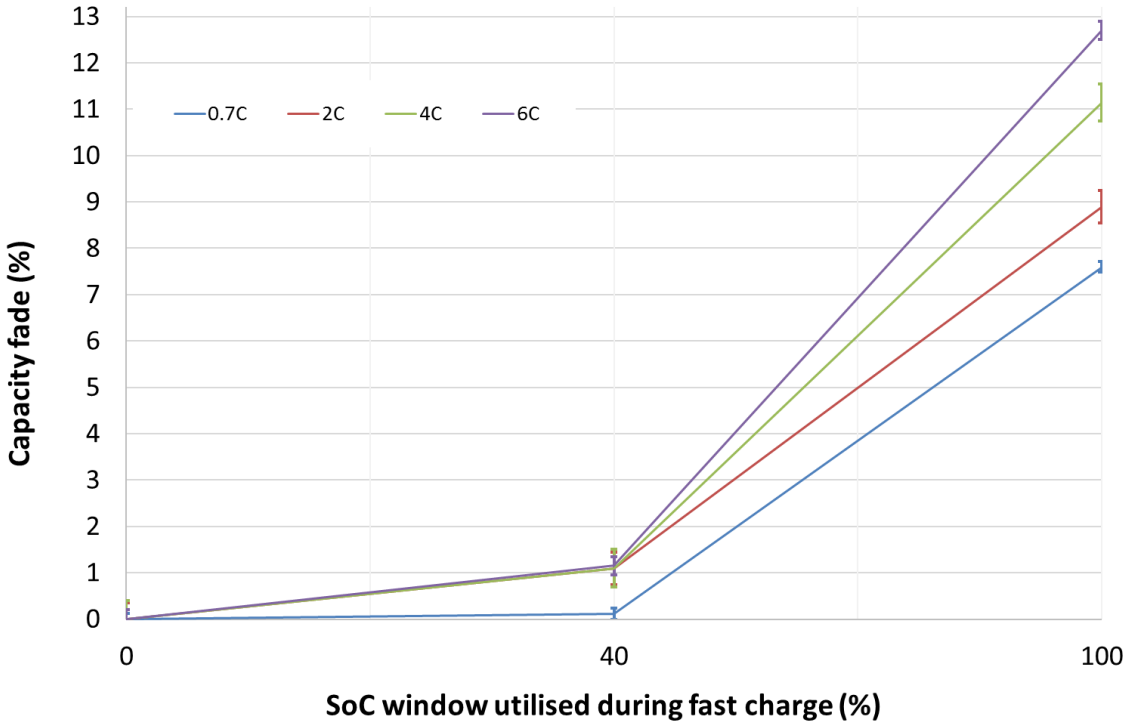

Figure 18. Impact of 'percentage change in state of charge' on cell capacity

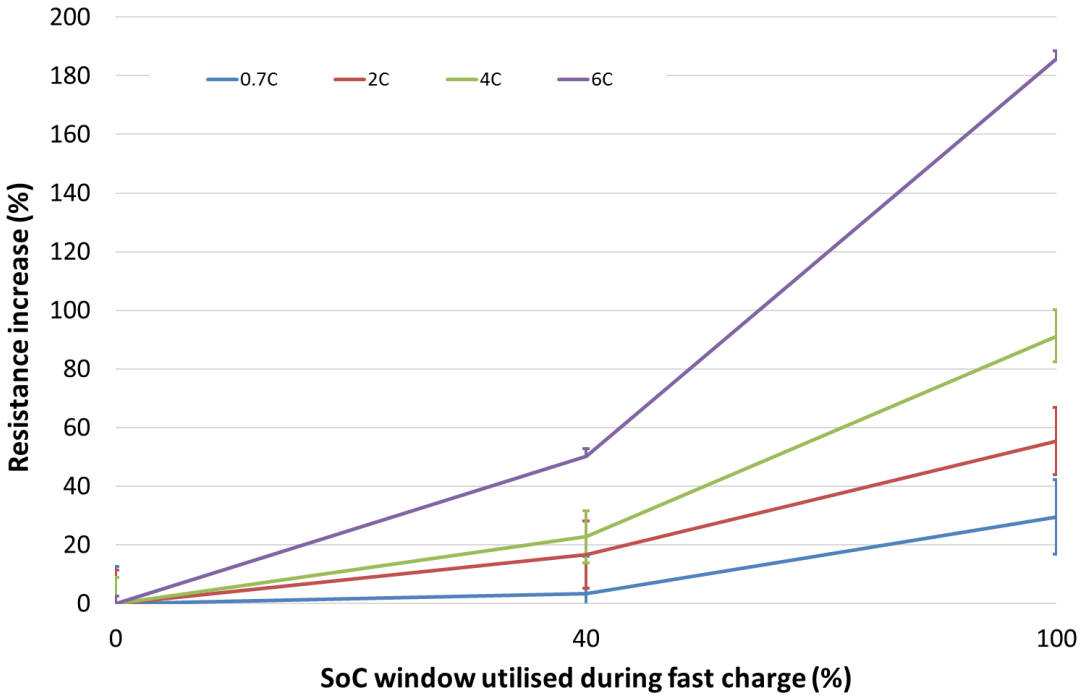

Figure 19. Impact of 'percentage change in state of charge' on cell resistance

5.6. Vibration

Cells were subjected to vibration (10 year accelerated profile) and non-vibration protocols to measure its impact over a prolonged period of time. The impact of vibration on cell capacity and resistance is summarised in Figure 20. Although the purpose of this work is not to explain why specific vibration profiles were used a brief overview is provided below for completeness.

A single axis electromagnetic shaker table was used to vibrate cells across three axes (x, y and z), the principal direction of vibration was differentiated by mounting the cells in different positions on the same table. The cells were mounted on aluminium blocks to limit undesirable fixture resonances caused by low specific stiffness. The actual vibration profile was the international standard test SAE J2380, which represents 100,000 miles driven across North America. The choice of vibration profile and test setup is explained further in the work of Hooper *et al.* [57].

Exposing a cell to vibration almost doubles the mean capacity loss, however, the error is large, s.d. 2.1% (not included on the graph because it is greater than the total axes length). This variation in capacity is well within the expected error of cells that have only been stored. Therefore, vibration has no impact on the capacity of lithium-ion cells.

This is not the case for the change in resistance. The resistance increased, and is more than 27 times higher after being vibrated when compared to the non-vibrated (control) cells. This shows that vibration does have an impact on resistance of the cells.

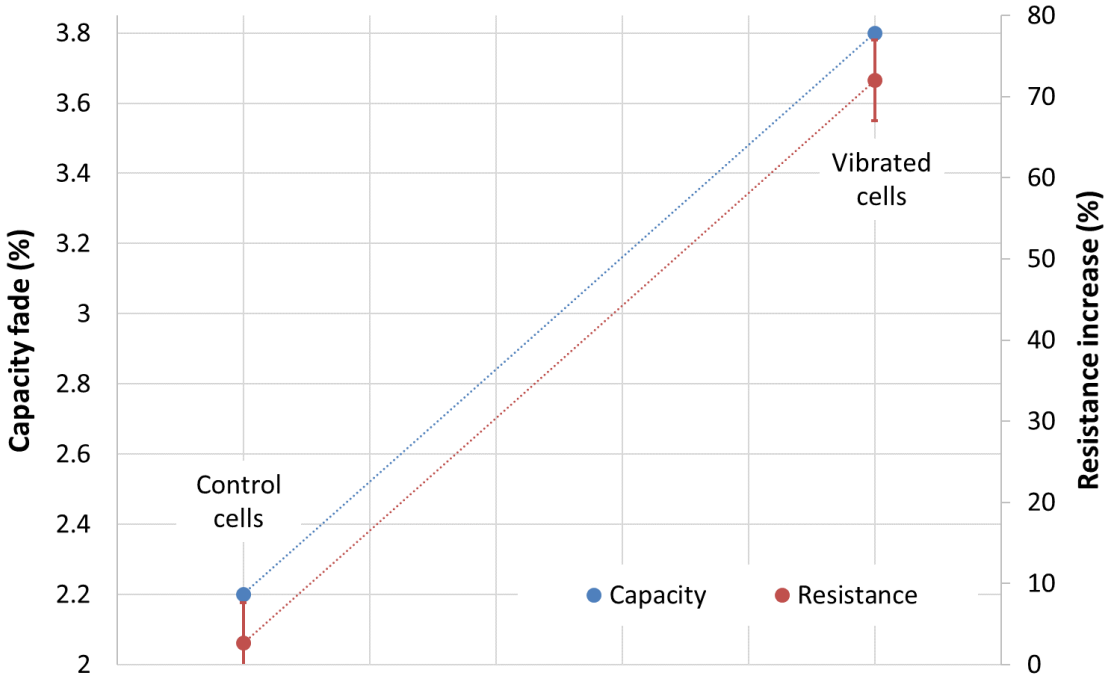

Figure 20. Impact of vibration on cell resistance and capacity

5.7. Pressure

Cells were stored for 633 days at a continuous pressure of either 0, 15 or 30 psi. The study was comprised of nine cells with three cells for each pressure. The impact of pressure on cell capacity and resistance is shown in Figure 21.

The capacity fade of cells increased from 2.4 % at 0 psi to 5.1% at 30 psi. This equates to a difference in capacity of 2.7%. With the error comparatively low for these samples it shows there may be a correlation between capacity and the pressure that is applied during storage. However, compared to the error inherent within the dataset, this error is still fairly low and would not be likely to contribute much to overall cell degradation. Therefore, pressure has no impact on capacity or resistance of lithium-ion cells.

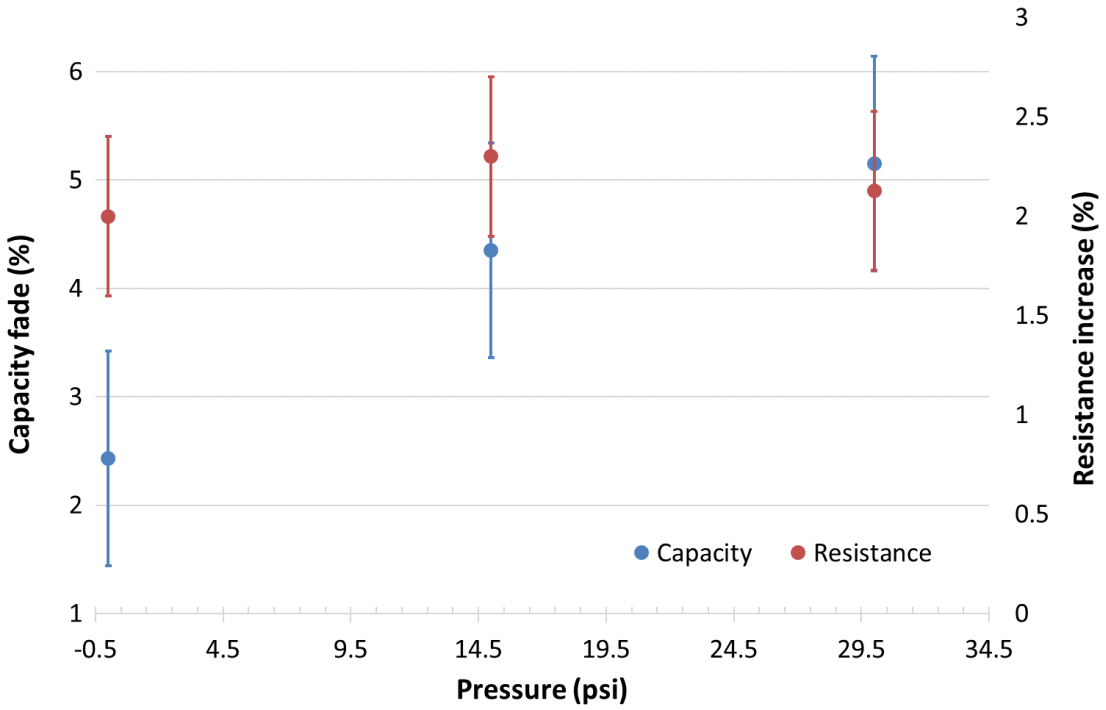

Figure 21. Impact of pressure on cell resistance and capacity

5.8. Orientation

Cells were stored for 633 days in a continuous orientation of either laying horizontally, being suspended with top cap facing downward (inverted) or with the top cap facing upward. The impact of orientation on cell capacity and resistance of cylindrical cells is shown in Figure 22.

The resistance increase of the cells varied from 1.8% whilst inverted to 3.3% whilst horizontal. However, the tests were conducted over a period of 20 months and this resistance increase over that period is negligible, compared to temperature tests and has comparable values with other cells. Therefore, orientation had no effect on either capacity or resistance and the slight downward trend in resistance is a consequence of natural variation. This work is consistent with the statement by Yardney© that orientation has no impact [163].

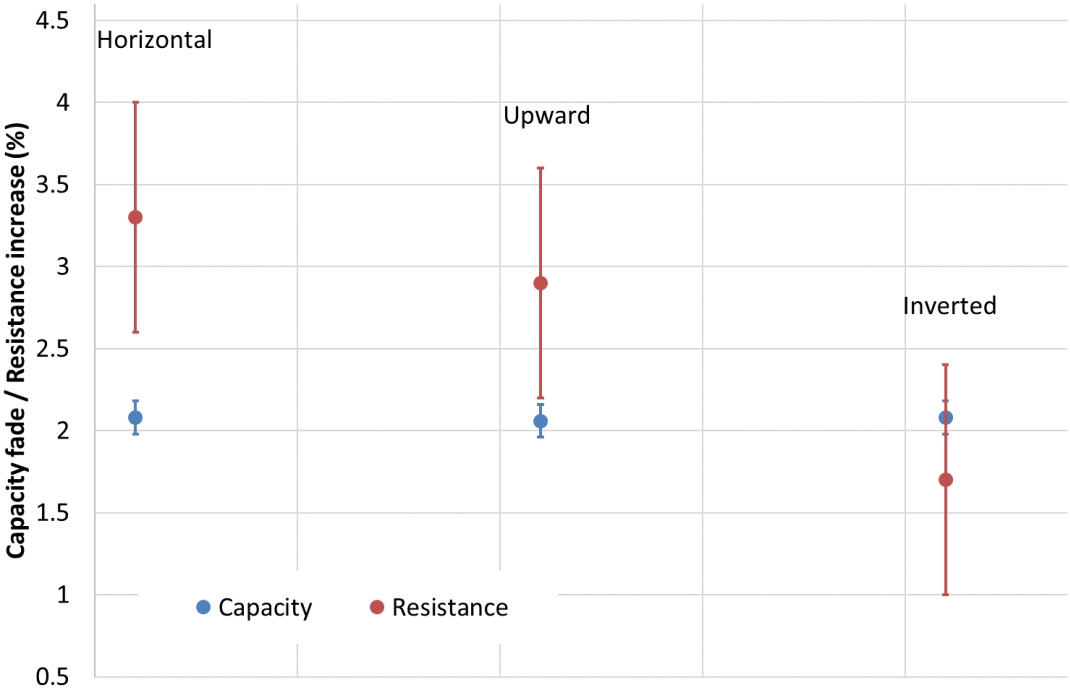

Figure 22. Impact of orientation on cell resistance and capacity

5.9. Discussion and conclusions

A study was undertaken including multiple institutions over years, culminating in thousands of testing hours. The electrical performance of each of the causes that impact lifetime was studied individually.

Table 4 shows the range in both capacity and resistance values for all the tested conditions. It shows that the upper limit in the range of both external cell pressure and orientation were consistently within the lower bracket of percentage from other causes. For example, the highest capacity and resistance values for orientation and pressure are within the error range of the larger temperature / SoC dataset for the time period. Therefore, neither external pressure nor orientation impacts the lifetime of lithium-ion cells because the degradation that did occur is within the expected values of cells stored for that same time and temperature.

This work shows that capacity is only impacted for changes in temperature, current rate and SoC. Vibration and % Δ SoC had no impact on capacity fade within the cells. The resistance of lithium-ion cells is affected by temperature, SoC, current rate, vibration and % Δ SoC. The condition that had the highest impact on the resistance was increased charge rates, temperature and then SoC. The smaller % Δ SoC condition was subjected to additional energy throughput in accordance with the USABC testing requirements, this may have added additional damage to the cells, but this was not obvious from the electrical data alone.

Table 4. Percentage changes in capacity and resistance for cells cycled under different conditions, colour indicates those values that are too low to relate to ageing (red) and high enough to suggest changes in cell conditions are responsible (green) values.

Cause	Capacity range (%)	Resistance range (%)
Temp. SoC	7-10	10-45
Current rate	7-13	20-180
% Δ SoC	0.2-1.2	5-45
Vibration	2.2-3.6	3-73
Orientation	2-5	2-2
Pressure	2.1-2.1	1.7-3.3

Electrical data collected on each of these seven usage conditions shows that the only causes of concern are temperature, SoC, % Δ SoC, current rate and vibration; it excludes the cases of cell orientation and external pressure (Chapter three). Although SoC, current rate, temperature and % Δ SoC were known as lifetime affecting factors, vibration was unknown; its impact on cell performance was dominated by a resistance increase.

The purpose of this testing regime was to isolate, as much as possible, each testing condition from the other causes of cell degradation. For this reason, the cells that underwent vibration, orientation, pressure, temperature and state of charge were not subjected to any charging or discharging. In contrast, the current rate and % Δ SoC were subjected to cycling conditions. In each instance, the additional conditions they were subjected to normalised as many of the other causal behaviours as possible, for example temperature was maintained at 25^{o}C, there was no vibration or imposed pressure.

The test method also accounted for in-use vehicle conditions. In the case of temperature and state of charge the test method utilised a matrix of conditions, to account for 10^{o}C through to

45°C and 20-80% SoC which are the conditions a traditional vehicle would experience during its lifetime. As mentioned previously, the vibration testing was designed as representative of an entire vehicle's vibration loading profile. This was also true for the selection of pressures and current rates.

The limitations within this dataset of electrical characterisation assumes that the electrical testing has been performed correctly and is comparable between institutions. No analysis has been performed within this work to ensure that the electrical testing was performed correctly. The potential implications of this assumption are shown by Barai [164] who states that the cell capacity measured can vary by as much as 5% just dependent on the length of the intermediary rest period between testing cycles. A variation of this much would call into question the entire capacity fade difference for temperature, SoC and current rate. However, the electrical data in this work is in general agreement with established trends within the literature for temperature and SoC [165], current rate [166] and % Δ SoC [91]. Therefore, it is reasonable to assume that the electrical values attributed to ageing are accurate and that the new values obtained for vibration, orientation and external pressure are also.

What this work did not do is perform further analysis with electrical impedance spectroscopy (EIS) and other non-destructive electrical techniques. Its absence is best explained by the work of Barai who shows that the time (up to 4 hours) between the removal of the electrical load and the impedance measurement impacts the results obtained [167]. Orazem and Tribollet also show that EIS is very sensitive and adjusting equipment, as well as model parameters and a myriad of other equipment components can significantly impact the results obtained [168]. Ultimately, EIS is a useful technique, as shown by numerous examples who performed analysis with EIS on temperature aged cells [165], to study lithium plating [169] and other ageing related phenomena [170]. However, equally, EIS analysis is difficult and the results obtained

are open to significant interpretation. There are many instances where previous interpretations have been proven incorrect [171], including within the battery community [172]. Therefore, due to these potential pit falls EIS results have not been included or studied within this work.

6. Preparation for post-mortem analysis

This chapter addresses objective two, which is:

Determine the post-mortem methods that allows connection between electrical performance data and material changes at the negative electrode. In order to partially achieve the second objective of this work two challenges need to be overcome, these are:

1. A method of opening 18650-type cylindrical cells without affecting the surface film
2. Understand the impact of rinsing electrodes on the surface film

This chapter addresses these two challenges by introducing a new method for opening 18650-type cells and contains a study on the impact of rinsing electrodes on the surface film. This chapter's position within this document as well as the wider portfolio is shown in Figure 23.

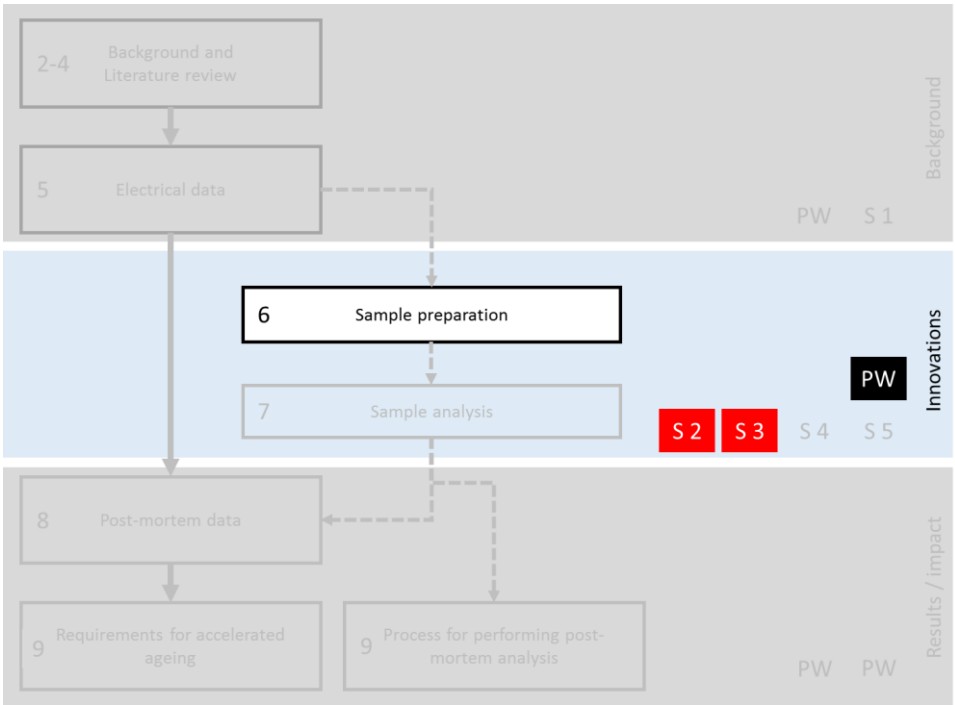

Figure 23. Outline of the engineering doctorate portfolio, chapters within this innovation report are shown as numbers to the left of white topic boxes. Red boxes labelled S1-5 represent the five portfolio submissions, the black PW boxes represent published work.

6.1. Cell opening

Figure 24 contains a chronological account of a new method to open 18650 cylindrical cells. It is different from the normal method in two ways. Firstly, it does not use a Dremel©, hacksaw or file to cut into the can but rather a pipe cutting tool; this eliminates the production of soot, steel and metal particles. Secondly, the can is not cut but rather peeled apart, like an orange, using pliers. This means that at no point does a cutting tool have to meet the active material jelly roll. The method used is:

1. The top of the 18650 cell was cut off with a pipe cutting tool (Figure 24, 1) above the electrode but below the top cap.
2. The top cap was removed (Figure 24, 2) by pulling directly away from the body of the can, while holding the cap with pliers.
3. The top crimped edge was peeled out and straightened. This causes the steel can to tear into small parts (Figure 24, 3).
4. The outer metal can was peeled apart in thin strips (Figure 24, 4 and 5).
5. The negative electrode tab welded to the bottom of the can was then separated from the outer steel casing completely by cutting the tab with ceramic scissors (Figure 24, 6).

Figure 24. Eight images chronologically mapping the opening of an 18650 cylindrical cell to remove the inner electrode roll

As shown in pictures 7 and 8 of Figure 24 the inner jelly roll was completely removed intact without the creation of dust or small metal particles. A total of 63 cells have been opened over

a period of two and a half years using this method, only one was short circuited (contact of pipe cutter with tab connecting the top cap) and created sparks. This can be avoided by placing insulating tape on the nose of the pliers. None of the cells opened with this method created any visible dust or other particulates.

Micrographs were collected and energy dispersive x-ray (EDAX) was performed on electrodes opened with and without the new method. Figure 25 contains these micrographs. Image a, which was opened with a Dremel© multi-saw. It has small white speckles that covered much of the electrode around the top and bottom of the jelly roll. Image b is from a cell opened with the new method and contains no white speckles and graphite particles appear more pristine. EDAX analysis shows that the white speckles contain high concentrations of carbon (45%) and oxygen (28%). EDAX also detected small concentrations (< 3%) of copper, manganese and iron that were only present in the cell opened with a Dremel© multi-saw.

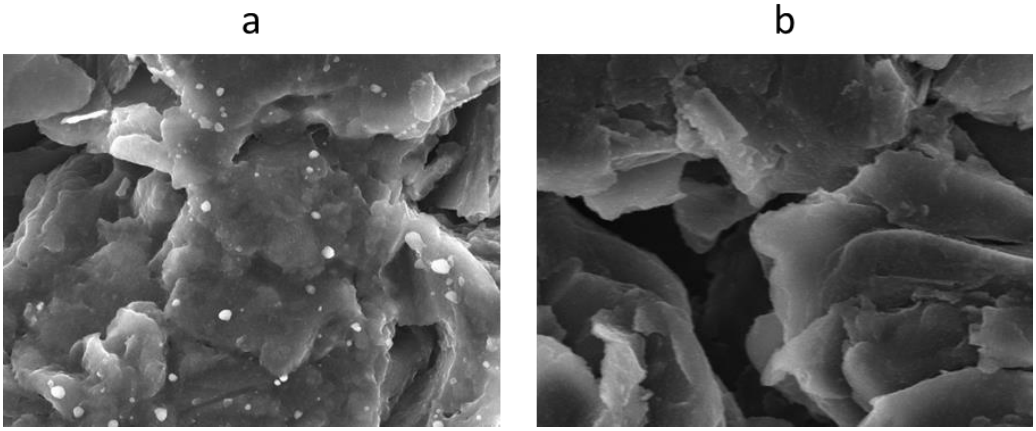

Figure 25. Micrographs of negative electrodes cut from the outside nearest the 18650-type cell can wall. Image a was opened with a dremel multi-saw whilst b was opened using the new method outlined in Figure 24.

6.1.1. Discussion

This work presents a solution to the problem of using rotating disc saws to open 18650-type cells through the use of a pipe-cutter and pliers. A study that shows the potentially negative impact of the rotating disc saw method is the work of Barrett et al. [173]. Their study investigated the presence of heavy metals for 50 non-rechargeable AA-type commercial cells. They opened each of the cells with a Dremel© tool and determined the concentration of various heavy metals present. They found vanadium, chromium, nickel, copper and a multitude of others. Some of them were at concentrations of less than one part per million (ppm). The problem is that many of these metals, such as vanadium [174], and nickel [175] are added to iron to improve the properties of steel. It is possible that when the steel outer casing of the AA-type can was cut, some of the steel found its way onto the samples and contaminated them – which contributed to their presence being detected. What is not known is the impact of such contamination on sensitive organic surface films in lithium-ion cells – in addition to the detection of their presence. Also, when the metal is cut the wheel and subsequent contaminating particles reach a temperature of at least a couple of hundred degrees Celsius [176]. It is well established that temperature changes the chemical composition of these surface films, and therefore, if surface film is analysed on an area where these particles have touched then they will not represent the in-use condition of the surface film. Therefore the new method presented in this work should be used instead.

6.1.2. Conclusion

The new method for opening 18650-type cells circumvents the problems associated with other methods of soot creation, short circuits and damage to the jelly roll. It makes it possible to trust the post-mortem results as indicative of the cells in-service conditions and circumvents a

significant source of error from surface film damage during cell opening. Further, it calls into question the results of any study that has opened cylindrical or other format cells with a Dremel© cutting tool and then makes conclusions based on analysis of the surface film's chemical composition. Due to the results of this work, this is now the only method used to open cylindrical cells for post-mortem analysis at Jaguar Land Rover, Argonne National Laboratory and WMG. It is proposed that all cylindrical cells be opened with this new method.

6.2. Sample preparation

This work investigates the impact of washing on electrode surface film. A foundational principle of this study was the use of real-world electrode materials (commercial cells) that had a known surface film composition. To do this the study uses vinylene carbonate (VC), which is known to preferentially react at the negative electrode surface and change the chemical composition of the surface film [177]. This study was performed using commercial 300 mAh, $LiCoO_2$/graphite pouch cells manufactured by Li-fun Technologies in China and shipped dry, with no electrolyte. Cells were then opened and electrolyte added, after which formation cycles were completed. The cells were manufactured with varying quantities of VC, these quantities were 0, 1, 2, 4 and 6 vol.% added to the electrolyte. After formation and preliminary cycles at rates of C/10 the cells were taken apart for post-mortem analysis. Electrode samples were cut from the same piece of electrode for each cell and then placed on sample evaporation dishes. Half were then bathed with 1.5 ml of DMC for one minute, and then left to dry for two minutes. The other half of the samples were not washed with DMC and remained in the evaporation dishes.

6.2.1. Results and discussion

Figure 26 contains micrographs of the negative electrode surface at each concentration of VC with and without washing. The micrographs presented are representative of the entire electrode surface. There are three distinct surface film environments present in the unwashed cells, these are those at 0 and 1% which appears like intertwined spider webs. A different film with a smoother appearance at 4-6% and the visual absence of a surface film at 2%. There is a film present, it just is not visible in this sample, because a surface film always forms at the electrode surface [93].

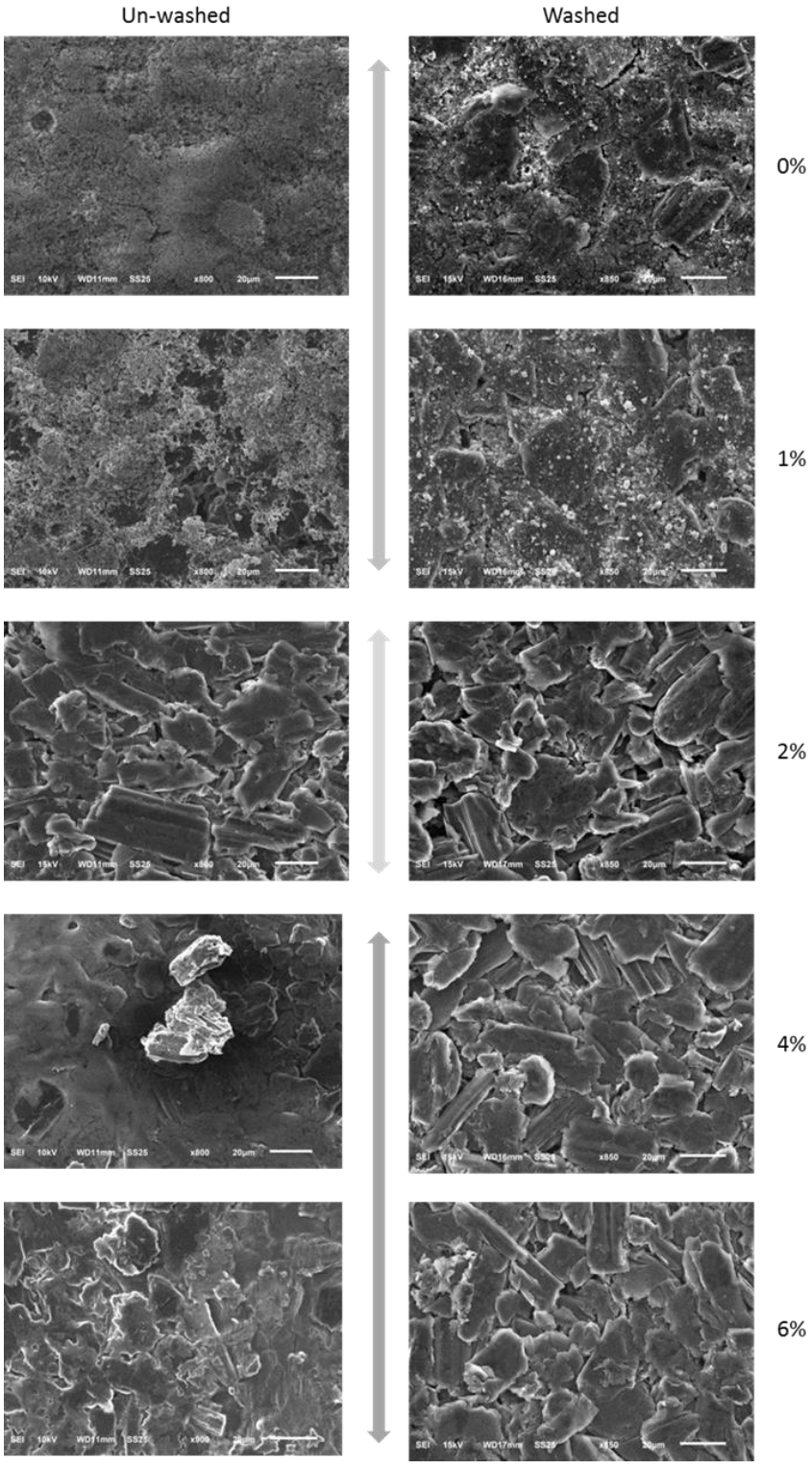

Figure 26. Micrographs of negative electrodes from cells containing varying concentrations (0-6 vol. %) of vinylene carbonate added to the electrolyte. Different arrows represent different appearances in the surface film of unwashed samples

The washed electrodes appear visually different to the unwashed electrodes. The spider web film at 0 and 1% has been completely changed by washing with the majority no longer present and graphite particles visible underneath. The film with a smooth appearance at 4 and 6% is also gone. The washed electrodes appear visually similar to normal graphite (2% washed and unwashed). If washing only removed salt and solvent then the film, which is visually different (and thus cannot be salt or solvent because this is identical) in different cells would not be affected.

The electrodes were also tested with IR. IR is used for the determination of organic (containing carbon) functional groups. It has two main regions; these are above 1500 cm^{-1} for vibrational frequencies indicative of chemical functional groups. And, below 1500 cm^{-1} which is indicative of a region called the fingerprint region. Although stretches in the fingerprint region are caused by specific functional groups the actual wavelength is significantly shifted by the environment and therefore is often only used as a 'fingerprint' to determine if two samples are identical. If the peak wavelengths and breadth are identical it is almost certain that the two compounds are the same [178].

N.B. more information on the theory and application of IR is available in Chapter Two, Section Five of Submission Three within this portfolio.

Figure 27 is an infra-red spectra of graphite across five concentrations of VC additive for both washed and unwashed electrodes. The first thing to note is that the unwashed electrodes have multiple troughs (stretches) whereas the corresponding washed electrodes do not. Washing has removed something from the surface of the electrode. However, the argument for using washing is to remove electrolyte salts, solvent and deposits. Therefore, the next step is to determine if this is what contributes to these stretches in the IR spectra.

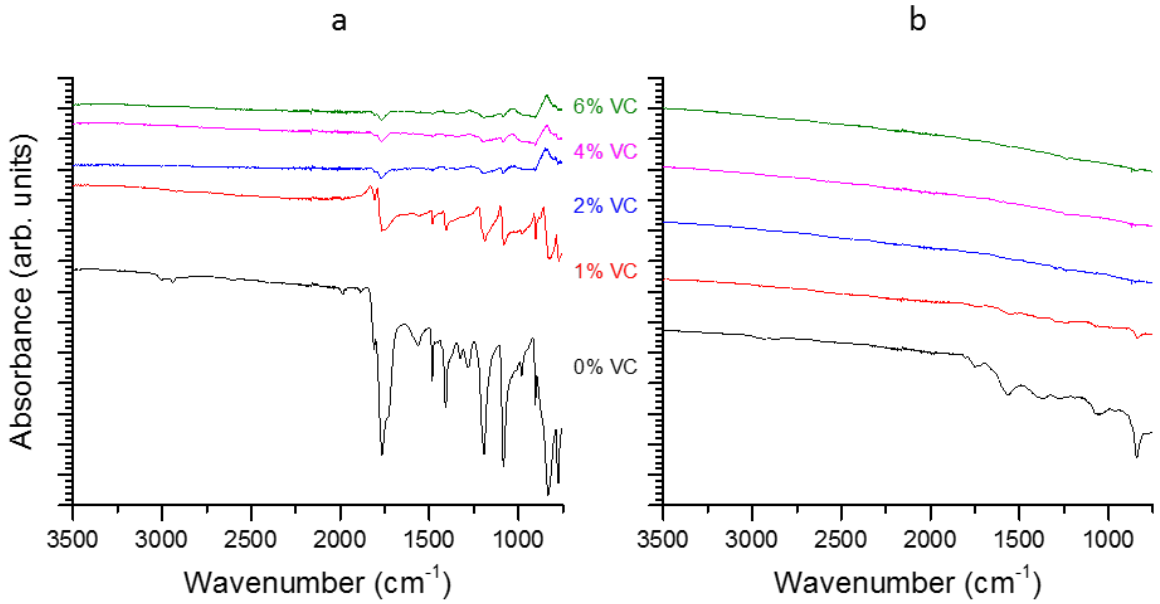

Figure 27. ATR-FTIR spectra of graphite electrodes with varying volume percentages of vinylene carbonate (VC) additive. The unwashed and washed IR spectra are shown in a and b, respectively.

The salt in these cells is $LiPF_6$, the P-F normally resonates within the fingerprint region at approximately 740 cm^{-1} [179]. Because this is not a pure sample it is not possible to definitively identify it because its wavelength will be shifted. However, there is an absorbance at 750cm^{-1} and therefore know it is present before washing and is possibly present, but reduced in intensity, after.

The high boiling point organic solvent (EC) has C-H and C=O functional groups which peak at around 2950-2990 cm^{-1} and 1750-1780 cm^{-1} respectively [178]. The solvent is only present if both of these two troughs are there. There is a triplet of troughs at 2970 cm^{-1} (C-H), but it is only present for the unwashed 0% VC electrode. The larger peak, present at all concentrations of the unwashed electrodes, occurs at 1770 cm^{-1} (C=O). The electrode from the cell containing 0% VC has the largest intensity for this peak and it reduces until 2% at which point it plateaus until 6%. Whilst the fingerprint region is similar across all concentrations, it is not identical,

and therefore this is represented as a single entity and is not used for identification. The intensity of stretches within this finger print region reduces as VC percentage increases. For the washed electrodes there are no discernible troughs for any concentration except 0% and even this is significantly reduced and broadened. Reduced intensity is caused by reduction in detected material whereas broadening suggests diversification in the energy of ground electronic states (changes in environment for the same functional group). Because Figure 27 does not have troughs at 2950-2990 cm^{-1} and 1750-1780 cm^{-1} it means that EC is not present at detectable concentrations of 1% VC and greater but may be present at 0% VC. This means that washing is not required to remove EC for the 1-6% sample.

It is possible to verify the presence of EC in the 0% VC sample by comparing the IR spectra of the 0% VC sample and pure EC (Figure 28). The two spectra look similar although not identical, EC could be present in the 0% VC sample but it is not the only chemical present, because there are absorbance present in the 0% VC sample (e.g. doublet of troughs at ~1300cm^{-1}) that are not present in the EC. This doublet of troughs is also removed by washing (Figure 28).

In summary, EC is definitely not present for the 1-6% VC cells and may be present for the 0% VC, but it is not the only chemical environment present. Chemical changes have occurred due to washing and this change is more than just removal of electrolyte salt and solvent.

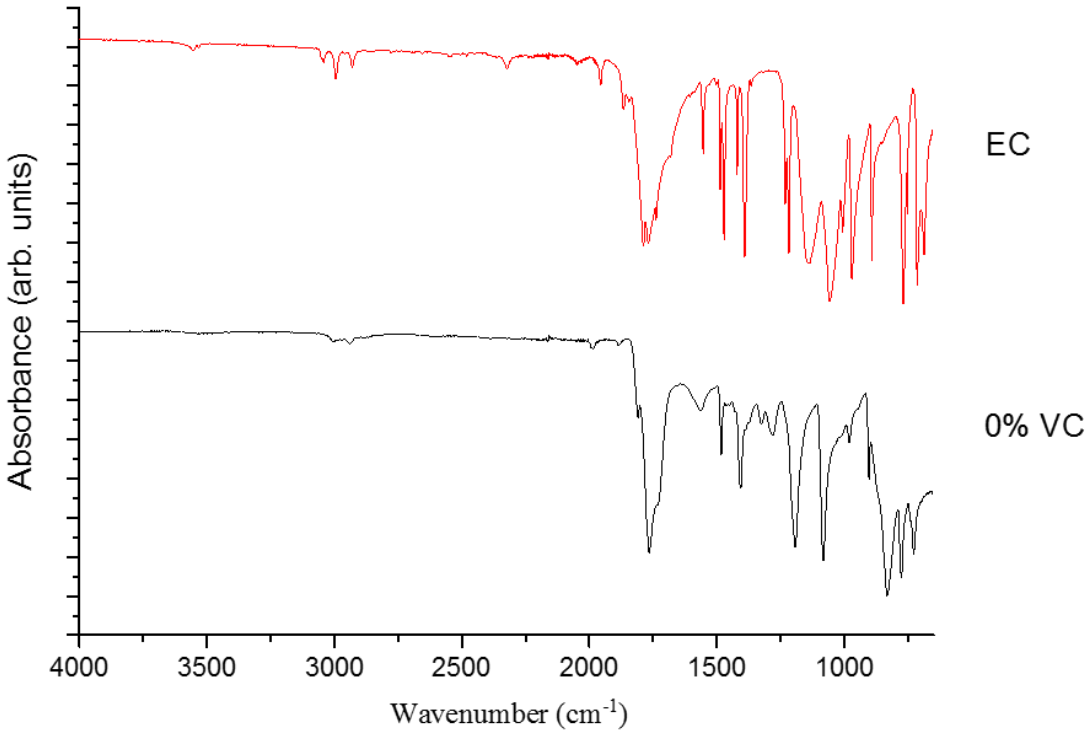

Figure 28. ATR-FTIR spectra of ethylene carbonate (EC) and a graphite electrode sample from a lithium-ion cell with no vinylene carbonate (VC) added to the electrolyte.

The conclusion that EC is not present in the unwashed samples is surprising because it was added to the cell and has not been knowingly removed prior to washing. Its absence can be explained by its vaporisation point dependence on pressure. Figure 29 contains a plot of data points from Chernyak et al. research on the vaporisation point of high boiling point solvents [180]. It shows that the effective vaporisation point of EC reduces with pressure. Using a logarithmic plot (R^2 > 99%) of the data equation (9) was obtained. Inserting two pressures, atmosphere (100kPa) to test the validity of the equation and a vacuum system ($1.3x10^{-6}$ kPa) it is possible to obtain (10) and (11) respectively. An XPS system is closer to (12) ($1.3x10^{-8}$ kPa).

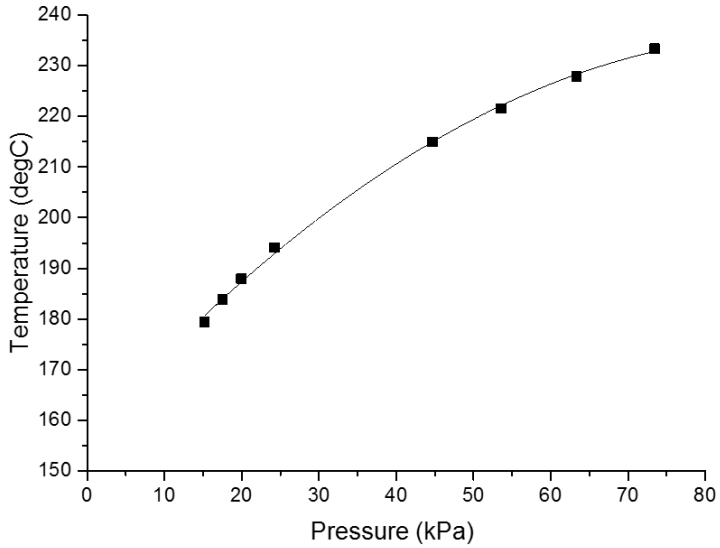

Figure 29. Plot of temperature (T) vs pressure (P) for ethylene carbonate vaporisation, data taken from Chernyak et al. work.

Using (9), the boiling point of EC at ambient pressure would be 244.7^{o}C; lower than the actual boiling point by 6%. The theoretical vaporisation point of ethylene carbonate under vacuum very quickly reduces (11), at XPS pressures it falls even further (12). Therefore, the pressures a typical sample sees for SEM or XPS analysis are orders of magnitude lower than required to completely vaporise EC from the sample surface. At the pressure and exposure time expected for XPS or SEM analysis; washing of electrodes to remove electrolyte solvents is unnecessary because the solvent will evaporate without it. To validate this conclusion, EC was ground with a pestle and mortar into a fine powder and placed it into a vacuum, after 30 minutes at $1x10^{-4}$ kPa it was no longer visible. This means that whatever is removed by washing (difference between a and b in Figure 27) is either surface film or surface film creation deposits.

Temperature = 34.481 x ln(Pressure) + 85.86 (9)

244.7 = 34.481 x ln(100) + 85.86 (10)

-381.5 = 34.481 x ln($1.3x10^{-6}$) + 85.86 (11)

-540.3 = 34.481 x ln($1.3x10^{-8}$) + 85.86 (12)

Although IR refutes the idea that washing is required to remove EC, and that it may reduce the quantity of salt, it does not address what is being removed, as shown in the micrographs (Figure 26).

To do this XPS analysis of washed and unwashed electrodes before and after sputtering was performed. Figure 30 shows the F 1s spectra obtained. F 1s was chosen because it represents the salt components and its absence or presence will indicate the effect of washing at removing salt. The other spectra are available in the published work of Somerville et al. [134]. There was one chemical environment which was present for both washed and unwashed electrodes; this was found at ~685 eV. For the washed electrodes this single peak was present both before and after sputtering and remains at the same binding energy with the same peak width. For the unwashed electrode there were two additional F chemical environments present, they were found at ~686 and 688 eV respectively. Prior to sputtering, the peak at 685 eV was most dominant, after sputtering the peak at 686 eV increased and the 685 eV peak decreased. The peak at 688 eV remained constant before and after sputtering.

According to the work of Ensling et al. [130] $LiPF_6$ salt in lithium-ion cells exhibits at two F 1s binding energies, $LiPF_6$ at 688 eV and Li_xPF_y at 687-688 eV. The surface film component

LiF at 685.5 eV. From these results Figure 30 shows that the unwashed electrode contains all three F environments. Once the bulk of the electrode material is reached by sputtering, the concentration of the Li_xPF_y component decreases and the LiF component increases. This occurs because the salt, which was suspended in the electrolyte before evaporation, deposits onto the surface and covers the surface film at its highest concentrations. When the sample is sputtered the deposited salt is removed and the bulk of the electrode is reached, this bulk contains a more representative mix of salt to electrolyte, as expected for the in-use cell conditions, and the percentage of surface film (measured as LiF) increases.

On the other hand, the washed sample, both before and after sputtering, contains no $LiPF_6$ component or LiF component and only Li_xPF_y. Tasaki et al. [181] performed a study on the solubility of salts found in typical surface films. In their work, graphite electrodes were soaked in DMC for upwards of an hour. They found that LiF salts were removed almost entirely from the electrode. The results presented here support this study but show that after washing for only two minutes DMC completely solvated at least LiF from the electrode.

The purpose of electrode washing, as cited within literature, is to remove the electrolyte solvents and salt [182]. This work discovered that washing was directly impacting the electrode surface film by removing some components and altering others. It also shows that it is not necessary to wash to remove the higher boiling point solvents, because these can be removed by exposure to low pressures. However, following on from the basic assumption of post-mortem analysis that the material being analysed is the same during post-mortem analysis as it is within the cell, washing cannot fulfil this requirement and therefore should not be used when analysis of the surface film is to be performed.

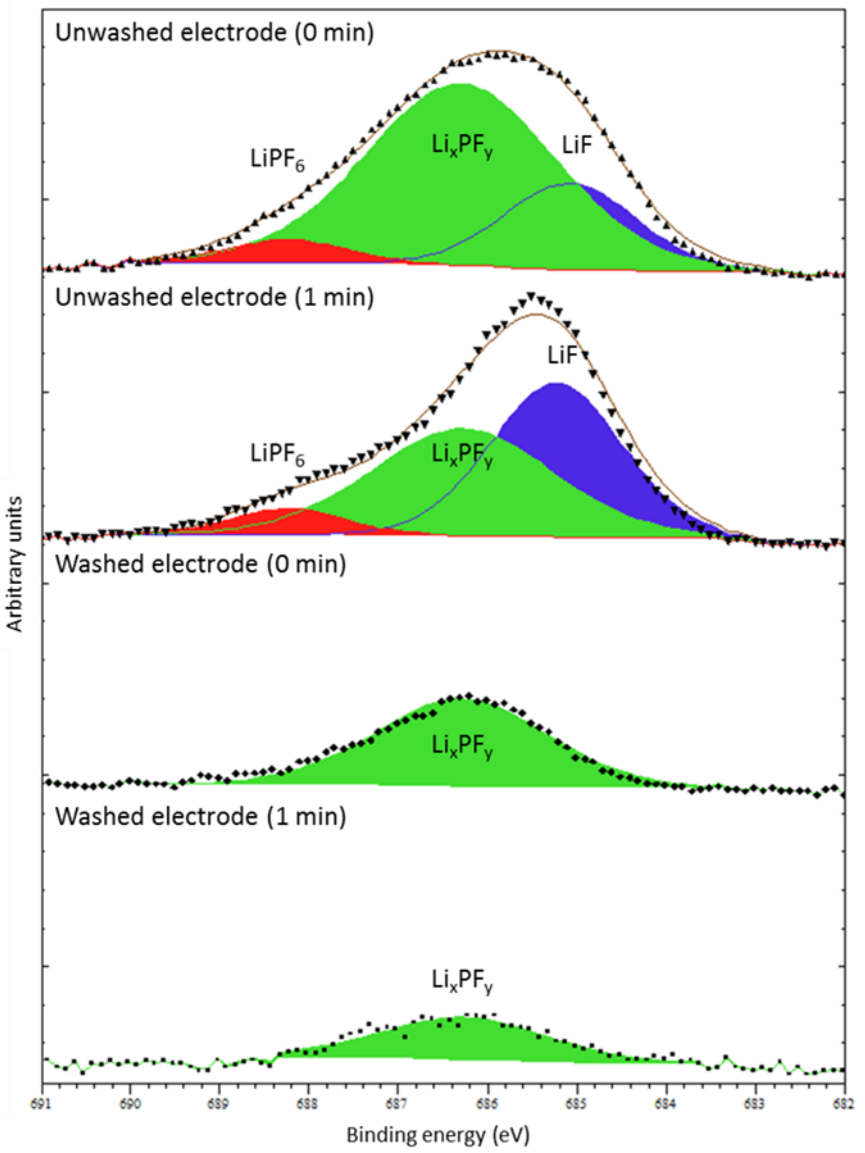

Figure 30. XPS of binding energy for F1s core electrons of both washed (with DMC) and unwashed samples. 0 min represents un-sputtered electrodes whereas 1 min represents the sample after sputtering with Ar^+ Ions for one minute.

6.3. Conclusions

There is no advantage to be gained in performing complicated, expensive, time consuming and delicate analysis of lithium-ion electrode surface films to study ageing mechanisms if the films, as studied, are significantly altered from their original nature during sample preparation. A study into how the processes may impact electrode surface films for each case is critical.

In general, opening pouch cells and gaining access to electrodes is simple and universally adhered to. Cylindrical cells are much more difficult and current practices using rotating saws creates dust, causes short circuits and contaminates the electrode surface. A new method that circumvents all of these problems was created. This allows electrodes to be extracted from cylindrical cells more easily and keeping the jelly roll intact.

Once electrodes are removed from the cell outer casing they are routinely washed to remove salt and solvent components. This process removes surface film, and especially impacted LiF concentration by solvation from throughout the electrode medium. The impact of this on results is that any subsequent analysis is tainted by preferential solvation. Or, more plainly, washing removes the compounds of interest.

It is suggested that cells should not be opened with rotating disc saws, but with the new method instead. And electrode samples should not be washed if study of the surface film is to be performed.

7. Analysis of surface film

The purpose of this chapter is to address challenges 3-5 in meeting objective two. These challenges are:

3. A process of studying the surface film composition separate from the electrolyte deposits
4. A process is required to determine the thickness of the electrode surface film
5. A process is required to stop $LiPF_6$ from affecting the chemical composition of the surface film in preparation for HPLC analysis

Its position within this document and the doctorate portfolio is shown in Figure 31.

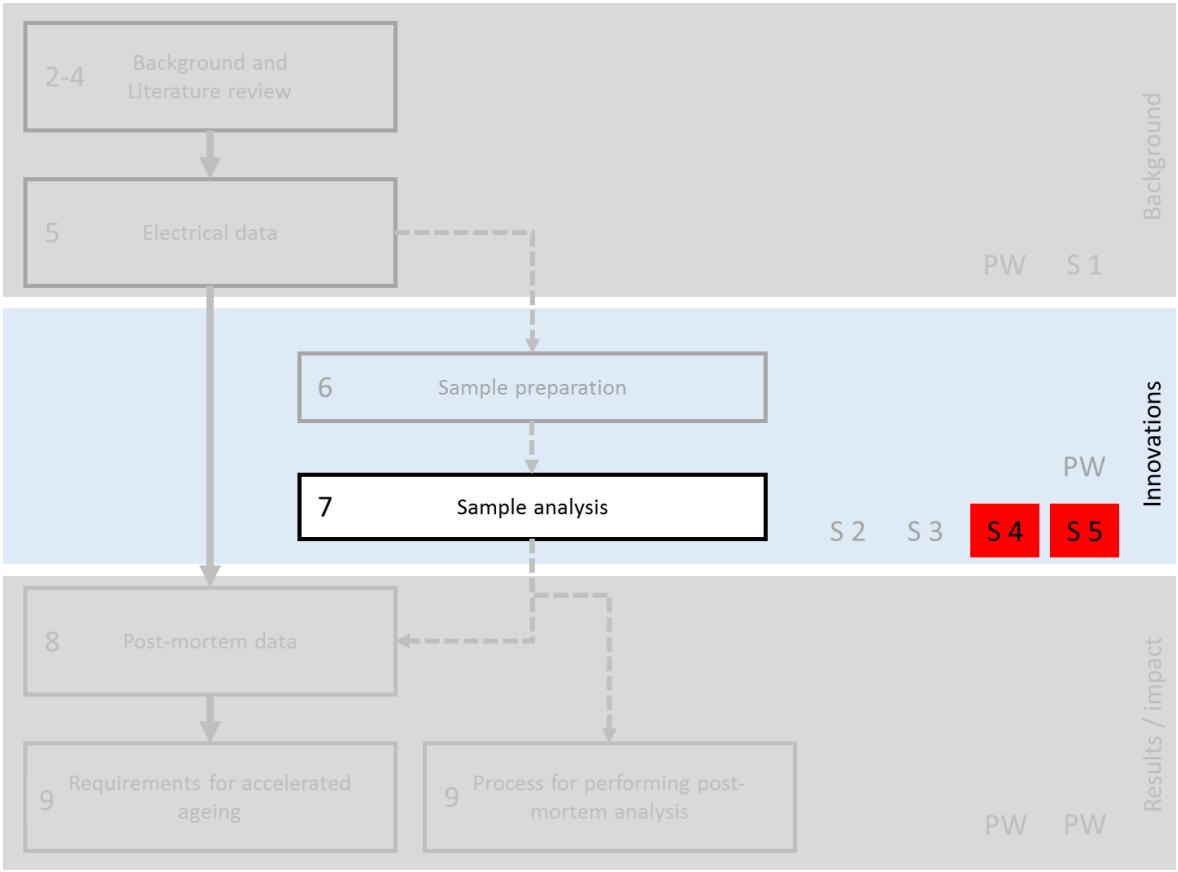

Figure 31. Outline of the engineering doctorate portfolio, chapters within this innovation report are shown as numbers to the left of white topic boxes. Red boxes labelled S1-5 represent the five portfolio submissions, the black PW boxes represent published work.

7.1. XPS analysis for differentiating between surface film and electrolyte deposits and for measuring surface film thickness

This section introduces the hypothesis for a novel method of determining surface film thickness and investigating the surface film separate from the electrolyte deposits with XPS. The application of this method is shown in chapter eight of this document.

N.B. This hypothesis relies on an understanding of fundamental XPS theory which is included in Chapters 1-5 of Submission Five within this portfolio.

7.1.1. Hypotheses

Figure 32 is a graphical representation of the electrode surface after it has been sputtered. It shows that in order to differentiate between the sample and the electrolyte deposits – which were on top - it is possible to sputter the sample instead of washing it. This means that the sample can be investigated with XPS before sputtering (with higher concentrations of deposits) and after sputtering to differentiate between electrolyte deposits (before sputtering – on top) and surface film (after sputtering - underneath). This suggests a method of how to differentiate between surface film and electrolyte deposits without washing electrodes.

Figure 32 also identifies that surface film does not form on 'electrodes' but rather on individual particles. It shows the impact that sputtering has in changing the chemical species identifiable with XPS (inset a) and to the material composition itself (inset b). The particles underneath the white box show how the surface deposits can be removed to reveal a lower concentration of these constituents without removing surface film completely. The significance of this is that surface film surrounds the individual particles. When sputtering occurs, it will sputter the different chemicals present at different rates. At some point, the rate of sputtering will reach a steady state, a point of equilibrium, where the quantity of material sputtered is equivalent for

all chemicals. This is because the materials with the lowest sputter yield will shield the particles with the highest sputter yield. Once this steady-state is reached it is then theoretically possible to detect variances within the surface film thickness by equating the concentration of surface film of cell a to b by the concentration of non-graphite carbon compared to graphite carbon. If the surface film of one electrode is thicker than another, then the concentration of the non-graphite carbon will increase.

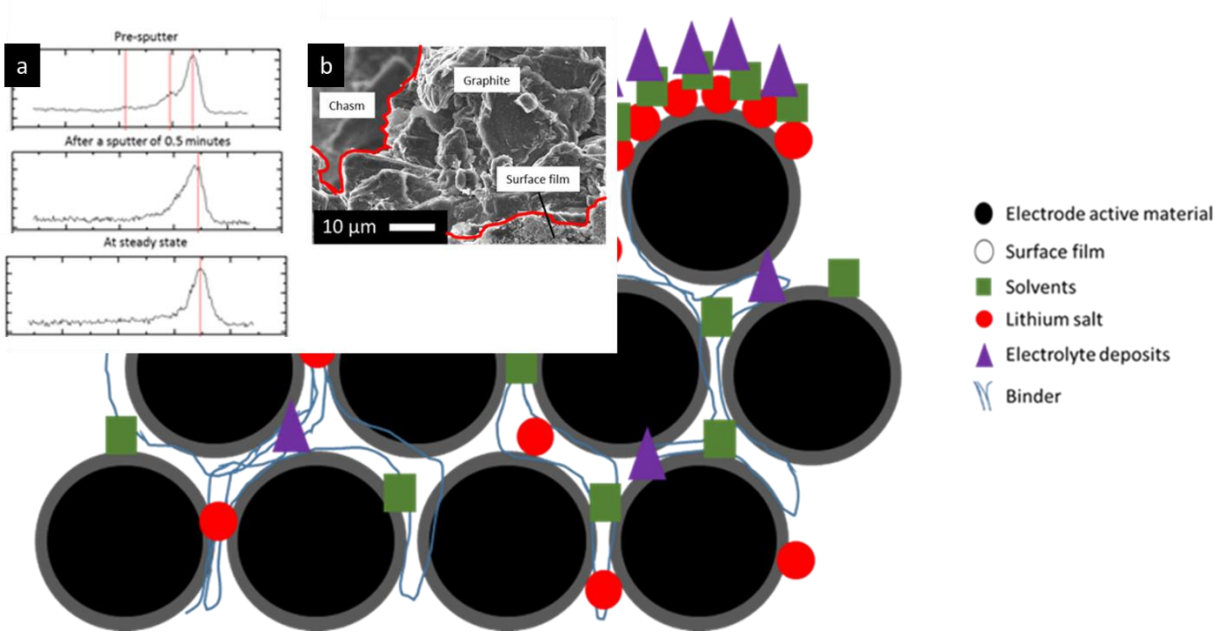

Figure 32. Impact of sputtering on a negative graphite electrode from a lithium-ion cell. The un-sputtered electrode is shown to the far right of the main image, whilst the impact of sputtering is represented by the removal of the surface solvents, salts and surface film. The impact of sputtering is shown at a material level by the XPS spectra-inset a, and the micrograph-inset b.

7.1.2. Discussion

The ability to determine the surface film thickness using XPS analysis is attractive. Not only is XPS extremely useful for studying the surface films chemical composition, its use for thickness calculations would reduce the total number of analytical techniques required.

However, the method currently employed within literature uses a sputter-depth profile method which is not suitable for lithium-ion negative electrode surface film analysis [139]. This calls

into question the results obtained. The method proposed within this work is able to overcome this problem by sputtering to a steady-state and then comparing the percentage of graphite environments to non-graphite.

However, the new method presented here is dependent on a number of factors:

First, that chemical variances throughout the electrode surface film should be normalised over the entire surface if the beam size encompasses sufficient particles. If it does not, then analysis of non-homogeneously oriented surfaces would be sporadic and different dependent on the location of the beam.

Second, that the comparable values are independent of the absolute counts recorded by the XPS detector but that percentage changes are comparable. In addition, it requires that any difference in percentage changes are greater than the error of the experiment, analysis and data processing.

Third, it assumes that the concentration of salts and deposits are less within the bulk of the material when a steady-state is reached than on the very surface. If this was not the case then changes in surface film would be saturated by the presence of these other species and detection would not be possible. This is a reasonable assumption because electrolyte is equally distributed throughout the available volume of electrolyte solvent. This is because after cell opening and solvent evaporation, the quantity of salt on the surface is higher because the volume of solvent is greater due to the volume of electrolyte between electrodes. This is reasonable because the difference in length between the electrodes is measured in microns whereas the XPS analysis depth is only a few nm thick.

Fourth, that irrespective of the chemical nature of the surface film, if non-graphitic bonds change relative to graphite bonds (C-C) the quantity of surface film must have increased. This assumption is reasonable because irrespective of the chemical structure being created (Figure

8) all of the surface film products contain a higher relative percentage of non-graphite bonds than graphite does. Therefore, if the chemical structure of the surface film on two samples is similar and, for example, the number of C-O components increases as a percentage of C-C component then the total quantity of surface film must have increased. However, it does not account for differences in chemical species present. A 50 and a 100 Da polymer with the same chemical functional group but a different number of C-C components would contribute the same number of non C-C components but different graphite components. This is why chemical changes in the surface film cannot be different to accurately determine surface film thickness with this method.

It should be noted that electrode surfaces before and after sputtering are inhomogeneous, stochastically ordered complex mixtures of unknown precise composition. Sputtering can move, rearrange and bury surface film components in such materials. By ensuring that the XPS detection area is large (100 µm diameter) it should be a representative cross section of the electrode surface, and militate against pockets or isolated regions causing bias in the results. To ensure that the samples collected are representative samples can be sputtered for 30 seconds interleaved with XPS analysis. This should continue until the spectra does not change between sputtering. As suggested by Steinberger et al. [183] the method also utilises low Ar^+ ion energy to reduce damage to the sample.

N.B. Assumptions one and two are tested within Submission Five of this portfolio and the results showed good agreement with the proposed method. Use of the method of electrode sputtering to support the fourth assumption has been applied to surface films that are chemically similar and these results are included in chapter eight of this document.

7.1.3. Conclusion

A hypothesis is presented that uses XPS to sputter to a steady-state within the active material and then study changes in the total percentage concentration of graphite components to non-graphite components, dependent on cell use. This would allow the relative thickness of surface films to be compared for samples that are of similar chemical structure. It also allows differentiation between surface film and electrolyte deposits. This theory is based on a number of assumptions that have been tested to verify their accuracy, these tests are included in Submission Five of this portfolio and validated for application in commercial cells in chapter eight of this document.

7.2. Selectively removing $LiPF_6$ from surface film samples

This section introduces a method of removing $LiPF_6$ salt from liquid electrode samples that have been collected by rinsing electrodes with solvent. The ultimate aim of the process is to prepare samples for analysis with HPLC and overcome the fifth problem highlighted from the literature which was:

A process is required to stop $LiPF_6$ from affecting the chemical composition of the surface film in preparation for HPLC analysis

N.B. Further information on the method of selectively removing $LiPF_6$ from liquid samples is provided in Submission Four of this portfolio.

7.2.1. New method

The method (illustrated in Figure 33) has been devised to passivate and subsequently remove $LiPF_6$ salt is:

1. An electrode of known area ($12cm^2$) and active material loading was rinsed with 20mL of dimethyl carbonate (DMC). $CaCO_3$ was added to the sample at a ratio of, at least, 0.0015g of $CaCo_3$ to every 12 cm^2 of electrode material.
2. This wash was then removed from the glove box, mixed with H_2O vigorously and then placed into a desiccator overnight to evaporate.
3. After evaporation, the residue was mixed with 20 ml each of first DCM (organic phase) and then water (aqueous phase). This was then mixed vigorously in a sealed round bottom flask.
4. The organic phase (at the bottom) was then extracted using a new long nose glass pipette and was then filtered through two sheets of filter paper (Herzberg speed of 2.3 min/ml^{-1}) which had just been soaked in DCM.
5. Depending on the HPLC system to be utilised the sample can then be directly injected for analysis or placed into the desiccator and re-solvated with another suitable solvent.

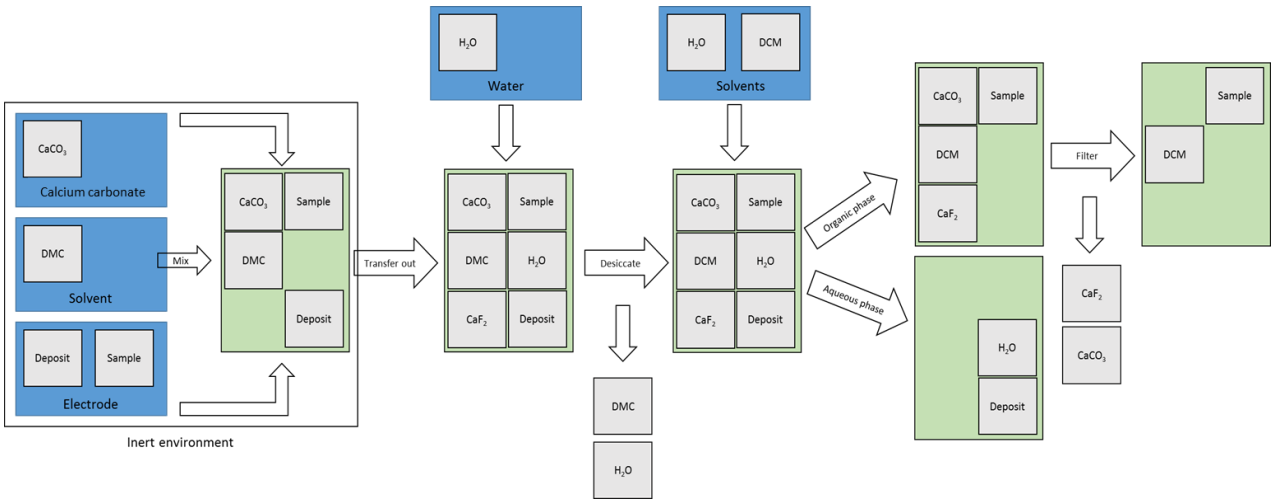

Figure 33. Illustration of the method to passivate $LiPF_6$ and selectively remove sample species prior to analysis with GC-MS and HPLC

7.2.2. Method verification

The viability of this method was tested using ion chromatography (IC). IC works by separating molecules dependent on their interaction with the stationary phase. More in-depth information on the technique can be found here [184]. However, for this work it is sufficient to report that it is able to detect the concentration of specific chemical elements. For this study the quantity of fluorine was calibrated to the system, this is done by creating standards of known concentrations of fluorine and comparing the sample with these standards. This was done with fluoride ion standards of 0.01, 0.05, 0.1, 0.5 and 1 $mg.l^{-1}$ solutions on an ICS 2500 ion chromatograph. This sample was then compared to purified and distilled tap water.

The Dionex software used only exported to PDF but screen prints of these are presented in Figure 34. It shows that the distilled and purified water contained 0.68 $mg.l^{-1}$ of fluoride ions. Whereas, the fluoride ions present in an electrode washed sample after using this new method was only 0.06 $mg.l^{-1}$. This is a difference of more than ten times less fluoride in the electrode washing sample than in purified water.

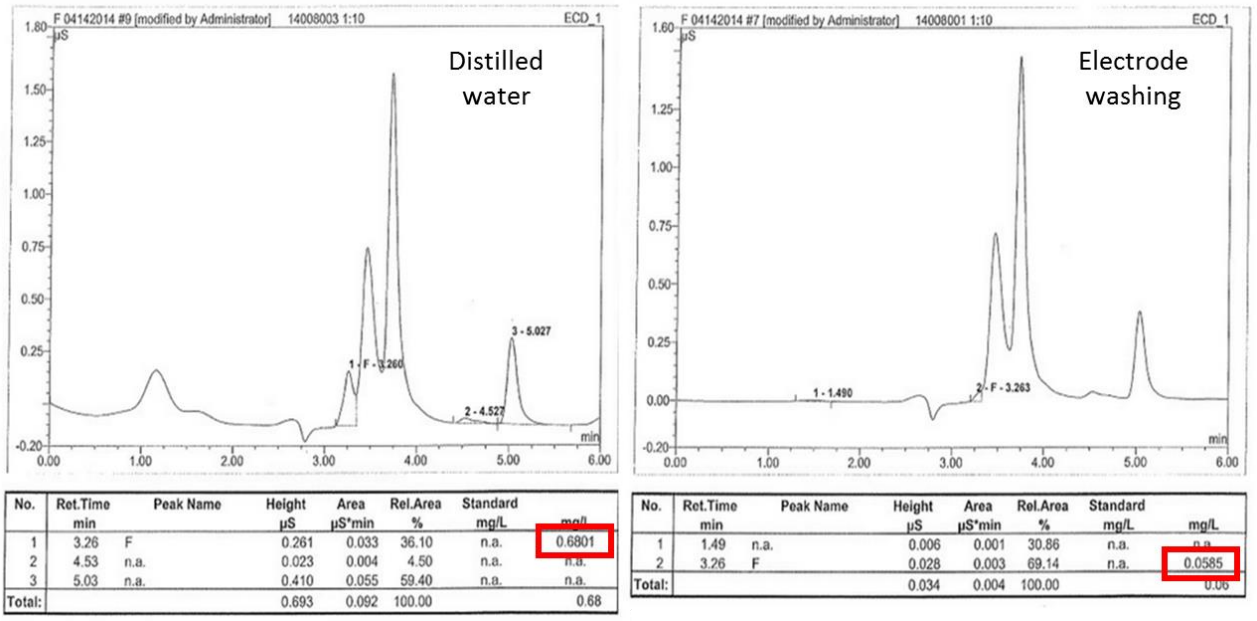

No.	Ret.Time min	Peak Name	Height µS	Area µS*min	Rel.Area %	Standard mg/L	mg/L
1	3.26	F	0.261	0.033	36.10	n.a.	0.6801
2	4.53	n.a.	0.023	0.004	4.50	n.a.	n.a.
3	5.03	n.a.	0.410	0.055	59.40	n.a.	n.a.
Total:			0.693	0.092	100.00		0.68

No.	Ret.Time min	Peak Name	Height µS	Area µS*min	Rel.Area %	Standard mg/L	mg/L
1	1.49	n.a.	0.006	0.001	30.86	n.a.	n.a.
2	3.26	F	0.028	0.003	69.14	n.a.	0.0585
Total:			0.034	0.004	100.00		0.06

Figure 34. Screen prints of the ion chromatography taken of distilled water and the electrode washing sample after processing with the method illustrated in Figure 33.

7.2.3. Discussion and conclusions

Using the method provided above the total quantity of F^- ions in the electrode washing sample was reduced to below distilled water levels. Because the sample was exposed to excess quantities of water the very small quantities of F^- ions present do not originate from either HF, or $LiPF_6$.

Previous to this work the only method of extracting $LiPF_6$ from samples was with a liquid-liquid extraction method proposed by Petibon et al. [146]. Their method exposed the sample to moisture prior to analysis meaning that the sample may have been contaminated by production of HF. The method proposed in this work circumvents these problems by initially mixing the solvent with the sample in an inert atmosphere. This introduces a problem with vaporisation points of solvents within a glove box environment which meant that a higher vaporisation point solvent had to be used in the glove box. The problem is that this solvent is highly soluble in

water and therefore an additional step had to be added to change the solvent being used so that the precipitates could be removed with the liquid phase, this was done with a desiccator and two additions of water.

The biggest step change is the addition of $CaCO_3$ to the sample prior to taking it out of the glove box and when it is hydrolysed. This means that any reaction which does occur prior to the sample being exposed to moisture creates Calcium difluoride (CaF_2) in place of reacting with the sample. This method of forming CaF_2 from Ca- containing compounds was established many years ago and is the basis for the use of fluoride within toothpaste [185]. The reaction between $CaCO_3$ and HF is shown explicitly in the work of Yasui et al. [186]. Therefore, the method presented here uses the same principles as Petibon et al. [146] but improves it by ensuring that there is no reaction between HF and the sample.

However, because the surface films chemical composition is unknown it is not possible to guarantee that some of it is not lost in the aqueous phase or chemically changed through the sample evaporation process. Therefore, this method is of most use in studying the oligomer compounds present within the surface film and not in building a complete picture of the surface film's composition with HPLC. XPS and other methods can be used to compliment this deficiency.

It should be noted that the spectra obtained for lithium-ion surface film samples is not typical of HPLC / GPC spectra (chapter eight); in that they are not well-resolved peaks. The only other spectra using HPLC on lithium-ion cells, also provides similarly unresolved peaks [187]. This means that that the results in this work are as optimised as they are likely to be for commercial samples. This is due to the variety of chemical products being resolved. This makes the technique no use for the absolute quantification of specific oligomers but is useful for the quantification of the sum of the polymeric components present.

7.3. Conclusions

XPS, FTIR, Raman and EDAX provide a means of analysing the chemical structure of the surface film. XPS was highlighted as being especially effective due to its high resolution in detecting chemical species in the <10nm range. However, analysis of the chemical structure only goes so far in describing the relationship between cell resistance or capacity and the surface film. Resistance of the cell can also increase due to an increase in the thickness of the surface film. Others have used traditional sputter-depth profile methods. However, this contains fundamental flaws for cell materials with inhomogeneous surfaces of unknown chemical composition. This work proposes a method of XPS analysis that sputters until a steady-state is reached in the material, at which point the relative concentrations can be used to determine the quantity of surface film relative to graphite. This comparison provides information on the thickness or quantity of surface film around each particle.

This innovative XPS method hinges on the assumption that the surface film components contain a greater quantity of non C-C environments than graphite, and that these non-graphite components are equivalent between samples. The problem is that XPS is not able to detect the length of oligomers within the surface film. Therefore, if oligomers are formed of different lengths, then it could appear as though the surface film had increased less than it has between different samples. This work proposes using HPLC to detect these polymeric species. However, $LiPF_6$ is present in the sample washing and this forms HF in the presence of water. This work proposes a method that stops reaction of HF with the oligomer species and allows analysis of the sample with HPLC through a wet-chemistry method. This method uses $CaCO_3$ to cause the HF to preferentially react with it, in place of the oligomers. However, the method has not been studied for its impact on non-polymeric species present in the surface film so should not be used for the study of these components with HPLC.

Chapters six and seven contribute work to tackle the second objective which is to:

Determine the optimum post-mortem methods that allow connection between electrical performance data and material changes at the negative electrode. This was done by overcoming five challenges and the optimum method for post-mortem analysis is:

- Open the cell (using the new method for 18650-type cells) inside a glove box and never expose samples to air
- Analyse with XPS to determine chemical composition of the electrolyte deposits
- Sputter the sample until a steady-state is reached
- Analyse with XPS to determine chemical composition of the surface film
- Compare the total concentration of graphite to non-graphite from the XPS results to determine surface film thickness
- Where further clarification is required on functional group assignment or morphology investigate with IR or SEM.
- Determine changes in polymeric species with HPLC using the new method for sample preparation outlined in section 7.2

This approach should avoid chemical changes to the surface film as a consequence of the preparation and analysis processes. It should also provide information on the chemical composition of the surface film, deposits and electrode thickness with XPS. Where XPS is not able to determine changes in surface film, HPLC can now be used to investigate changes in the polymeric species present. It also uses a minimal number of techniques making characterisation simpler by reducing the time involved with multiple sample preparations.

8. Post-mortem analysis of lithium-ion cells

The purpose of this chapter is to complete objectives three and four, which are:

1. Perform post-mortem analysis on the negative electrode surface film of cells at each of the lifetime affecting conditions to determine viability of the method and investigate the causes of lifetime reduction within lithium-ion cells
2. Determine whether material changes to the surface film at the negative electrode can be correlated to the cells electrical performance

This chapter applies the information and innovations to post-mortem analysis highlighted within this report and applies them to the lithium-ion cells characterised electrically in Chapter Three. Each testing condition post-mortem analysis is contained within its own sub-section. Its position within the context of the wider portfolio and this document is shown in Figure 35.

It should be noted that XPS analysis and its repeatability across samples is shown in Submission Five of this portfolio. Although samples are inhomogeneous, there is good agreement between samples and the results presented here should be representative. However, XPS costs up to £750 a day and although this work processed over 100 samples, this cost limitation impeded the study, especially for different temperature / SoC samples. The temperature / SoC samples were only performed on five different cells and therefore further analysis would be required to ensure these results are representative.

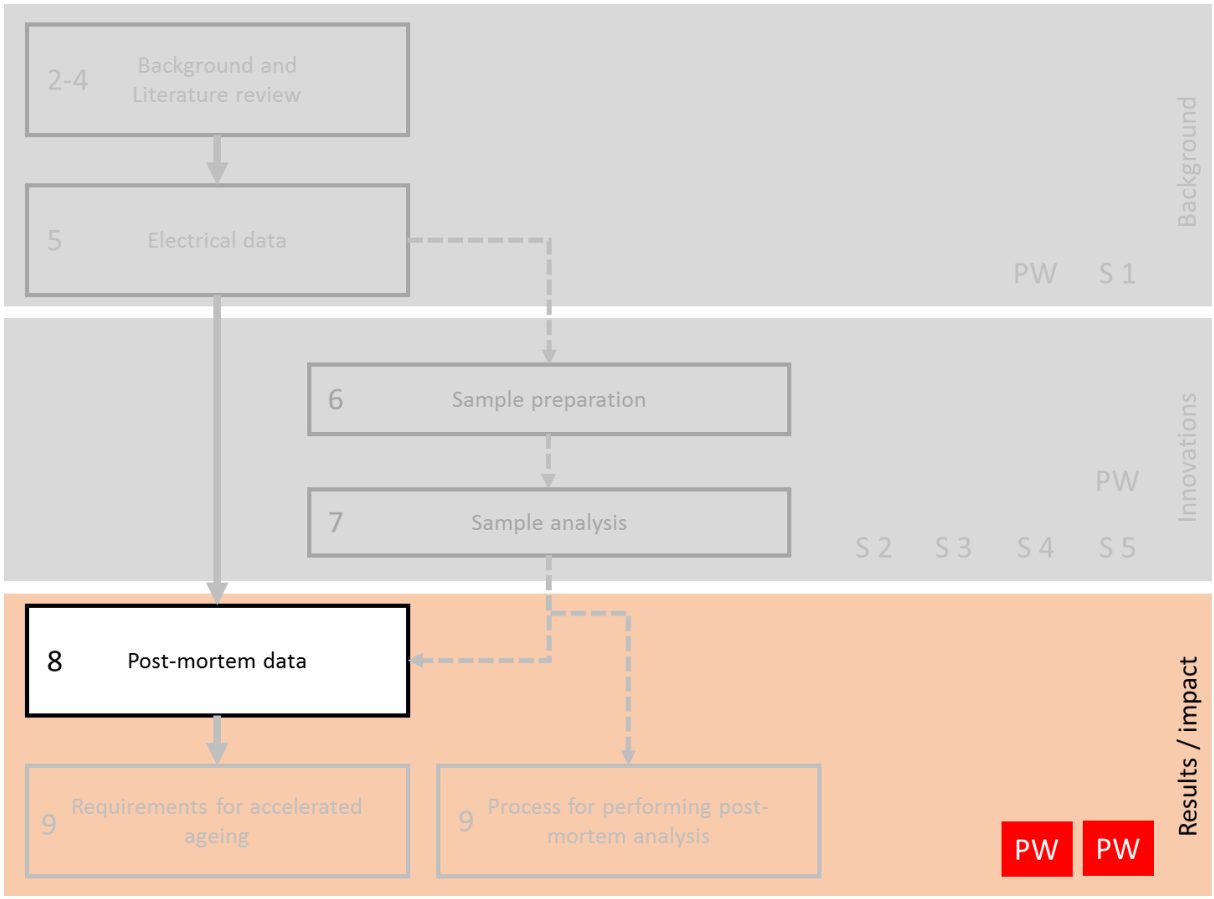

Figure 35. Outline of the engineering doctorate portfolio, chapters within this innovation report are shown as numbers to the left of white topic boxes.

8.1. Increased current rate during charge

Some of the information contained in this section is explained in further detail in *Chapter Six of Submission Five within this portfolio*.

8.1.1. Visual changes

Figure 36 depicts the physical appearance of the negative electrodes at each charge rate based on the photograph from [162]. The 0.7- and 2-C electrodes look identical in colour, shading, and appearance. The 4-C electrode is mostly similar in colour and appearance but has a single grey band covering approximately one-third of the middle of the electrode roll. The electrode from the cell subjected to a charge rate of 6-C also has a band; however it covers only one-quarter of the electrode. The active material is delaminated from the current collector so that the copper is visible in places underneath. The presence of the grey-coloured band in the centre of the 4-C charged electrode and the delamination along the centre of the 6-C charged electrode indicates that the increased charge rate is affecting the middle sections at the 4- and 6-C rates of charge differently. This difference is highlighted further by the Figure 36 inset, which is a magnified photograph of the 6-C electrode. It shows that the electrode changes in colour across the electrode surface. It is multi-coloured with white patches in the middle (far right), and moving from the middle to the outside of the electrode (far left). The colour changes from greenish to blue to lighter blue to grey. Although chemical changes in surface film do not always present themselves visually, changes in colour always indicate a change in the thickness or chemistry of the material under study.

Delamination of the 6-C electrode had a uniform pattern in the centre and across the length of the electrode roll. This pattern of delamination comes in and back out like two opposing sinusoidal waves. Part of this pattern is caused by lines in the electrode material running from

the bottom of the can to the top cap that are repeated in an almost equidistant pattern along the length. These lines perfectly aligned with the current collector tabs when the electrode is rolled up, which were at either end of the negative electrode and in the middle of the positive electrode.

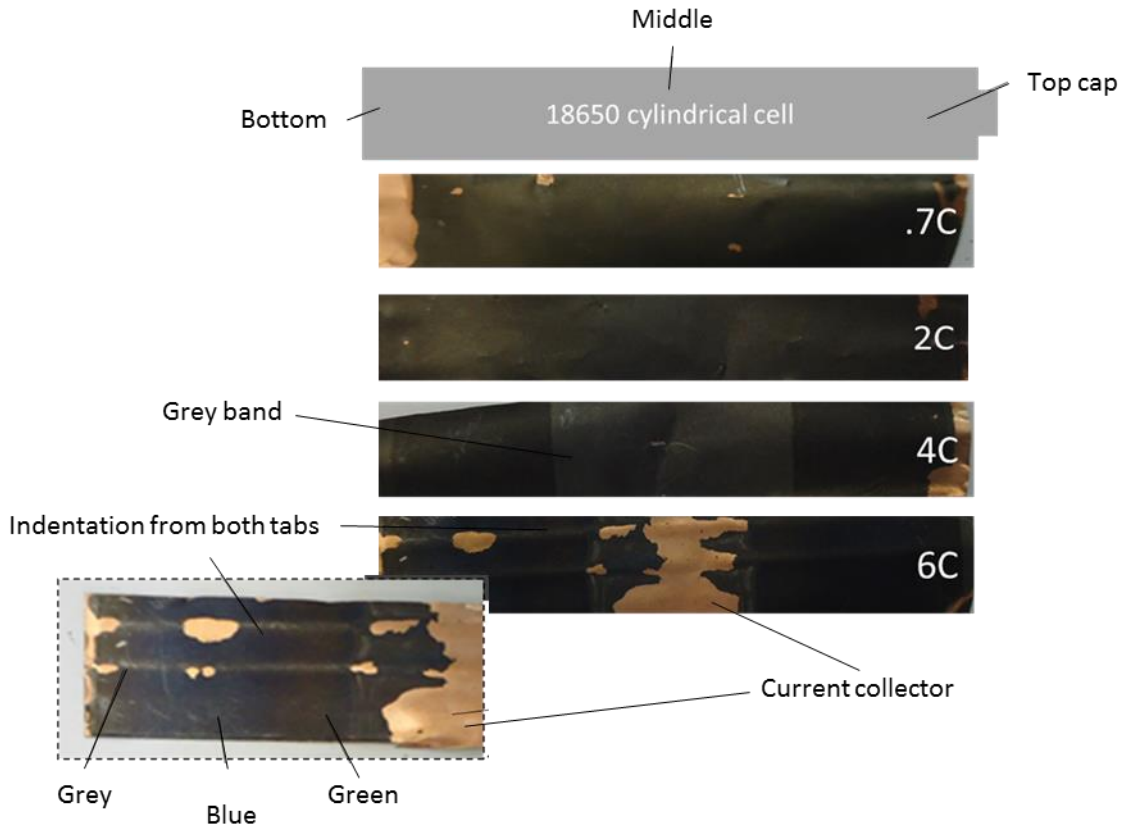

Figure 36. Photographs of graphite electrodes from commercial 18650-type lithium-ion cells that have been subjected to different rates of charge (0.7-, 2-, 4-, and 6-C). The photograph (inset) shows one side of the 6-C electrode at higher magnification.

8.1.2. Microstructural changes

Figure 37 contains micrographs of the negative electrodes from cells charged from 0.7-C to 6-C. These images are from both the middle and the outside (close to the top cap/bottom) of the electrode roll. There are two key points to be made. First, the outside part of the roll for the 0.7-C and 2-C charged electrodes' active material looks like pristine graphite. At 4-C, small, lighter-coloured dots are present, and at 6-C, it is more difficult to identify individual graphite

particles because of a surface covering. The middle of the electrode roll is not visually the same as pristine graphite at any rate of charge because a film is visible. A trend is not clear, using SEM, of the extent of surface film growth on the middle track of the electrode roll as it is for the outer track. However, the middle track appears to have a greater amount of surface film than that on the outside in each case except for 6-C, which is visually similar for both the middle and outside.

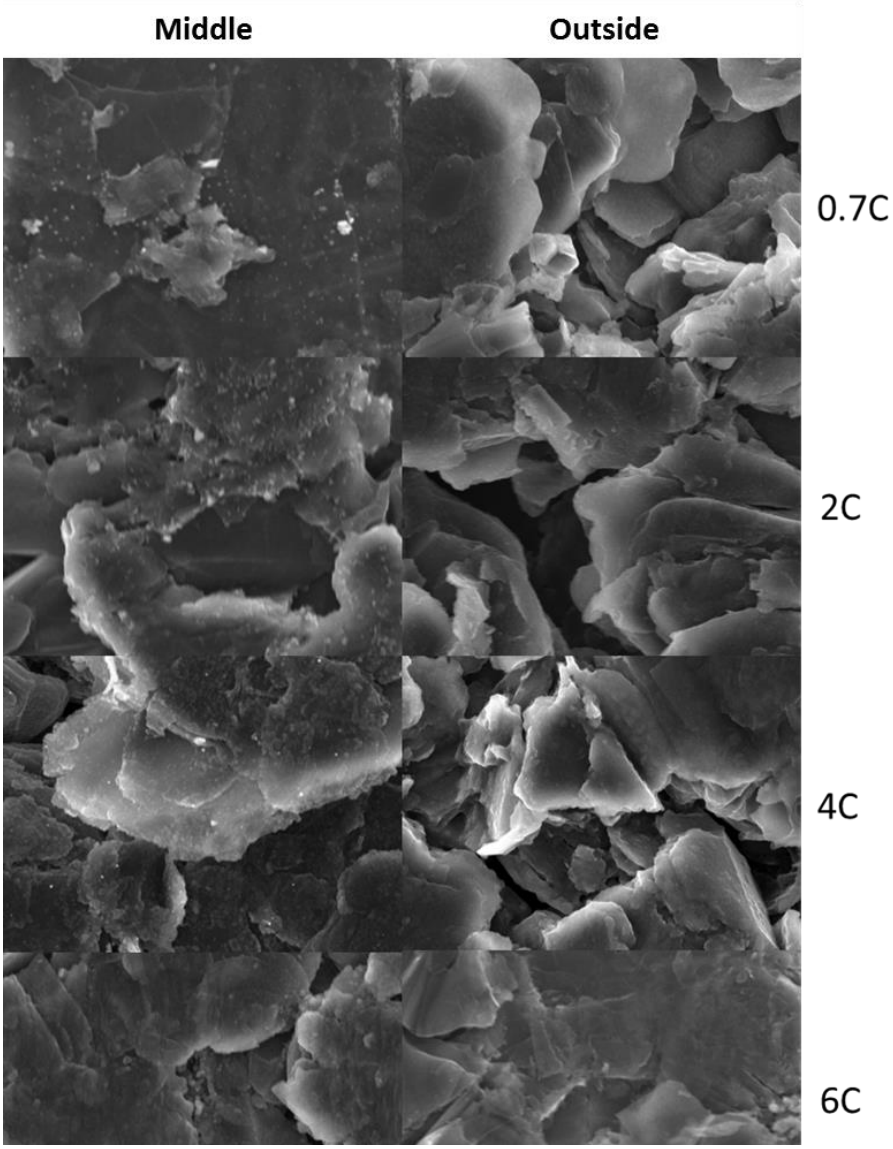

Figure 37. Micrographs of graphite electrodes from commercially available 18650 cells that were subjected to different rates of charge (0.7-, 2-, 4-, and 6-C). The "Middle" and "Outside" labels refer to micrographs taken furthest from the top cap and bottom of the 18650 size cell (Middle) and those taken closest to them (Outside).

8.1.3. Surface film chemical composition

Figure 38 is the liquid chromatogram of the surface film removed from the electrodes at each C-rate from samples cut from the outside of the electrode material. The Figure 38 inset shows the total intensity within each minute (marked by colour bands).

Results from the 0.7-, 2-, and 4-C electrodes are almost identical. In contrast, results from the 6-C electrode are considerably different. They contain much higher concentrations in the 9–10 and 10–11 minute time intervals. The size exclusion columns used elute higher molecular weight (MW) / more branched oligomers soonest and lower MW, less-branched oligomers later. Therefore, the 6-C electrode had a higher concentration of higher MW oligomers compared to the others. This finding suggests that the surface film of the 6-C electrode is chemically different from those at other C-rates. This is because the total counts are almost identical at less than 9.5 minutes and after 14 minutes, indicating that this difference is from the addition of a greater concentration of higher MW oligomers only.

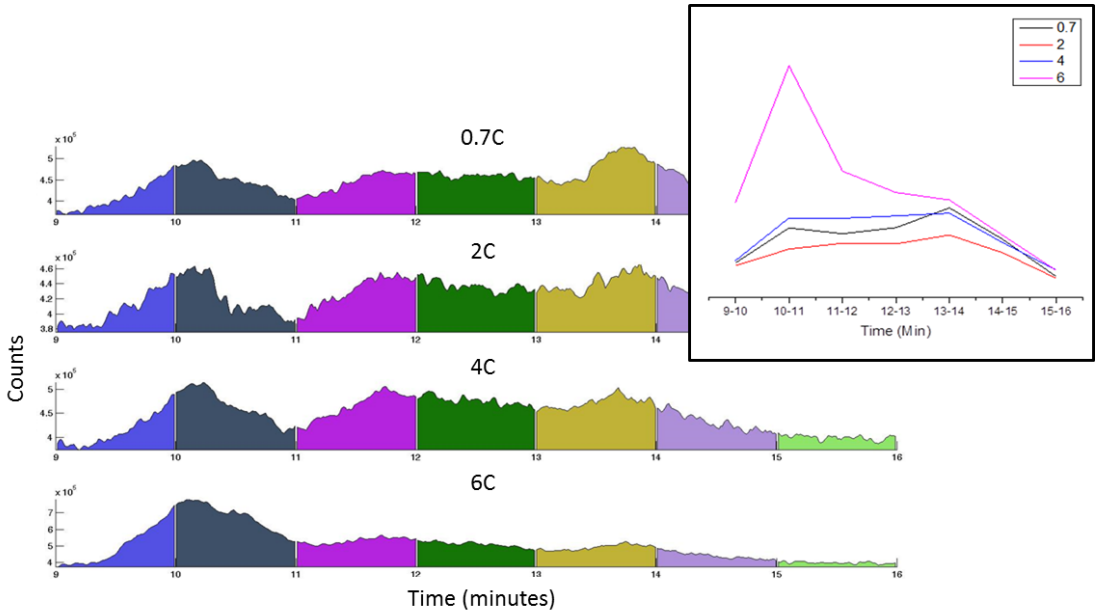

Figure 38. High-performance liquid chromatography of electrode surface film removed from cells that have been subjected to different rates of charge (0.7-, 2-, 4-, and 6-C). The inset is the integration of the total counts for each 1-minute period.

Figure 39 shows the XPS spectra of the C1s spectra of the outside of the electrodes at each C-rate. The 0.7-C to 4-C spectra peak positions align almost perfectly (<0.15eV). Whereas the 6-C electrode C-O peak requires an adjustment of 0.6 eV to lower binding energy and also an increase in its FWHM of 0.5 eV. Because the other samples align so tightly it suggests that this shift is from a change in chemical species. The re-alignment is from an adjustment in the chemical environments that are present. The assignment of peaks to specific chemical environments is according to previous XPS studies of graphite electrodes [19,124].

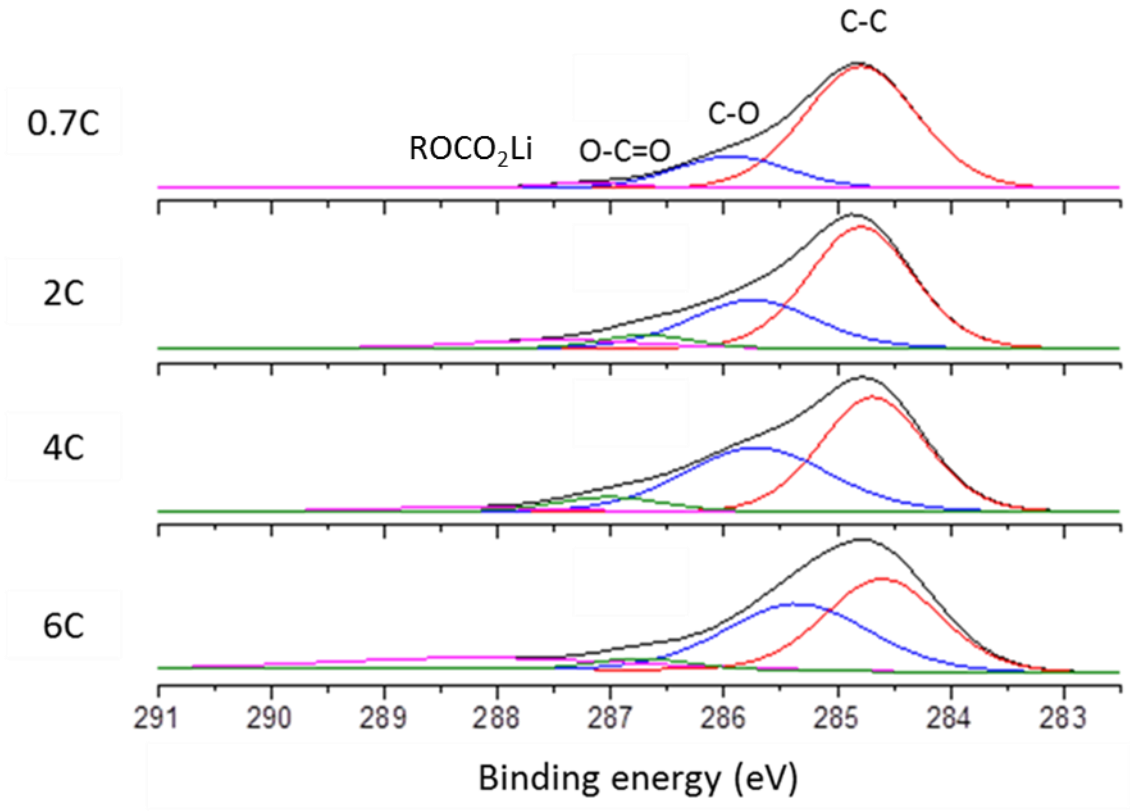

Figure 39. C1s XPS spectra of graphite electrodes after sputtering from commercial 18650 cells subjected to different rates of charge (0.7-, 2-, 4-, and 6-C).

Figure 40 shows the C1s spectra of the middle and outside of the 2-C electrode. The findings indicate that there is a chemical difference. The O-C=O component is not present on the outside, whereas it is present in the middle. In addition, the contributions of both C-O and $ROCO_2Li$ increase by 38% and 103% in the middle, compared to the outside. The graphite reduces from 62% on the outside to 39% on the middle, a reduction of approximately one third and an increase in non-graphite peaks of one half. The shift of the C-O and $ROCO_2Li$ peaks to a lower binding energy for the middle sample suggests that the surface film containing these groups is chemically reduced or that an additional chemical environment is present. XPS shows that the middle contains a greater quantity of non-graphite compared to the outside. This same trend, shown here for 2-C electrodes, was consistent across C-rates. The middle always contains a higher quantity (>20%) of surface film compared to the outside.

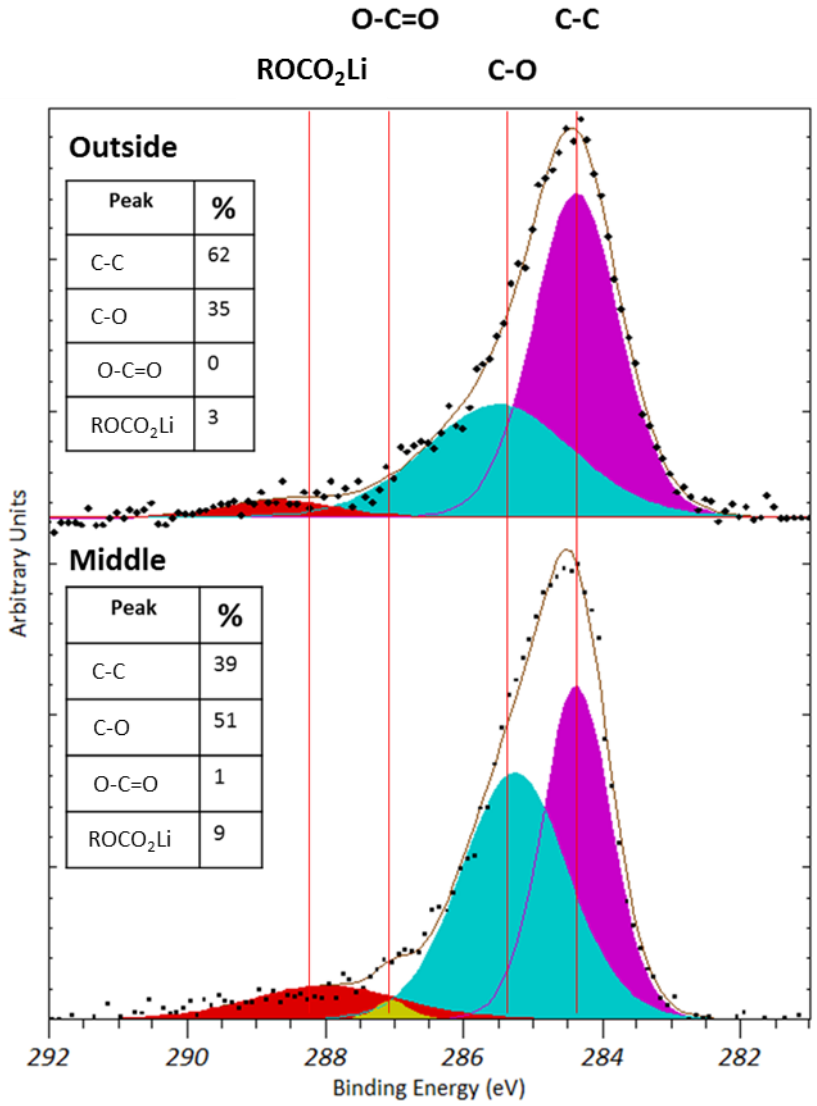

Figure 40. C1s XPS spectra of a graphite electrode from a cell subjected to a charge rate of 2-C. The *middle* refers to the electrode furthest from the top and bottom of the 18650-size cell, whereas the outside refers to the electrode closest to the top or bottom of the electrode roll.

8.1.4. Discussion

8.1.4.1. Position dependent surface film changes

Figure 36 shows that as the C-rate increased, it had a different impact on the middle track of the electrode roll than on the outside. Although this effect is most pronounced for the 6-C electrode that had delaminated in places, the 4-C electrode similarly had a grey band in the middle. The micrographs show that although not visually quantifiable, the C-rate had consistently increased the concentration of surface film and more so in the middle than on the outside. While it was not possible to see any surface film in the micrographs on the outside track of the cells charged at 0.7- and 2-C, the middle track showed that surface film was covering the graphite particles. Figure 40 supports this finding by showing that the non-graphite surface film components of the middle of the electrode roll were 20% greater than on the outside. This increase in surface film cannot be a consequence of the current path preferentially moving along the middle track. This is because the current collector tabs were located at both ends of the unrolled negative electrode and in the centre of the positive electrode.

A possible reason for this increase in surface film along the middle of the electrode roll is presented in the work of Wood et al. [188]. They show that wetting of the electrode roll during cell manufacture is a "bottleneck" to the formation and manufacture of lithium-ion cells because it takes much longer to perform. The wetting process involves the injection of electrolyte both on top of the jelly roll and at the bottom of the cell through the mandrel hole. However, because the process is dependent on capillary action the middle will never contain the same quantity as those areas closest to where the electrolyte is first inserted. Reeves and Morris [189] note that an electrode's active material that is not sufficiently wetted increases

both electronic and charge transfer resistance. This is consistent with differences noted in the electrical performance of cells subjected to different C-rates.

At the highest C-rate (6-C), the electrode active material in the middle had delaminated in places. The delamination only occurs along the middle of the electrode roll and is most pronounced when it aligns with the tabs. This suggests it is caused by an increase in temperature because it is well known that the tabs are the hottest parts of the cell because they are subjected to higher current throughput [190]. Therefore, at 6-C, the temperature of the middle of the electrode roll (which is hotter due to wettability issues and coupled with the tab temperature rise) increases so that the binder properties are negatively affected. This finding is consistent with the much steeper decrease in cell electrical performance at 6-C as noted in [162].

This hypothesis was tested by placing samples of electrode material cut from the outside and the middle of the cell subjected to 6-C into environmental chambers at various temperatures. Photographs from this test are shown in Figure 41. The electrode from the outside of the cell maintained adhesion at 30^{o}C (Figure 41 a), whereas the electrode from the middle delaminated at 30^{o}C (Figure 41 b) and turned to paste at 55^{o}C (Figure 41 c). The increase in temperature permanently affected the chemical properties of the binder such that it reduced its adhesion to the current collector.

This means that the temperature in the middle of the graphite electrode from the 6-C charged cell was sufficient to permanently affect the properties of the binder, such that the electrode delaminated from the current collector at temperatures of 30^{o}C which is well within the normal operating conditions of the cell. Better electrolyte wetting could potentially mitigate this from happening and may increase the charge rates that can be implemented. However, this study does not conclusively prove that it is electrode wetting that is the cause of the higher temperature along this central band. It is possible that the higher temperature is because this is

the longest distance of the heat conducting path to the outside of the cell can. The temperature of the thermal chambers were kept at a constant 25ºC. Therefore, at the end of a charge period at high C-rates this central core will be higher, even if it was sufficiently wet.

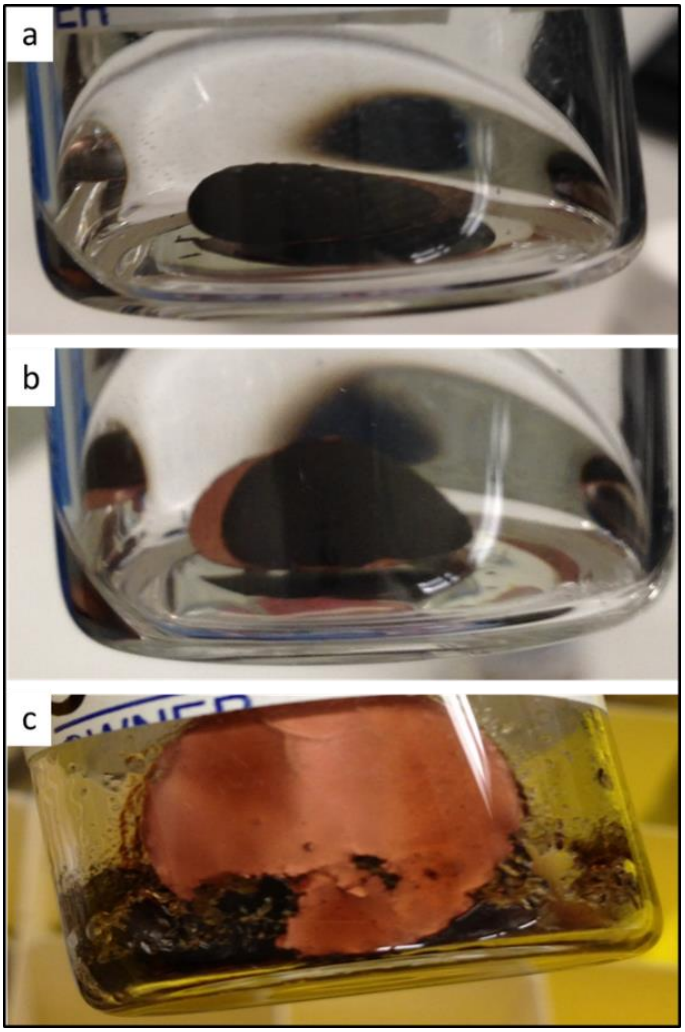

Figure 41. Photographs of graphite electrodes cut from commercial cylindrical cells from the outside (a) and *middle* (b and c) of the electrode roll and stored at 30ºC (a and b) and 55ºC (c) in typical electrolyte organic solvent.

8.1.4.2. Changes to the surface films chemical composition

Figures 38 and 39 show that with the exception of the 6-C cell the chemical composition of the surface film at 0.7- to 4-C is almost identical. At 6-C, however, the surface film chemical

composition changes significantly. The HPLC data shows a much higher concentration of longer chain, more branched oligomer compounds suggesting that the surface film and / or electrolyte components are increasing in size. This difference suggests that surface film thickness determination is not possible for 6-C cells using the method outlined in Chapter Five. Therefore, it is not a suitable condition for accelerating the ageing mechanism. Changes to the chemical composition of the surface film suggest different mechanisms to those used during normal ageing conditions. What this suggests is that it is possible to use charging rates of up to 4-C for accelerated ageing testing without chemically altering the surface film material that is formed.

8.1.4.3. Surface film thickness

Figure 42 presents the relative peak areas for each chemical environment (a) and for all C-C graphite and non-graphite peaks (b) according to the fitting used in Figure 39. Figure 42a shows that as the C-rate increases, the percentage of C-C graphite decreases, whereas the concentration of C-O and O-C=O species, from the surface film, increase. The concentration of $ROCO_2Li$ species remains between 0% at 0.7-C and 8% at 2-C but does not show a trend with C-rate. When the sum of these non-graphite environments (C-O, O-C=O, and $ROCO_2Li$) is compared to the C-C graphite environments (Figure 42b), there is an increase in surface film as the C-rate increases. At 6-C, however, the concentration of surface film to graphite is 57% surface film to 43% graphite. In each case, as the C-rate increases, so too does the concentration of surface film compared to graphite. Because the chemical environment has changed for the 6-C cell surface film, not only can the XPS method employed not account for change in path length but its value, if it could be calculated, could not be used in comparison to other samples.

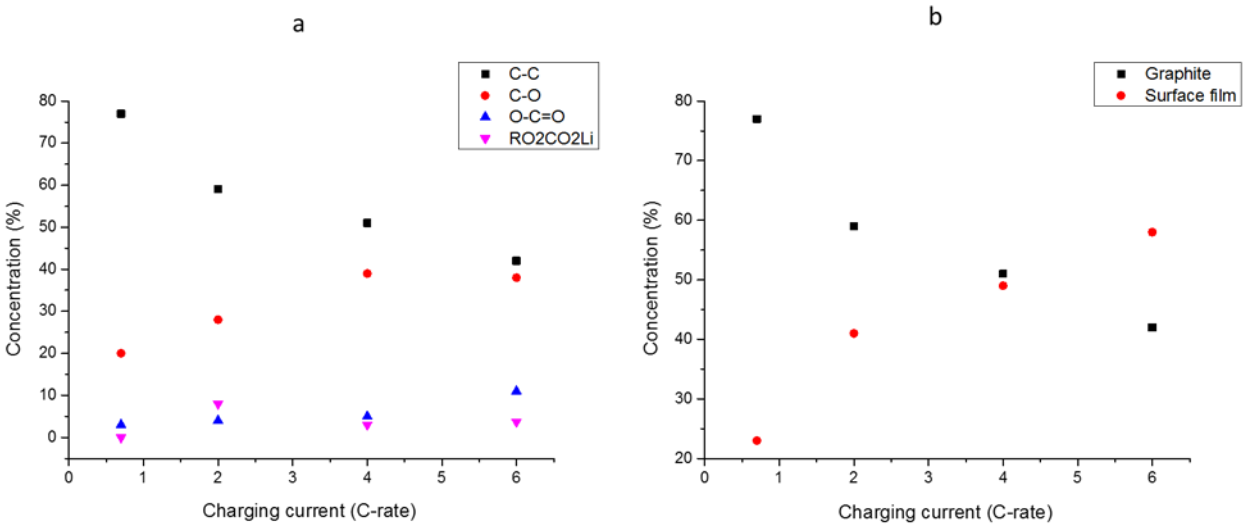

Figure 42. *(a) The peak areas plotted as a percentage of total C1s environments and (b) the sum of all non C-C environments (surface film) compared to all C-C environments.*

Increasing the C-rate of the cell (up to 4-C) does not appear to impact the material composition of the film formed but does impact the concentration of surface film relative to graphite. Figure 43 shows the surface film concentrations recorded in Figure 42b and relates them to the cells resistance. It shows a consistent increase in surface film percentage that tracks the cell resistance. What is more interesting is that although the trend line follows all points, including the point at 6-C, because the surface film has altered in the 6-C instance the value has no significance. With this value disregarded, the surface film growth is linear with C-rate.

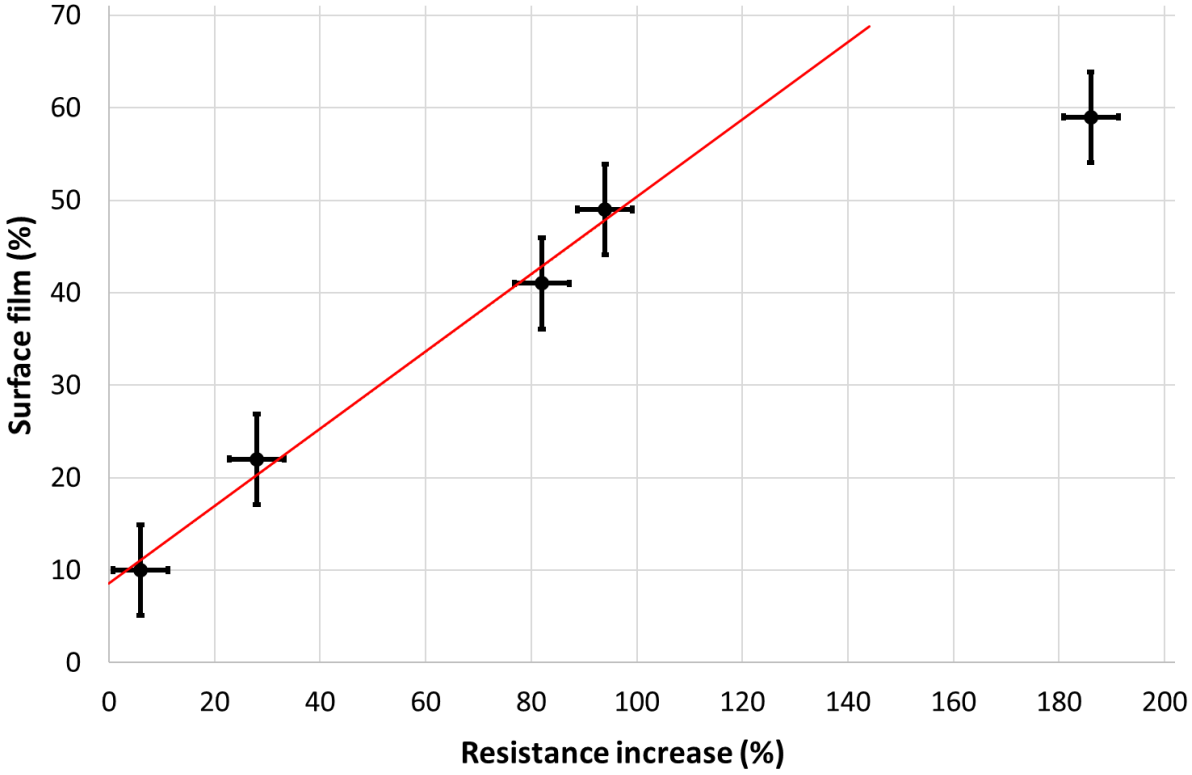

Figure 43. Cell resistance relative to the total quantity of surface film for lithium-ion cells subjected to varied rates of charge. R^2 value of fitting line (red) is >0.98%.

In the one instance where the chemical nature of the film changes the XPS method employed for determining surface film thickness breaks down and cannot be employed – precisely as predicted.

It should be noted that there is nothing special about the 4-C rate for lithium-ion cells in general because this rate will change with cells, materials and chemistry. Instead, it is important to look at the wider picture of ageing and lifetime prediction of lithium-ion cells with post-mortem analysis. Using the analytical methods and techniques presented in this work, it is possible to identify and quantify chemical changes in the materials themselves; these could not be detected by electrical performance data alone. Therefore, what is important is that the surface film does not chemically alter until after a charge rate of 4-C. The moment that the surface film alters,

Arrhenius kinetics cannot be assumed and the rate of degradation must be tracked through lower charging rates. If the chemical structure of the surface film does not change, then it is possible to use the XPS method presented here to determine the relative surface film thickness and define a specific rate, for a specific cell, chemistry and usage case. Therefore, post-mortem analysis can provide answers that are both more in-depth and quicker than electrical performance alone. For these cells, that rate was 4-C, but was not 6-C.

8.2. Percentage change in state of charge

This section investigates the impact of the percentage change in state of charge on the surface film of the negative electrode surface film. This study was completed in tandem with those cells analysed in section 8.1 and uses the same charge rates (0.7-, 2-, 4- and 6-C) but a smaller percentage of the charge window (40-80%). It uses the United States Advanced Battery Consortium (USABC) standard of testing, to determine the difference between those charged between 0-100% SoC and 40-80% SoC.

Photographs of the electrodes taken from cells subjected to % Δ SoC during charge, and at different charge rates, are shown in Figure 44. The cells subjected to a smaller SoC window are severely delaminated along both sides of the electrode and across the entire electrode roll. In contrast, only the cell charged at 6C is delaminated along the central band. The cause of this central band delamination is addressed in section 8.1 above. However, the delamination noted in these samples cannot be the same cause as that for the 40-80% SoC cells. The main problem is that the electrode active material is completely bound to the separator and not the current collector. Analysis of the surface film within this work has occurred assuming the electrolyte evaporates from the top of the electrode surface. This work has not addressed the potential chemical differences in surface film with distance from the current collector. Nor is it possible to study the electrolyte deposits due to the uncertainty with deposition on the back side of the electrode. The greatest challenge for post-mortem analysis of these samples is therefore not surface film analysis but why the delamination of the electrode active material from the current collector has occurred.

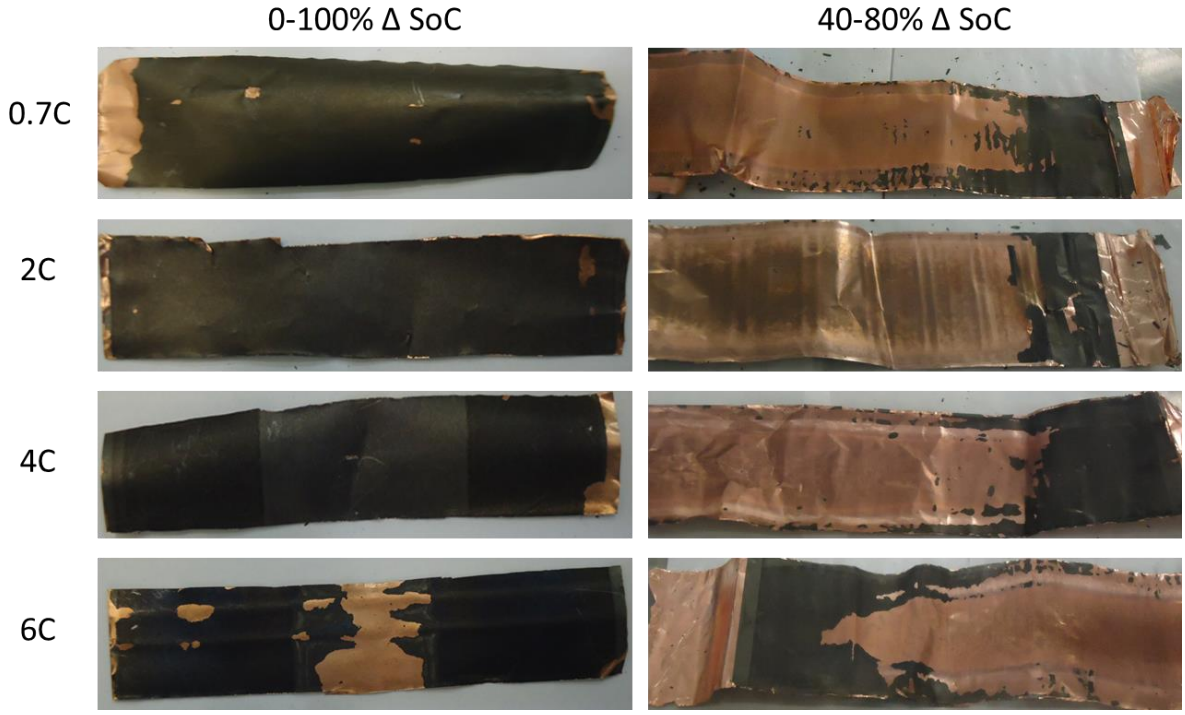

Figure 44. Photographs of electrodes subjected to different charging rates (0.7- to 6-C) through 100% of the state of charge window (0-100% Δ SoC) and 40% of the state of charge window (40-80% Δ SoC)

Figure 45 shows micrographs of the current collector (CC) from the outside band of the electrode roll (where the 6-C cells have not delaminated). In all cases, prior to analysis, the current collector was cleaned with N-methyl pyrrolidone on a cotton wool bud to remove the electrode active material. The 40-80% micrographs are completely different from the pristine Cu CC. It is possible to see the individual grains of Cu, whereas in the pristine cell, these individual grains are not shown. This is because when the Cu CCs are formed they are hot pressed between rollers that align the individual grains, they are then polished to create the smooth surface. The roller marks are shown as streaks through the Cu. Therefore, the polishing removes differentiation between grains. In the 0-100% case it is possible to see the polished surface of the electrode roll (similar to pristine) but it also contains small localised imperfections.

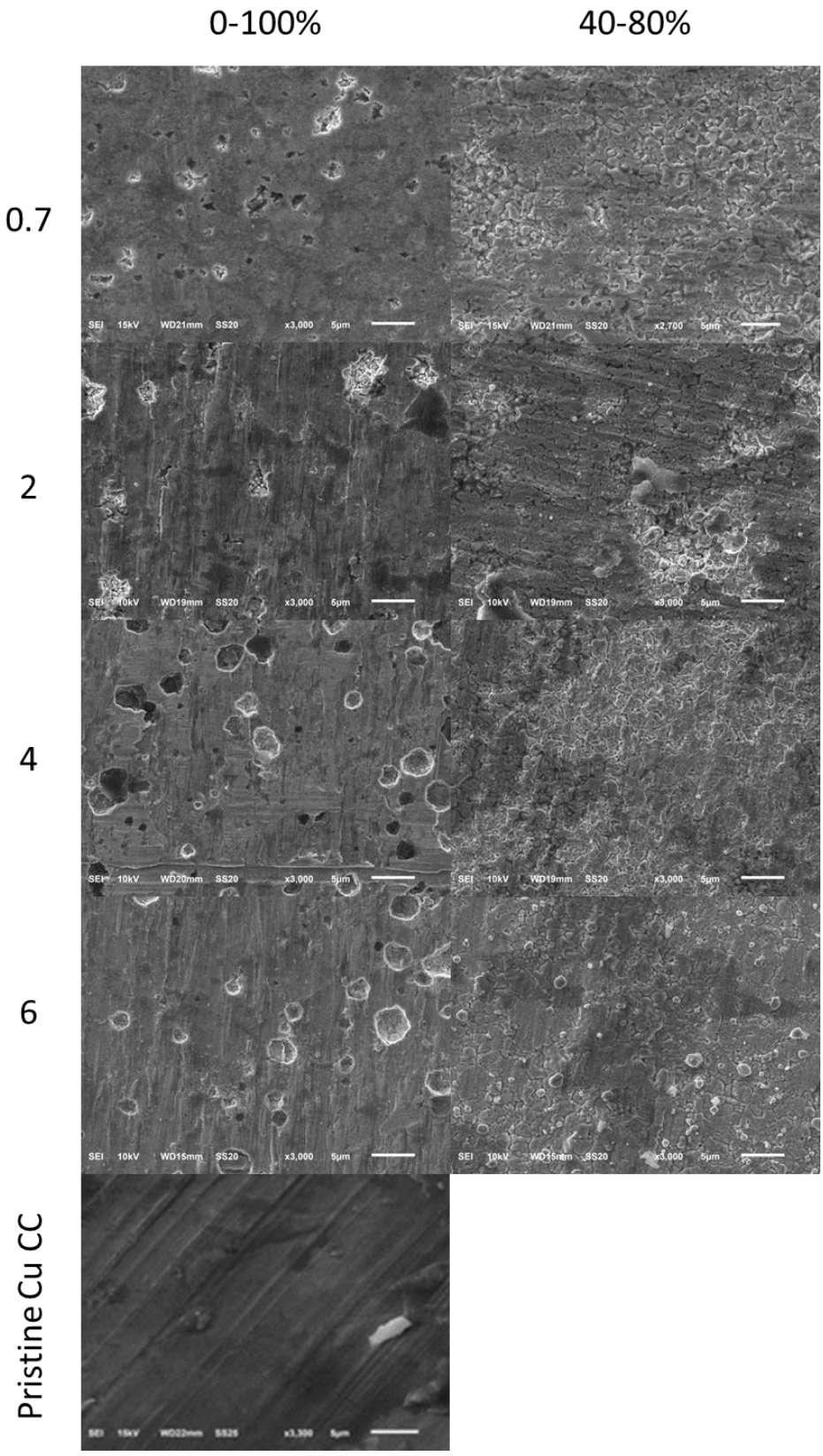

Figure 45. Micrographs of copper current collectors from cells subjected to different charging rates (0.7- to 6-C) through 100% of the state of charge window (0-100% Δ SoC) and 40% of the state of charge window (40-80% Δ SoC)

According to Braithwaite et al. who studied Cu CC corrosion these localised imperfections are revelation of the grain boundary [191] and they occur when four things happen. First, the material must have been 'work hardened', or polished, to impose an artificial material surface. The electrode potential must be close to 0.0V, the grains must be large (although no specific size is defined), and there must be alkali metals present. These cells (40-80% and 0-100%) were subjected to the same conditions, including a discharge to 0.5-0.8V (total cell voltage) prior to post-mortem analysis. However, under these conditions, copper current collectors can also be subject to pitting [192].

Figure 46 contains micrographs collected from the two sets of cells and from a Cu CC that was forced to higher potentials (0.0V) in the presence of an aggressive alkali metal salt solution to create pitting of the materials. The 0-100% cell CC has corroded but only to reveal the grain boundaries. This is because it is possible to see the grains at the bottom of the corroded sections, this is different to the pitted CC. Frankel et al. [192] state that once pitting begins the process self-propagates due to the creation of a potential difference within the pit through expulsion of cationic species. What this means, with respect to this work, is that pitting does not stop at the grain boundary. This is evident because the pitted CC in Figure 46 does not have any grains present at the bottom of the created pit. Therefore, it is not pitting but grain boundary revelation or 'etching' that is the cause of the delamination for the 40-80% cells. Whereas, in the 0-100% cells that etching is stochastic. This suggests that one of the four factors required for grain boundary etching has increased for the 40-80% cells and not the 0-100% cells. It cannot be concentration of alkali metals because the cells are identical. It also cannot be CC polishing or grain boundary size because the cells were chemically identical when manufactured. This only leaves the potential of the electrode, therefore, the potential of the negative electrode must be lower for the 40-80% cells than for the 0-100% cells. The only time that either set of cells was taken to this low potential was during complete discharge prior to post-mortem analysis.

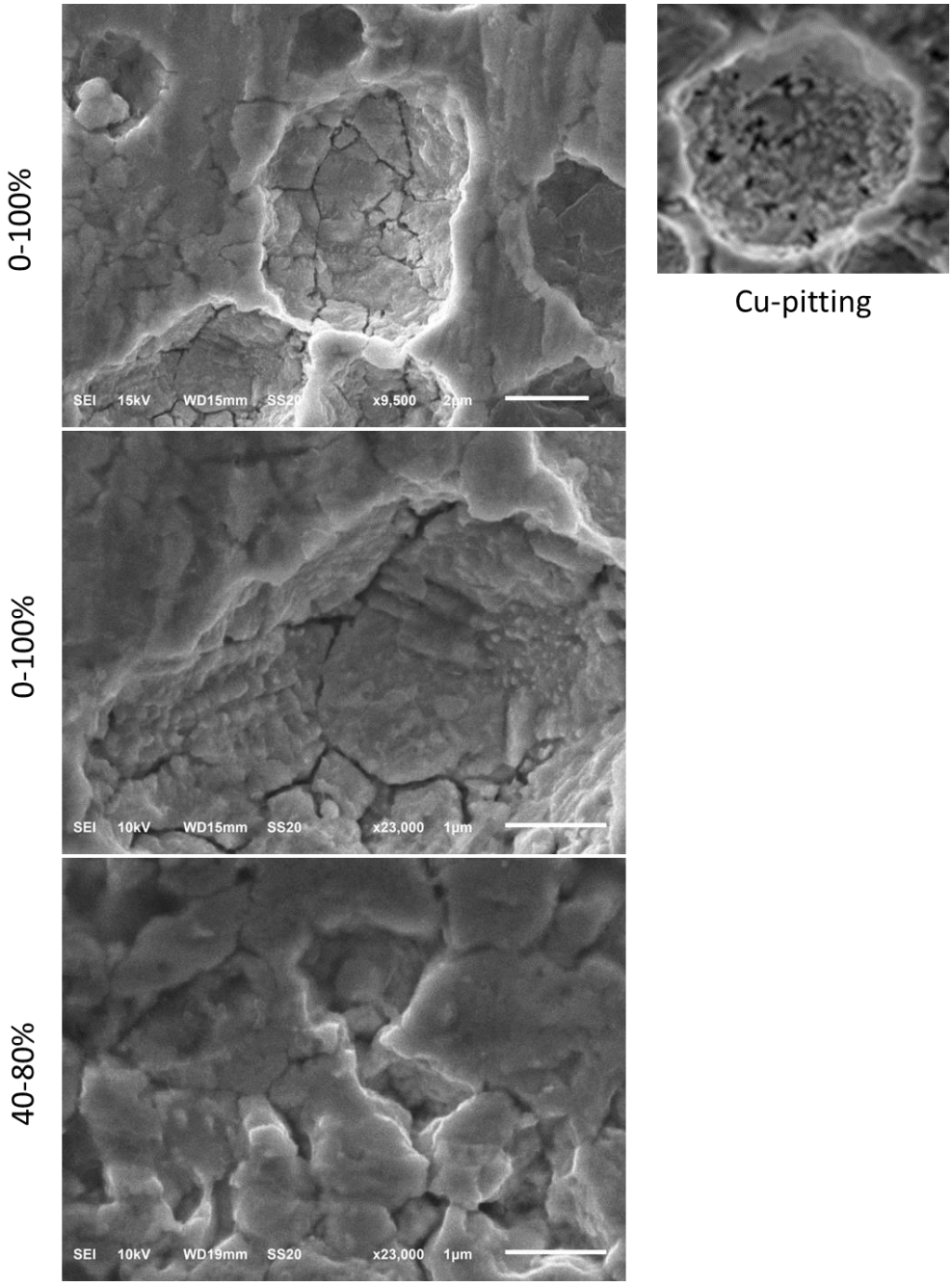

Figure 46. Micrographs of copper current collectors from cells charged through 100% of the state of charge window (0-100% Δ SoC) and 40% of the state of charge window (40-80% Δ SoC) and of a Cu current collector after pitting damage

Using results from section 8.1 shows that the middle track of the electrode should have delaminated prior to discharging the cell for post-mortem analysis. Therefore, the CC along this central track should not have been etched when the cell was discharged prior to post-

mortem analysis. Figure 47 shows the difference between the middle and the outside of the 40-80% Δ SoC cell. It shows that the grain boundaries of the outside are clearly visible. Whereas, the grain boundaries of the middle are not. This is consistent with both of the presented hypotheses, that the middle of the electrode roll is delaminated prior to post-mortem analysis and that the negative electrode active material is at a lower potential for the 40-80% Δ SoC cell than the cells subjected to 0-100% Δ SoC.

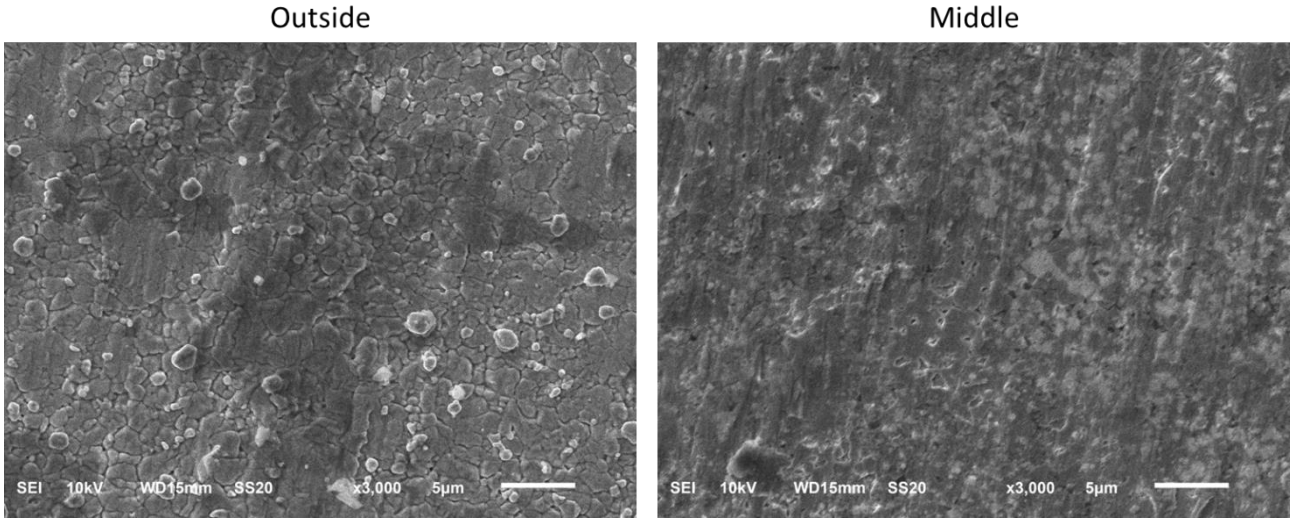

Figure 47. Micrographs of copper current collectors from a cell charged at a rate of 6-C through 40% of the state of charge window (40-80% SoC) from the middle of the electrode roll and the outside

A possible reason for this is proposed by Bloom et al. [193], and a method for its study is provided by Dahn et al. [194]. These works showed that over time the absolute potential of individual electrodes can shift. The result would be a shift in the potential of a single electrode. Applied to the cell presented here, when the 40-80% Δ SoC cells were discharged the negative electrode went to a lower potential because it had shifted and therefore the copper was etched. When the etching happens, the copper that is bound to the active material of the electrode is separated from the current collector and the delamination occurs.

These tests were performed according to the USABC electric-vehicle battery test procedures manual [195], for determining the difference between small and large changes in a cells % Δ SoC. This procedure is the standard used for comparison of manufacturer cell performance but was created for Ni-MH cell chemistry. It uses a repeat cycle to re-determine the cell voltage limits due to hysteresis effects that are inherent within Ni-MH technology. The 0-100% and 40-80% Δ SoC cycling program from the USABC Electric Vehicles Manual is shown in Figure 48. It shows that for each complete charge a 0-100% cell uses, the 40-80% Δ SoC undergoes an additional 40% charge and 40% discharge. In addition, the cut-off voltages of the next electrical cycle are dictated by the previous charge-discharge profile and so there is some ambiguity as to whether the percentage limits used are consistent between the two tests.

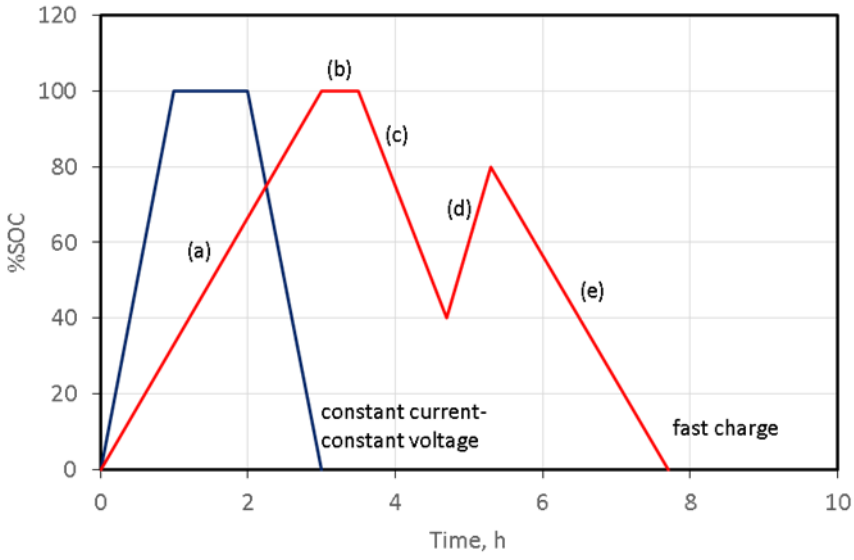

Figure 48. Profile of the charge discharge cycle standard testing procedure from the USABC for testing of damage induced by a percentage change in a cells state of charge utilised during charging.

This ambiguity with respect to charge voltage start and stop limits and additional cycles may be the cause for the electrode potential slippage. It also shows the damage that can be imposed

on lithium-ion cells with respect to electrode potential if the USABC standard is used. It is the author's recommendation that the USABC standard be changed to accommodate for lithium-ion technology. In addition, it is recommend that any future tests are not performed according to this current standard, because its impact of electrode slippage on electrical performance is unknown and may lead to incorrect results. Additional cycles are well-known to impact cell performance. Therefore, for lithium-ion cells these additional cycles should be removed and such comparison should be completed by a test that does not contain them.

8.3. Vibration

This section contains post-mortem analysis of the cells that were vibrated compared to a cell that was not. These cells are the same as those in the work of Hooper et al. [196]. A method of XPS analysis that sputters off surface deposits to determine differences between surface film and electrolyte deposits has been used. The chemical composition of these two materials is presented separately.

8.3.1. Surface film (Negative electrode post-sputter)

This section presents chemical analysis of the surface film of the vibrated cell. Figure 49 contains C 1s XPS spectra of the negative electrode surface film from the control cell and the three vibrated cells and shows differences in the chemical composition of surface film between cells. There are three chemical environments which can be attributed to the spectra of the control cell; these are C-C from graphite (284.4 eV) [19,124,126] which will invariably include some C-H components that broaden the FWHM of the peak. A carbide, C-Li (282.8 eV), which is a component of the surface film [197] and also C-O (286.3 eV) which is similarly a

component of the surface film [19]. For each of the cells that have been vibrated an additional component within the surface film was present (O-C=O) at 289 eV [133]. On the basis that this component was not found in the control sample and yet is present in all of the vibrated cells, its presence is a direct consequence of the cells being exposed to a vibration loading.

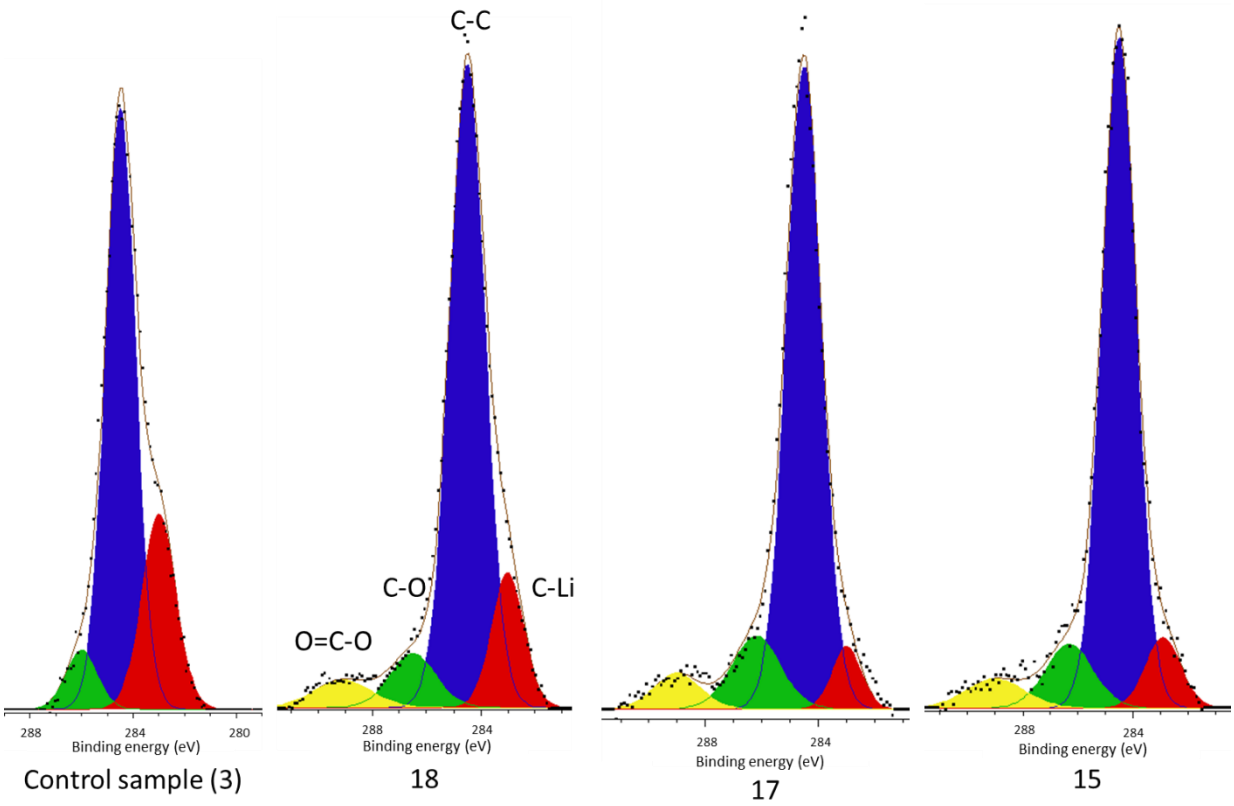

Figure 49. XPS spectra of the negative electrode for C 1s from four cells (3, 15, 17 and 18) after sputtering with Ar^+ ions. The chemical environments (C-Li etc.) are shown by tags in cell 18 and are identical in position and colour to those shown in the other cells.

Figure 50 also supports the finding that there is no C=O in the control cell surface film. The O 1s spectra shows no evidence of the C=O environment at 533.6 eV for the control cell and yet it is present in each of the other cells which have been vibrated. The F 1s and P 2p spectra are included to show that there were no other significant changes in the chemical structure of the

surface film with no evidence of additional bonding environments. The control, and cell 17's F 1s spectra, does contain a peak at 682.5eV. This has been attributed to NaF contamination, which is consistent with the NIST XPS database allocation [198]. There was also some Na present in the XPS spectra in these two cases but the spectra was exceptionally noisy due to the very low concentrations present. In both cases the contribution from NaF is less than 1% of the total F environments; and thus negligible.

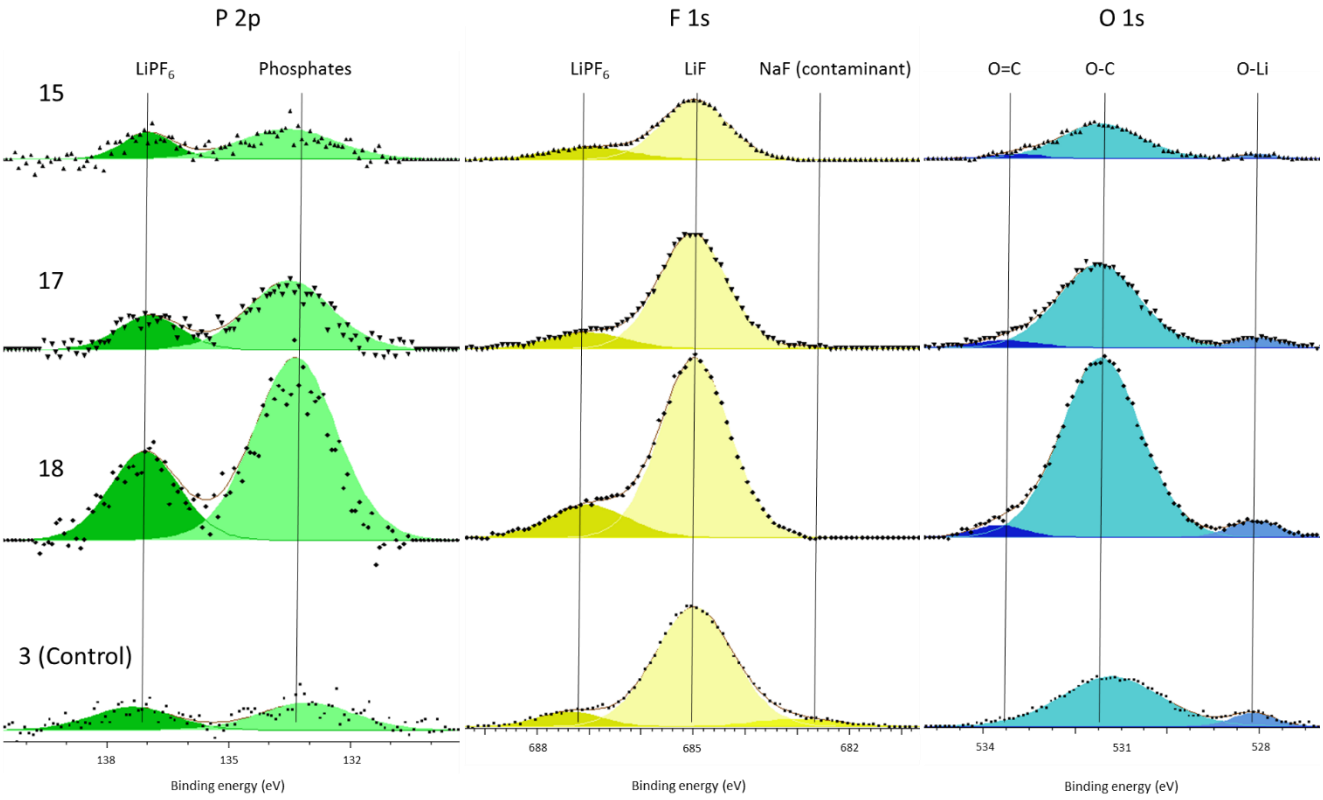

Figure 50. XPS spectra of the negative electrode for P 2p, F 1s and O 1s from four cells (3, 15, 17 and 18) after sputtering with Ar^+ ions. The chemical environments are represented by tags (e.g. LiF) and lines which indicate the relative binding energy alignment.

All C environments in the C 1s spectra have been determined from the concentration of that peak relative to total carbon environments. Peak concentrations for species concentrations come from the P 2p spectra and the F 1s spectra because these are only present within the cell

as $LiPF_6$ initially and thus any decomposition products containing either P or F must come from the same absolute concentration of $LiPF_6$.

Table 5 contains percentage concentrations of chemical environments detected from XPS. It shows an increase in the components corresponding to decomposition of the electrolyte in each of the vibrated cells. This is most notable for the phosphates which increased from 57% of P 2p environments to a minimum of 68% and a maximum of 73% in the vibrated cells. This represents the chemical degradation of $LiPF_6$ salt to form phosphates; it is most pronounced in vibrated cells. In addition, the absence of C=O containing compounds in the control sample, yet presence in the vibrated cells shows that the chemical composition has changed.

Table 5. Relative percentages of chemical environments from chosen peaks and elemental environments in surface film

Cell	LiF (F 1s)	C-O (C 1s)	C=O (C 1s)	Phosphates (P 2p)	C-Li (C 1s)
3 (control)	12%	9%	0%	57%	9%
15	21%	12%	20%	73%	6%
17	14%	14%	6%	68%	3%
18	17%	10%	22%	71%	3%

8.3.2. Electrolyte decomposition products (Negative electrode pre-sputter)

This section presents chemical analysis of the electrolyte deposits present on the negative electrodes of cells subjected to vibration. Figure 51 contains XPS spectra of the negative electrode from the control cell and the three vibrated cells before sputtering and represents changes in the electrolyte deposits. Attribution of chemical environment is identical to those shown in Figure 49. However, while the control sample contains C-C/C-H, C-O and O=C-O environments, it does not contain a carbide peak (C-Li) at 282.8 eV. Given the absence of C-Li in the control sample but its presence in all vibrated cells, vibration is most likely.

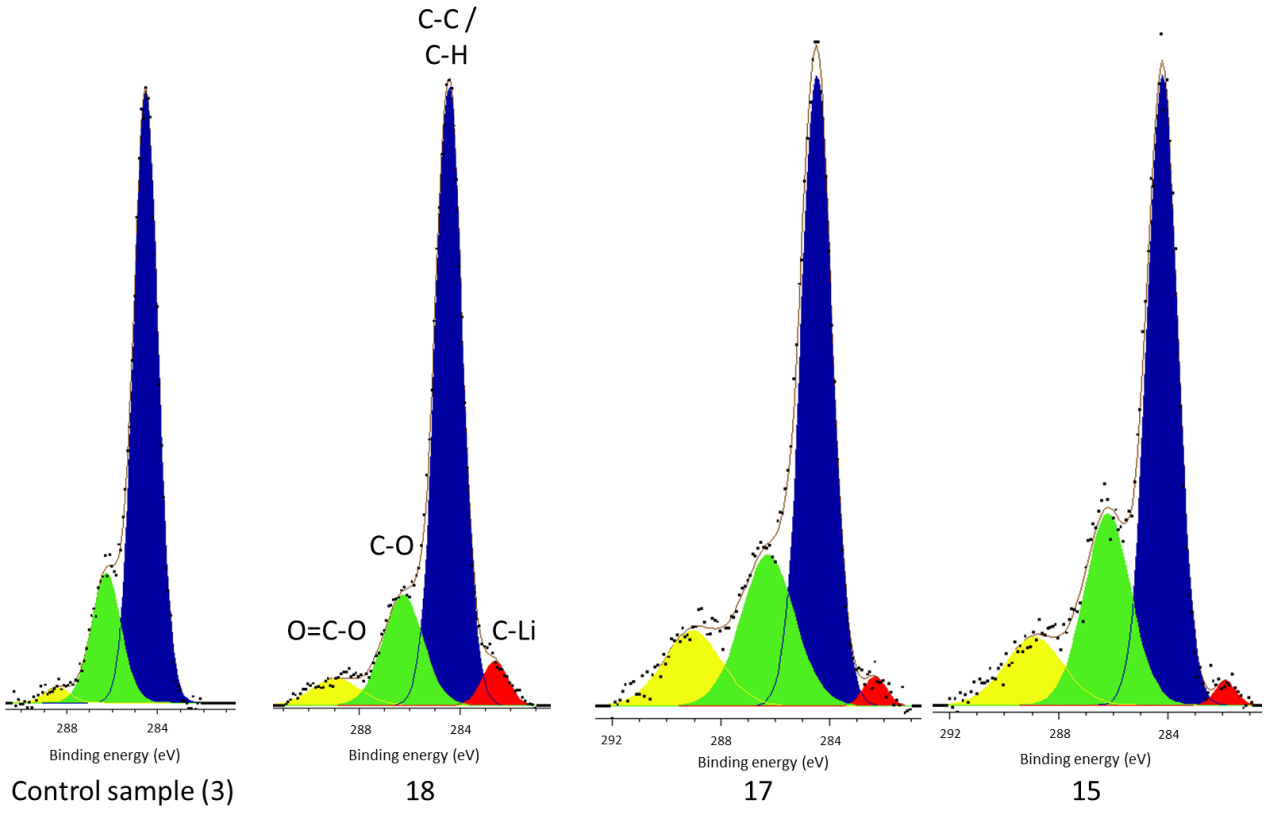

Figure 51. XPS spectra of the negative electrode for C 1s from four cells (3, 15, 17 and 18) before sputtering. The chemical environments (C-O etc.) are shown by tags in cell 18 and are identical to those shown in the other cells

Figure 52 contains XPS spectra from the P 2p, F 1s and O 1s chemical environments of the electrodes pre-sputter. There are two key differences between the control cell and the cells which had been vibrated. First is that in each vibrated cell the percentage concentration from phosphates increases significantly when compared to the P 2p salt component. Secondly, there is an increase in total quantity of O-C chemical environments present in the vibrated cells compared to the control sample.

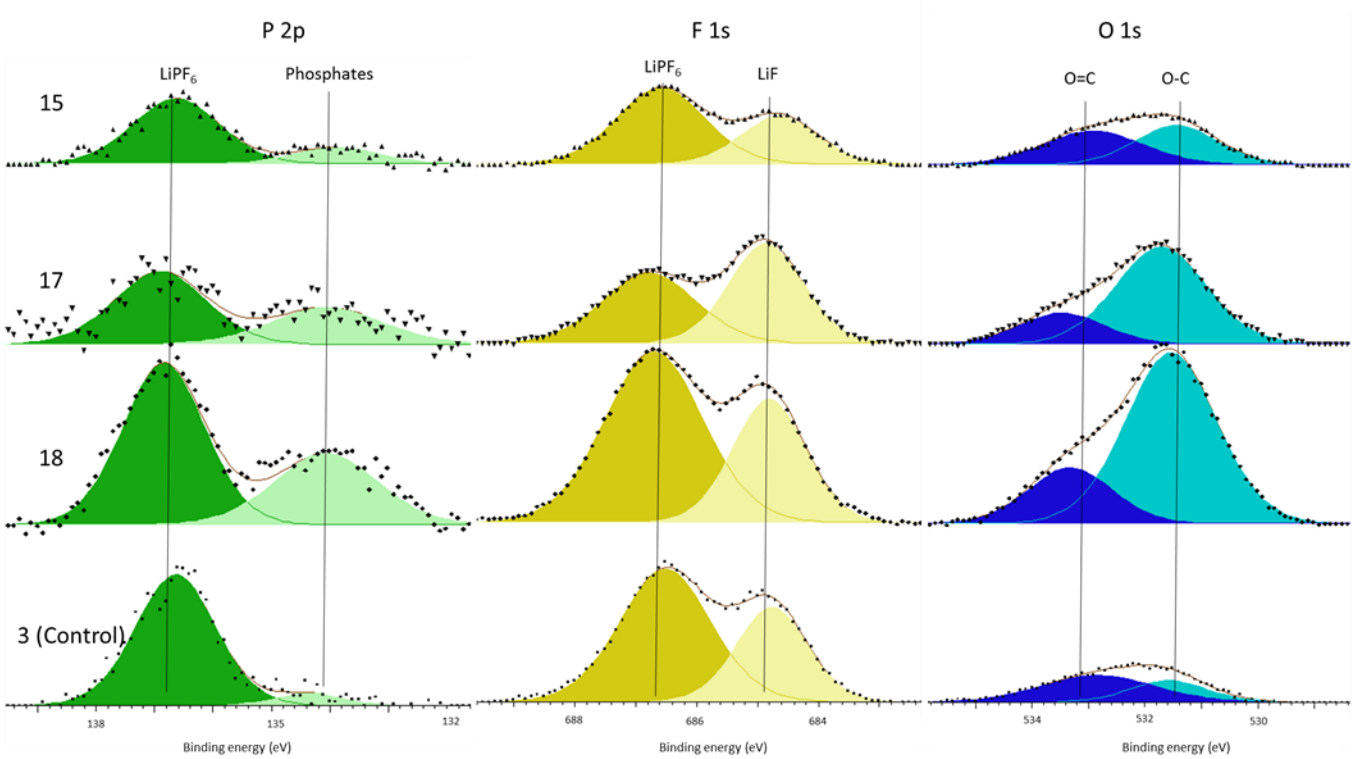

Figure 52. XPS spectra of the negative electrode for P 2p, F 1s and O 1s from four cells (3, 15, 17 and 18) before sputtering. The chemical environments are represented by tags (e.g. LiF) and lines which indicate the relative binding energy alignment

Table 6 contains percentage concentrations of different chemical environments from the electrolyte deposited products. Whilst the LiF concentration remains essentially identical (except for cell 17); the other three environments each show a significant increase in cells subjected to vibration. When comparing the vibrated cells to the control sample the phosphate

component increases by a factor of 2.5 to 5.5 in the vibrated cells whereas the C=O component increases by a factor of 2.25 to 6. The C-O component has also increased, by a factor of 1.4 to 2.2 in the vibrated cells.

Table 6. Relative percentages of chemical environments from chosen peaks and elemental environments in electrolyte deposits

Cell	**LiF (F 1s)**	**C-O (C 1s)**	**C=O (C 1s)**	**Phosphates (P 2p)**	**C-Li (C 1s)**
3 (control)	36%	35%	3%	7%	0%
15	35%	49%	18%	20%	6%
17	53%	77%	19%	39%	5%
18	35%	77%	7%	36%	6%

8.3.3. Discussion

From this work it can be concluded that vibration impacts the lifetime of lithium-ion cells through the removal and reformation of surface film at the negative electrode. This is validated by C-Li being present within the surface film decomposition products of only the vibrated cells and indicates that vibration is the cause. This is because its formation happens shortly after manufacture [104], therefore vibration did not create the Li-C, but rather removed it with the surface film. During vibration some of the surface film (including Li-C) breaks away from the electrode and is subsequently deposited within the cell electrolyte. The cell level manifestation of this reaction is an increase in resistance [196].

In support of this principal mechanism increased phosphate concentrations can be seen within the surface film and electrolyte decomposition products of the vibrated cells. The only source

of Phosphates is the $LiPF_6$ salt. Therefore, the salt must have decomposed to form the additional phosphate components. Kawamura et al. show a possible mechanism for this phosphate formation in their work on the decomposition of $LiPF_6$ [123].

In addition to lithium carbide in the electrolyte of vibrated cells and increased phosphate concentrations, the vibrated cells also contained higher concentrations of C-O and C=O environments in the electrolyte and increased LiF and C-O components in the surface film. It is well established within the academic literature that this suggests an increase in surface film forming reactions [19,124,133].

The presence of O-C=O environments within the vibrated cell surface film, with its absence in the control cell, further supports the previously suggested mechanism. Which is that vibration caused the removal of surface film from the electrode and then new surface film took its place. Because the conditions are different (i.e. lower concentrations of H_2O), the chemical composition of the new surface film is different, hence the inclusion of O-C=O components. Etacheri et al. showed that the main reduction products for ethylene carbonate, propylene carbonate and DMC contain ester compounds (O-C=O) [199]. Commercial cells use additives such as vinylene carbonate to selectively react at the surface of electrodes initially [200] to stop reduction of these species. They use specific quantities of these additives to form a surface film which uses up as little of the useful electrolyte components as possible without impeding cell function later [177]. Therefore, the product (new surface film formed after vibration) is likely to lead to an increased concentration of ester environments, causing an increased impedance and increased cell resistance as the surface film is no longer selectively formed for its role.

It could be recommended that lithium-ion cell manufacturers and users implement a vibration profile within accelerated testing profiles to determine the expected cell lifetime. Especially because the mechanism is different from those dependent on temperature, SoC, current rate

and % Δ SoC. However, the electrical performance for these cells, which is provided here [196] contains large errors dependent on vibration profile and between cells. Therefore, although the mechanism showed consistency within post-mortem analysis there remains a question about its impact for other cells, manufacturers and chemistries.

8.4. Change in temperature and SoC

This section contains post-mortem XPS analysis results from the surface film of cells subjected to different storage temperatures and SoC. The cells tested were one from each condition of temperature and SoC.

8.4.1. Introduction

Figures 53-55 contain XPS spectra of the negative electrode from binding energies that represent the C 1s, O 1s, F 1s and P 2p chemical environments respectively. They are presented in such a way as to make trends dependent on temperature or SoC easier to distinguish.

Assignment of peaks to specific chemical environments is representative of those presented by others [19,124]. Although such assignments are always open to interpretation, the $ROCO_2Li$ peak is especially spurious. It is possible that this peak is actually a satellite graphite peak that occurs with high concentration of sp^2 hybridised carbon (graphite) [126]. Its presence is typically distinguishable if there is an asymmetric tail toward higher binding energy for the 284.4 eV peak. The problem with these samples is that this tailing may also be due to the presence of C-O functionalities. Although the $ROCO_2Li$ component is shown in two samples, due to this ambiguity, the conclusions drawn from the spectra assume it is not present at all.

The principal peak for 45ºC and 80% SoC in Figure 53 is from C-O functionalities and not graphite. It is possible to adjust this peak so that this main peak is C 1s graphite at 284.4 eV. However, because this shifting occurs for all chemical environments if this is done, it would also adjust the O 1s 'C-O (2)' peak 1.3 eV to lower binding energy, which would move it to 0.7 eV less than the O-Li peak present in the other samples. There are two reasons this is not chemically possible, only metal oxides are present at binding energies that are within this region and there were no other metallic species present in the survey scan of the material.

Secondly, even if it had bound to another metal; a lithium ion is the smallest, and is a highly charged metallic species. Binding with other metals would move the peak to higher not lower binding energy. Therefore, it would move the O 1s peak outside of the possible values for these samples. This problem is echoed in the F 1s peak positions, including the shifting of LiF out of the demonstrable area of the F 1s spectra. Assuming that the simplest explanation is the most likely, the C-O peak has been assigned as the principal peak of the C 1s spectra.

8.4.2. Surface film chemical composition

The C-O component of the C 1s spectra of Figure 53 is approximately equal at 10ºC, irrespective of SoC. There is no change at a higher temperature (25ºC) and low SoC but a significant change at the highest temperature (45ºC) and low SoC, an increase in percentage of C-O to 32% of all C 1s environments. Once the SoC increases from 20% to 80% the concentration of C-O component relative to other C 1s functionalities increases further. Going from a C-O concentration of 32% at 20% SoC to 75% at 80% SoC.

Because there is no chemical reaction that involves reversible formation of C-O within lithium-ion cells, it is assumed that this formation is from irreversible reduction of electrolyte solvents at the surface of the electrode. As temperature increases the concentration of C=O-C species also increases, moving from 1-2% at 10ºC irrespective of SoC, and 0% at 25ºC, to 30% and then 76% at 45ºC for 20% and 80% SoC respectively. This shows that temperature is the primary factor in C-O formation / reduction of electrolyte until at higher temperatures and SoC at which point the increase is much sharper than expected. What it also suggests is that the species formed at these higher temperatures are primarily small carbonates for the 45ºC / 80% SoC condition. This is because if polymeric or longer chain carbonates were the primary reaction product then non-graphite C-C bonding would still dominate. However, in this case

C-O bonding is primarily the product. Therefore, it contains a higher concentration of methyl carbonate derivatives because these contain less C-C bonding (refer back to Figure 9). This conclusion is supported by increased concentrations of O=C-O functionalities in the C 1s and the O 1s spectra (Figure 54) with increasing temperature, which is similarly indicative of electrolyte reduction.

What this means is that surface film formation is most affected by temperature, and that formation of surface film is primarily methyl carbonate type derivatives at 45^{o}C / 80% SoC.

Section 3.2.4.1 refers to the underlying theory behind lithium plating at increased current rates. The specific chemical mechanism highlighted here, of changes in the chemical species as a consequence of lithium plating may be specific to the cells used. In this case the cells used were NMC-type cathode materials with graphite negative electrodes. It is likely that cells with other chemistries, particle sizes, electrolyte selection or additives will not induce the same mechanisms. What it does show however is that post-mortem analysis can be a critical component of any electrical model to validate or refute assumptions made with respect to surface film growth or alteration with temperature, SoC or other operating conditions. For other chemistries and cells it is possible to apply a higher temperature profile to induce a faster rate of degradation without chemically altering the surface film composition. What this work does show, is that it is not possible to know if this assumption is correct without post-mortem analysis.

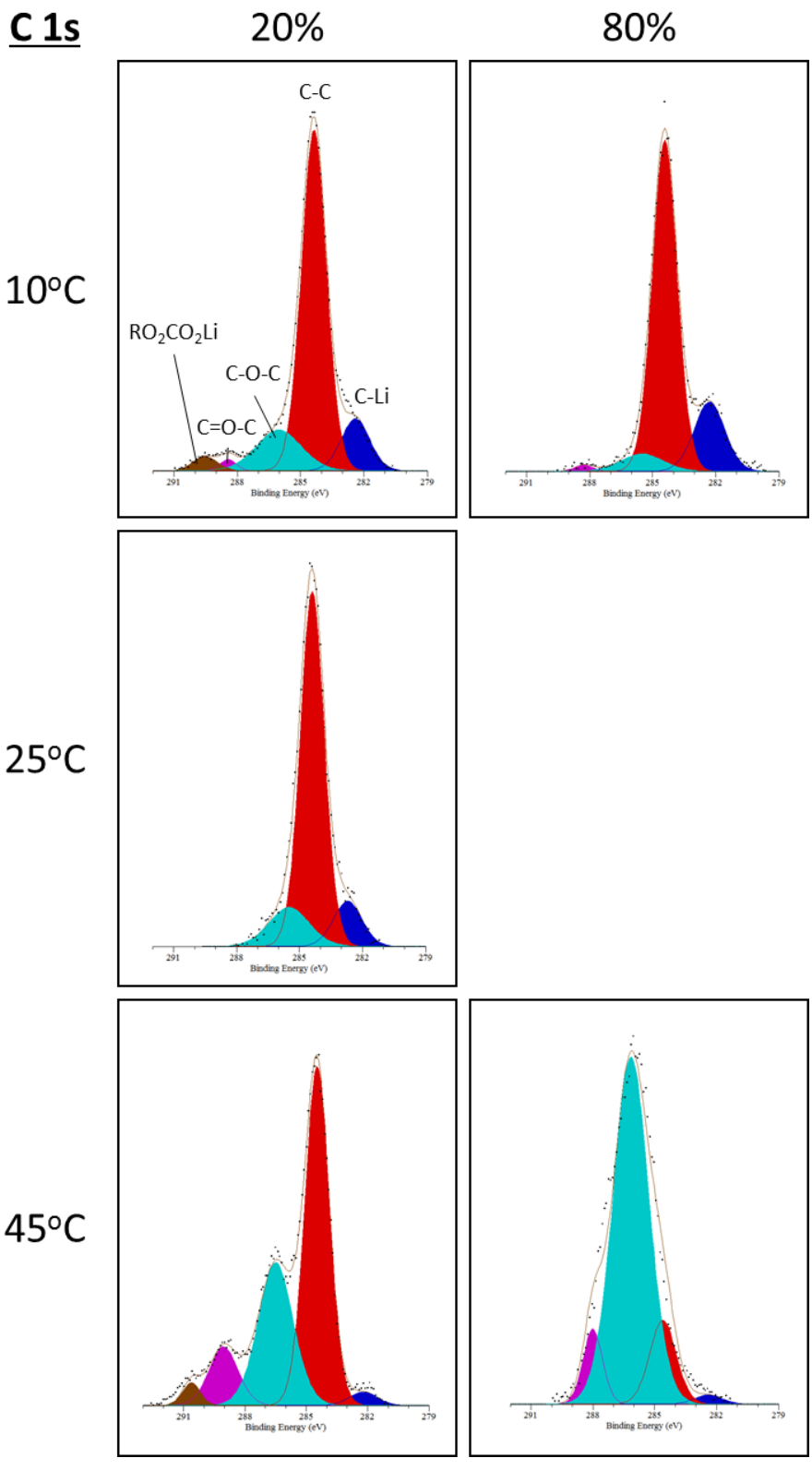

Figure 53. C 1s x-ray photoelectron spectra from the negative electrode of cells subjected to different temperatures and states of charge during storage for a period of 30 months. Identical peak colours represent the same chemical environment based on peak binding energy and width values

The O 1s spectra (Figure 54) is difficult to de-convolute for specific chemical environments due to the variety of chemical species that exhibit at the same binding energy (e.g. phosphates, carbonates, alumina, silicon oxides and organic C-O components). This is not true for the metal oxides, which tend to exhibit at 1-1.5 eV lower than the metal carbonates (e.g. C-O) and phosphates [201]. This lithium metal oxide peak is present in electrodes at 10^{o}C and 25^{o}C but not 45^{o}C. What is interesting is that the relative percentage of this peak is approximately the same for samples at 20% SoC (6-9%) irrespective of temperature but increases to 25% of total O 1s environments at 80% SoC and 10^{o}C. Aurbach et al. [202] have shown that Li-O is a product from plated lithium. This work shows the highest concentration of Li-O in the samples from cells stored at 10^{o}C and 80% SoC. Ely and Garcia note lithium nucleation growth during storage without cycling [203]. This is reasonable because lithium plating is produced by two kinetically rate limited but competing reactions occurring at the surface of the electrode, intercalation and lithium plating [68]. Lithium is still present at the surface of the electrode during storage and this work shows it has caused lithium plating to occur, but at a much slower rate.

However, there is no guarantee that these results can be extrapolated to all cell types. Smart and Ratnakumar proposed this competing mechanism interpretation by showing that lithium plating can be limited and even stopped through electrolyte choice [68]. It is possible that the detection of plated lithium at the 25^{o}C condition in these cells is a result of higher concentrations of ethylene carbonate (EC) or electrolyte additives. A cell with lower concentrations of EC or electrolyte additives may not show formation of Li-O species due to a reduction in plated lithium.

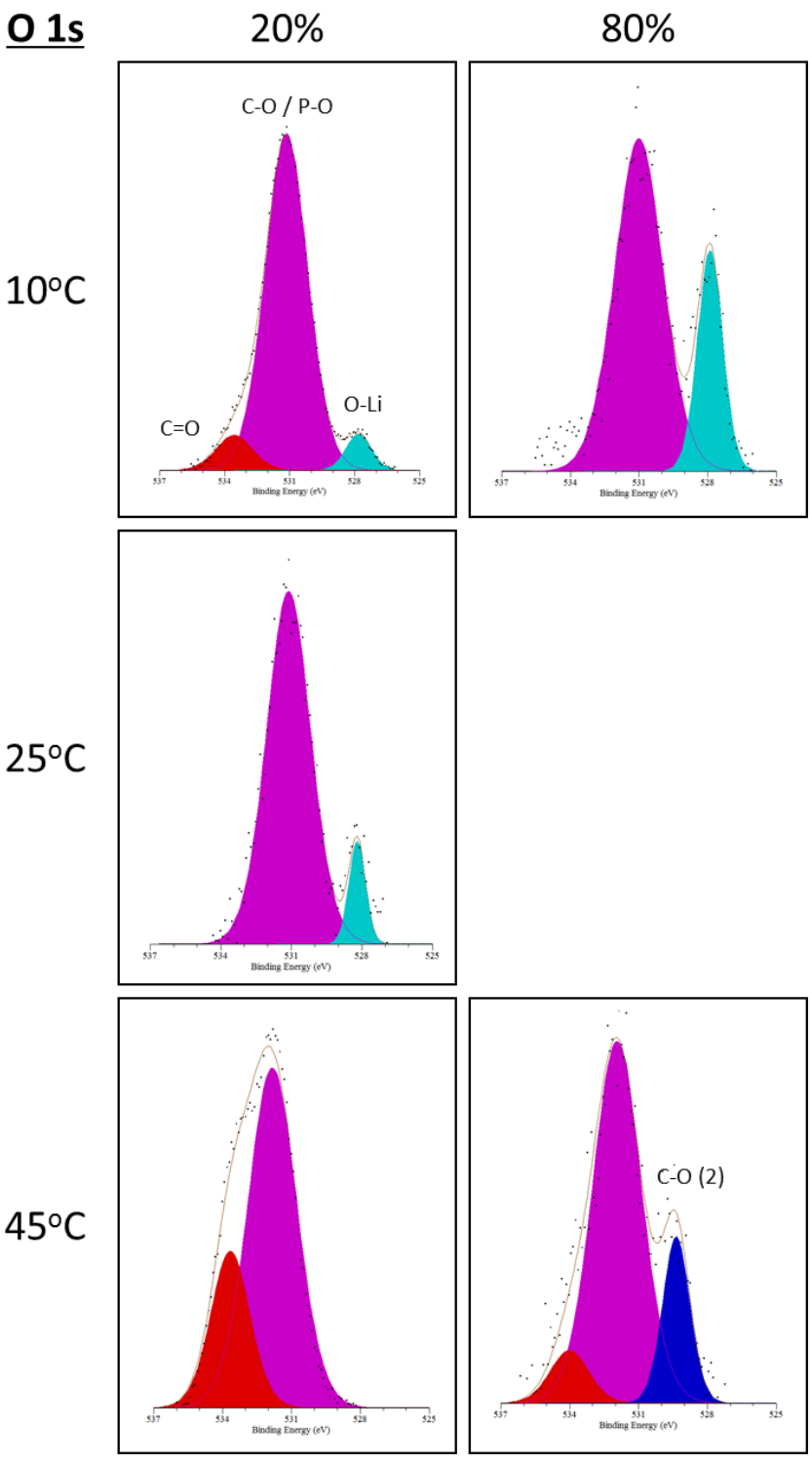

Figure 54. O 1s x-ray photoelectron spectra from the negative electrode of cells subjected to different temperatures and states of charge during storage for a period of 30 months. Identical peak colours represent the same chemical environment based on peak binding energy and width values.

The final point of interest is the formation of LiF, which is a component of the surface film [124]. The F 1s spectra shows that as the temperature increases the concentration of LiF relative to the $LiPF_6$ salt reduces to nothing at 45ºC and 80% SoC. Assuming the salt concentration of initial cell formation is consistent across samples means that increased temperature is reducing the quantity of LiF formed. At 45ºC and 80% SoC there is no LiF present at all, and only a $LiPF_6$ component. At 80% SoC and 10ºC the highest concentration of LiF (82%) is present. Dedryvère et al. [127] noted the increase depends on higher SoC and proposed a mechanism of LiF formation from small lithium methyl carbonates. This mechanism is supported in these results, because when the carbonate concentration is at its highest (45ºC / 80% SoC) LiF is not present in any concentration.

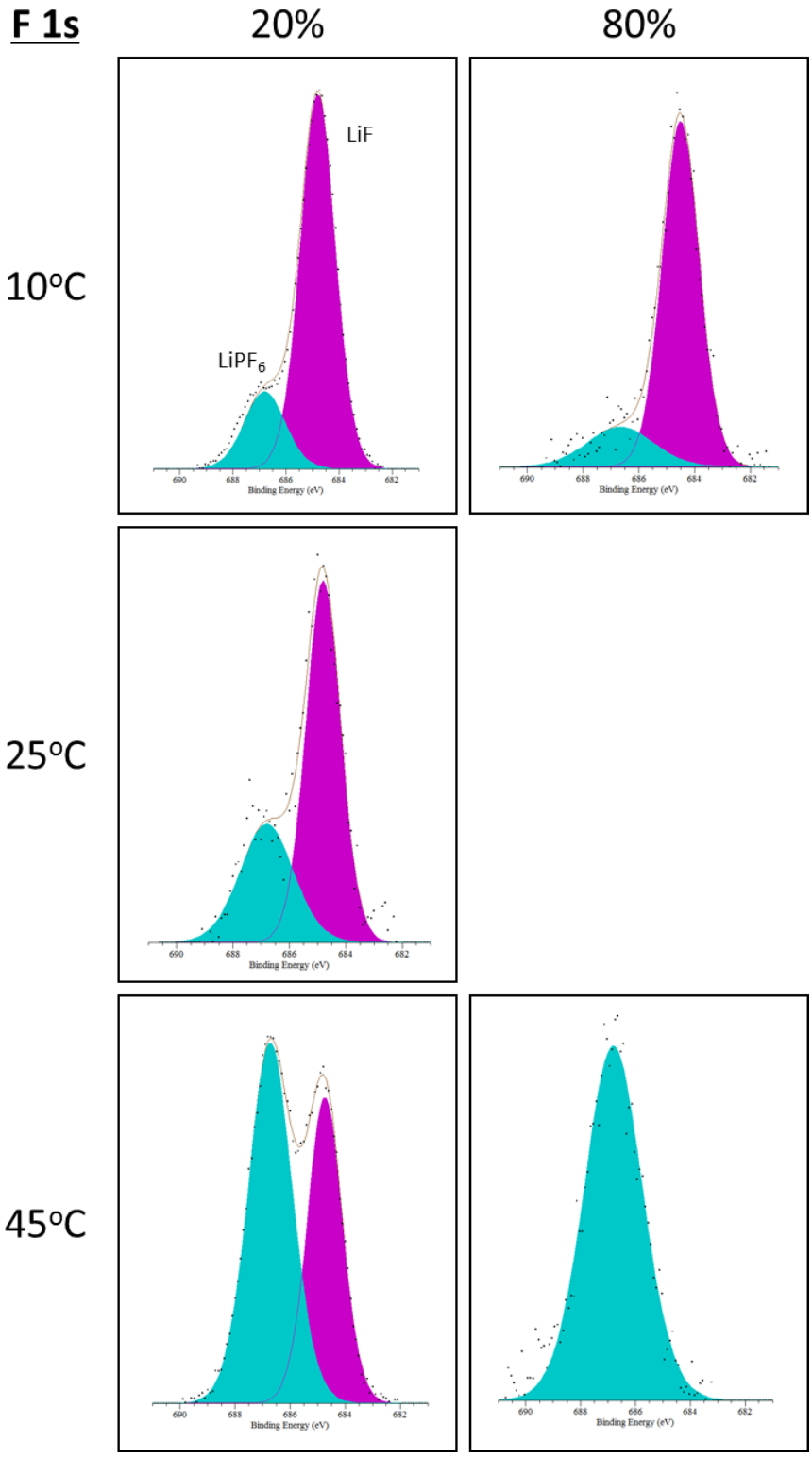

Figure 55. F1s x-ray photoelectron spectra from the negative electrode of cells subjected to different temperatures and states of charge during storage for a period of 30 months. Identical peak colours represent the same chemical environment based on peak binding energy and width values.

8.4.3. Discussion and conclusions

All of this means that SoC and temperature primarily introduce two different mechanisms of degradation. One at temperatures of 10^{o}C and another at 45^{o}C. This general conclusion has been shown by Waldmann et al. [22] and is consistent with this study's electrical data that shows these two conditions as impacting cell performance the most. However, this is not the only reaction occurring otherwise the low temperature would have the highest capacity fade, which it does not. This is a limitation within these results where only the negative electrode surface film has been studied. It is possible that reactions at the cathode contribute to the capacity fade, as noted in the work of Guan et al. [204] but are not studied for these cells.

What is useful is that it also shows post-mortem analysis can be used to track certain markers that can be attributed to specific storage conditions. These are the increase in C-O component and reduction in LiF, at higher temperature and accelerated by higher SoC. And, the increase in the O-Li component, which forms at low temperatures and is similarly accelerated by high SoC.

What this could mean to accelerated testing of lithium-ion cells in the future is that increasing SoC but lowering temperatures may speed up Li-O formation by a factor of up to four. Reducing the time spent performing testing by the same factor. After this has been completed, it may be possible to then focus on increasing the C-O component of the cell by maintaining a cell at 80% SoC and 45^{o}C for one hour instead of cycling at 25^{o}C for 6 hours.

However, it is not this simple, it is also possible to see many instances where the chemical composition of the electrode varies with SoC and temperature in other ways. The disappearance of the C=O functionalities at 20% SoC and 25^{o}C shows that the surface film is too complex to be able to do this type of acceleration with accuracy. The specific chemical composition of the surface film has changed at these conditions. Therefore, although this work shows an

accelerated ageing profile might be able to use two extreme conditions this is no different from previous work [22]. It also could have been inferred from the electrical data shown in Chapter Five. What the electrical data did not show however is that the surface film alters at this intermediate temperature. This is not consistent with the Arrhenius type acceleration that is often used to support accelerated ageing tests [205]. As Spotnitz makes clear [16], if the chemical composition of the film alters then the Arrhenius relationship cannot be used because it is no longer a single reaction that is taking place. The post-mortem results from this work suggest that an accelerated test profile requires multiple different temperatures to be consistent with actual cell conditions.

9. Discussion

This chapter discusses the process used for post-mortem analysis and the requirements for accelerated ageing. This is done within the context of whether post-mortem analysis can be used to detect material changes in commercial lithium-ion cells after accelerated lifetime testing.

The position of this chapter within the context of this innovation report and the wider portfolio is shown in Figure 56.

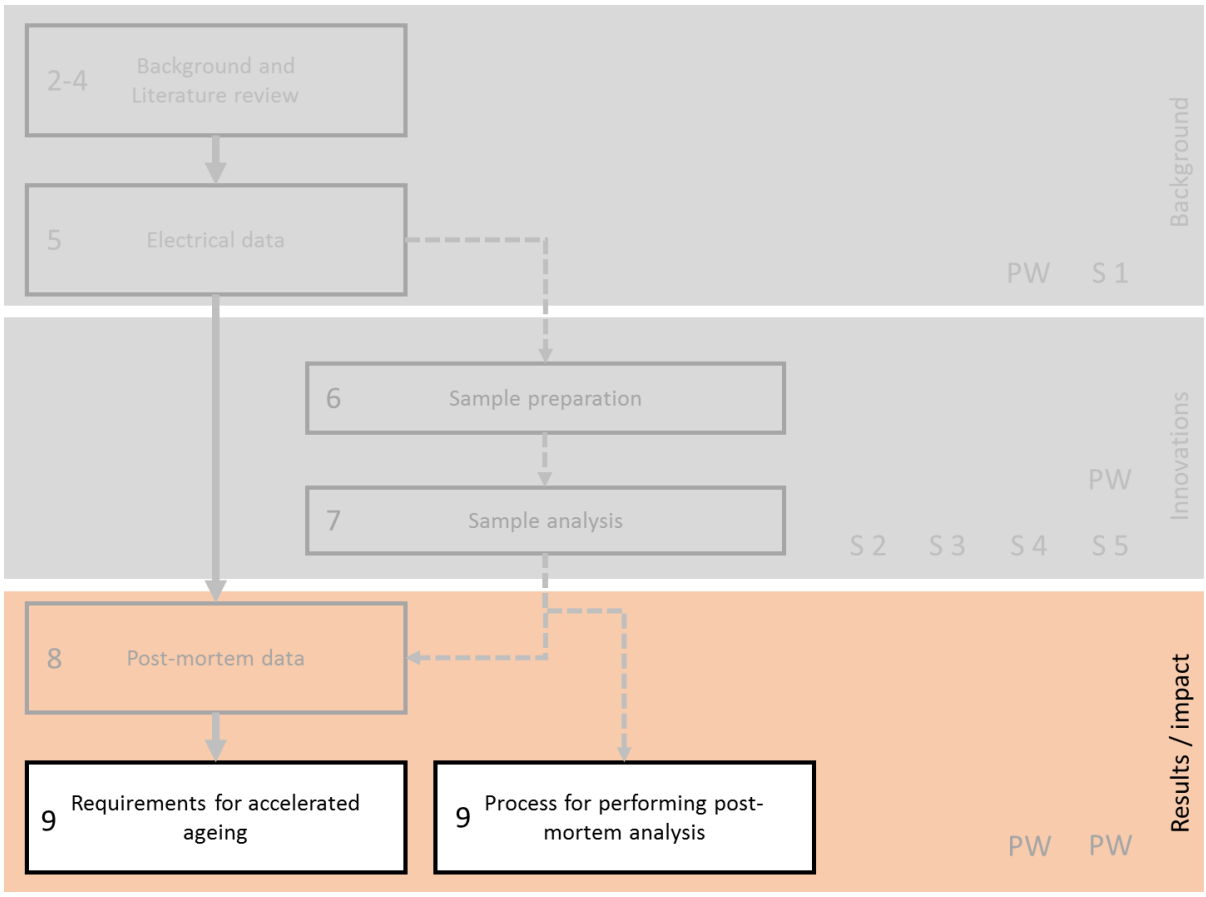

Figure 56. Outline of the engineering doctorate portfolio, chapters within this innovation report are shown as numbers to the left of white topic boxes.

Post-mortem analysis was performed on cells subjected to different operating conditions over accelerated testing periods. Because post-mortem analysis of this type is so common

[206,22,205] it might be expected that the processes used within literature do not alter the sample itself. And, that the methods of studying the organic [19], inorganic [127] and polymeric components [187] as well as overall thickness [139,140] of the surface film are well established. However, this work revealed that the methods used to open 18650-type cells [22], process the harvested samples [207], study the films polymeric component [146] and the surface films thickness with XPS [140] contained significant limitations that either affected the chemical composition of the film or did not do what was being proposed.

After overcoming these limitations, it was possible to create an optimum method of performing post-mortem analysis on cells subjected to different accelerated conditions. Using this method this work shows how vibration is a potentially critical component of any accelerated testing profile. That changes to the chemical composition of the surface film from increased charging rates causes primarily increases in surface film thickness. And how the assumption there is no change in the chemical composition of the surface film with changes in temperature and SoC was not true for these cells.

9.1. Post-mortem analysis

9.1.1. Opening and sample processing

Our work shows that it is possible previous post-mortem analysis may have observed changes that were caused by the process of cell opening and sample processing. This may have been the case in the work of Barrett et al. [173] for example. Considered within the framework of post-mortem analysis such results could lead to spurious conclusions on chemical changes to surface film and create a skewed materials based evidence process from inaccurate results. The process of opening 18650-type cells with rotating disc-saws [208,176,173,209] and washing the electrode surface with low-boiling point solvents [105,210,139] is done in the vast majority of post-mortem analysis studies.

Although there had been some discussion about the impact of washing on the surface film being analysed [158] a systematic study had not been performed. This work shows that this is an oversight because washing removes surface film material and selectively removes LiF. Furthermore, washing has been shown to be unnecessary as the low boiling point solvents evaporate at low pressures and therefore a low temperature antechamber is more suitable.

The process of cell opening with a rotating disc-saw for anyone who actually performs it should raise concerns. It creates large quantities of dust, heated metal can be observed and the jelly-roll, in this work, was always cut, creating short-circuits. This work provides evidence that the process of cutting cells open with a rotating disc-saw can cause changes in the surface film of the electrode. Jungst et al. [211] for example, opened a 18650-type cell with a rotating disc-saw and then wash the electrodes prior to investigating the quantity of metals in the cell. They mention that washing did not reduce the quantity of metals present- suggesting that they understand this could be a potential factor. However, there is no mention of the impact that opening the cell had on those concentrations, or where the sample was taken from within the jelly roll. They found aluminium, nickel, cobalt and copper at both electrodes which are all present in steel. This work also noted increases in metals, especially copper, but exclusively in the samples that were opened with a rotating disc-saw. Therefore, the impact of using these methods has implications on analysis of the surface film. There are a large number of ways that a delicate surface film of unknown chemical composition could be chemically altered as a consequence of these processes due to heat, solvation and contamination. Therefore, further analysis of films after such interference is unlikely to be representative of the in-use conditions. Not only does this uncertainty of potential contamination invalidate post-mortem results but in some cases, such as Jungst et al. [211] and Barrett et al. [173] the conclusions drawn have a direct connection to the method used.

Opening of 18650-type cells with a rotating disc-saw appears to be unnecessary and instead the process created in this work of using a pipe cutter and peeling the can open could be employed in its place. The effect of washing the electrode surface should be considered important where study of that surface is required. If these processes are not adhered to, the results obtained may be incorrect and cause conclusions to also be incorrect – this may have costly implications for OEM who would rely on post-mortem analysis. Because they may rely on them for long term accelerated ageing tests.

9.1.2. Analysis of the surface film

XPS is the most common method for chemical species analysis of the electrode surface film [126,155,127,156]. In addition, there is a requirement to understand the thickness of the electrode surface film in validating the impact that accelerating conditions have if they do not alter the surface films chemical composition. This is commonly performed with XPS, using sputter-depth profiling [139,140]. However, the process of sputtering is not uniform for all materials because the rate of sputtering differs dependent on chemical composition [212], Li^+ species can also migrate during analysis [212], and morphology of the sample changes the absolute counts [212]. Cell electrode surface films are also highly inhomogeneous [213]. This means that sputter depth-profiling should not be used to determine surface film thickness. It is possible to overcome these limitations by sputtering until a steady-state is reached and then comparing the concentration of non-graphite C 1s components to graphite C 1s components. This work shows this method being used to determine the thickness of negative electrode surface films from cells subjected to different rates of charge and different temperatures and states of charge. It shows that where the chemical composition of the material does not change the quantity of surface film increases linearly with resistance. Therefore, this method provides

a different method of analysis and allows relative thickness of the electrode surface film to be estimated using XPS.

Analysis of polymeric species with HPLC / GPC systems is also important in understanding the surface chemistries of these samples because XPS cannot be used to determine the polymeric component [133]. And therefore, making a calculation of surface film thickness may be skewed by identical XPS results but non-identical surface film composition. HPLC can be used to measure these compounds, however the presence of $LiPF_6$ and subsequent formation of HF [135] mean that samples cannot be processed without first removing $LiPF_6$ salts [146]. A method has been previously used to remove this salt from the sample prior to analysis with gas chromatography [146]. However, this method used water during the sample preparation outside of the glove box. And, although their work noticed no impact on equipment over a number of years, there appears to be no system in the method of stopping reaction between the sample and moisture, during the intermediate period. Reaction with the sample may cause error in later analysis of the surface film. It is possible to overcome this problem by adding $CaCO_3$ to the sample within an inert environment; because calcium preferentially reacts with fluorine to form CaF_2. In addition, the use of a high boiling point solvent means that they can be used within the glove box environment. This requires a re-solvation and evaporation period after use. It is recommended that a Ca containing substitute be added to the sample prior to hydrolysis and that this be performed inside a glove box. This then allows HPLC to be used in analysis of the polymeric components of lithium-ion cell electrodes without damage to the sample.

9.2. Accelerated ageing tests

Accelerated ageing experiments operate on the assumption that under accelerated ageing conditions the chemical composition of the surface film does not change [16]. The results of this work augment the findings of Bloom et al. [17] that chemical changes to the surface film occur under different cell operating conditions other than temperature. This work extends their work to include vibration and increased current rates during charge. It also improves on this previous work by showing the chemical changes from analysis of the materials contained inside the cell. This works results diverge from Bloom et al. work [17] in that variations in temperature from 10^{o}C to 45^{o}C contained differences in the chemical composition of the surface film. This may be due to the fact that Bloom et al. work was performed at temperatures of 40-70^{o}C whilst this study was performed at temperatures of 10-45^{o}C. Therefore, it is possible that higher temperatures do follow Arrhenius behaviour without a change in chemical composition to the surface film, as they indicate. However, as shown by the surface film composition of the cells kept at a temperature of 25^{o}C, this assumption was not consistent for this work.

9.2.1. Increased current rate during charge

The impact of charging rate had been electrically characterised before [214] and more recent studies have shown similar electrical performance to those presented in this work [215] primarily that increased C-rate decreased cell performance. However, electrical performance suggests that increased C-rate would linearly impact the capacity fade of the cell and that an accelerated testing profile may be able to use C-rates of up to 6-C. Post-mortem analysis of the negative electrode surface film showed that C-rates of up to 4-C could be used in an accelerated test profile to increase the resistance and capacity fade during lifetime of lithium-ion cells under charging conditions. It showed that at least part of the degradation observed was caused by

temperature. Although results from this work cannot decouple the effects of temperature and charge rate it shows that temperature gradients exist within the electrode material that follow manufacturing induced faults that may have been created by insufficient electrode wetting, and by association increased temperature gradients. This non-uniform ageing supports the conclusions of Klett *et al.* [206] in their tests on commercial cylindrical cells with a different chemistry which, suggests that electrolyte wetting is the probable cause – and therefore that this failure may not be induced in other format cells. As mentioned previously, this explanation of electrode wetting is not the only potential source of temperature gradients. Because the centre of the electrode roll is furthest from the negative and positive tabs, and the outer cell can, over prolonged charging periods the temperature along this central core will increase. Such an increase may have caused the delamination and surface film alterations irrespective of whether it was sufficiently wet. This work, does not prove that electrode wetting is the source, only that the damage is associated with increased temperatures.

The consequence of these results to JLR come from the speed with which testing can be performed during a fast charge section of an accelerated testing profile. Instead of taking 85 minutes to charge at 0.7-C, the cell could be charged at 4-C reducing the testing time to 15 minutes. This equates to an increase in the speed of a fast charge profile by 5.6 times. This testing profile provides value to the type of accelerated testing that JLR performs by reducing the time that it can be performed in and could not have been predicted from electrical performance alone.

There is a difficulty in coming to this conclusion from this data alone. It is that this work assumes increasing the c-rate of charge only impacts the negative electrode surface film. Other studies have shown that increased charge currents can also crack the graphite particles [216]. This may lead to loss of lithium sites available for intercalation [217] and thus effect cell performance. If this has occurred for these cells, then a measurement of the surface film

compared to cell resistance is not the entire story. Although a rise in surface film percentage was consistent with a rise in C-rate and resistance further work would be required to exclude particle fracture from the picture completely. Therefore, this work would benefit from further analysis with XRD to verify whether this assumption about surface film being the main cause of performance decline is true.

9.2.2. Vibration

The impact of vibration on the materials within lithium-ion cells had not been studied previously for long-term ageing studies. Damage from vibration had referred to damage occurring in electrical connections [218] and not in changes to the surface films composition. The presence of Li-C components in the surface film, formed during the cells first cycles in the presence of H_2O, shows that the surface film on the electrode may become detached from the electrode surface during vibration. This is then replaced by a non-selectively formed surface film. This work suggests that vibration follows a dissolution of surface film type profile, typically only observed at much higher temperatures [219]. This means that any accelerated ageing lifetime tests for lithium-ion cells should contain a vibration profile.

There are limitations to the conclusions that can be drawn from this method and reaction mechanism in isolation. It is possible that changes in temperature, SoC, current rate or other conditions might be catalysed by the surface film being removed. Malmgren et al. show that reduction of the electrolyte on the surface of freshly passivated electrodes caused a much higher reduction in capacity than with non-passivated electrodes [18]. Therefore, when this vibration induced mechanism is coupled with a high-capacity fade mechanism the rate of performance decline may be different. This means that vibration must be coupled with capacity fading mechanisms like temperature or increased SoC to determine its absolute impact.

In addition, the cells undergoing post-mortem type analysis assumes that the vibration profile employed is representative of 10 years of vibration. If the vibration profile used in this study is more aggressive than in a real-world condition, then the mechanism seen in these results may not be accurate. Although, it is beyond the scope of this work to investigate the accelerated profile conditions themselves. The post-mortem methods applied here could be used to investigate changes to the surface films composition during different vibration profiles to address this.

9.2.3. Temperature / SoC

Ecker et al. suggest that Arrhenius type acceleration works for storage conditions of different temperature below 60^{o}C [205]. Spotnitz et al. state that this is dependent on if the chemical structure of the surface film does not change [16]. The results in this work directly contradict the proposition of Ecker et al. by showing that different surface film compounds are formed at different temperatures and SoC [205]. Most notably, this is O-Li products at low temperature originating from lithium plating and C-O components at high temperature.

It may be possible to integrate the two worst conditions and ignore the intermediary conditions. The composition of the two extremes suggest that using a 45^{o}C or 25^{o}C with higher SoC may cover the worst case scenario of cell performance decline. An accelerated test profile would therefore only need to include low temperature / high SoC and high temperature / high SoC to cover both types of surface film composition. This means that the study within this work could be duplicated with six cells, instead of 27 reducing the cost by up to 78%; this is a significant cost and time reduction. However, it also shows that there is no short cut to accelerated testing if accuracy of prediction is required. The Arrhenius assumption that it is only the reaction rate of identical reactions being accelerated does not appear accurate.

9.2.4. Percentage change in SoC

Post-mortem analysis of the cells subjected to different % Δ SoC was handicapped by a USABC electrical test-profile which induced damage that was not representative of real-world conditions. It is most likely that the additional cycles caused a shift in the negative electrode potential which caused grain boundary etching and delamination making it not possible to study the surface film.

Although this test does not show any useable results for accelerated testing requirements, it provides an opportunity to highlight the advantages of post-mortem testing. The test profile used gave electrical performance that was consistent with previous work that predicted its impact [7]. Indeed, the cells showed much better electrical performance with a reduced percentage change in SoC than with the 0-100% SoC profile. This is probably the reason that other groups who were also using it had not highlighted the USABC test requirements as a problem.

Upon cell opening it became clear that the test profile had induced damage that was inconsistent with that expected from electrical data. Post-mortem analysis showed another condition which supported the binder degradation mechanism. Without post-mortem analysis this supporting information would not have been available. It would be assumed that the USABC test profile was sufficient and that the degradation recorded in capacity and power was accurate. This was not the case, and as a direct consequence of this work the USABC have been reviewing this information for future revisions of the manual. Dr Ira Bloom presented this information to them in the autumn of 2015.

For the purposes of understanding the impact of a % Δ SoC on the cells internal materials and whether it is equivalent to other conditions, these tests must be performed again on new cells, without the additional cycles.

9.3. Collective impact for JLR

This work proposes that instead of submitting cells to multiple SoC and temperatures, instead focus could be made on the low temperature / high SoC condition and the high SoC / high temperature conditions to accelerate testing time. In addition, instead of using multiple charging rates a single rate of 4-C could be applied to track the capacity and resistance. Therefore, acceleration of each charging portion of the accelerated test profile could be improved by more than an hour.

For this work, the type of test time saving presented would reduce the total number of temperature / SoC cells from 27 to 6, reducing the total cost by up to 78%. For current rate, using only a 4-C test profile calculated as representative of cell conditions would reduce cell numbers required from 24 to 6 reducing the cost by 75%. For vibration, by removing three cells the total cost savings would be 33%. With the removal of the need to test for orientation or pressure as well the total cost savings would be up to 75%.

A deliverable for JLR is that the time it takes to perform an accelerated test profile can be reduced without chemical changes to the surface film at the negative electrode. This is possible by charging at rates of 4-C, storing cells at 80% SoC for both 10^{o}C and 45^{o}C. It also shows that for the accelerated ageing tests to be representative they should include a vibration profile.

This work presents methods that can process key parts and components of the cell without causing damage. It addresses how to open cells, process them and the main techniques to use – and how to use them to abstract the optimal amount of information. The aim of this work was to investigate how post-mortem analysis can be used to detect material changes in commercial lithium-ion cells after accelerated lifetime testing.

This work has drawn direct comparison between cell conditions during accelerated cell conditions and material changes at the negative electrode surface film. It brings together a vast sum of information into a single method.

This does not mean that it is perfect. The approach applied for XPS and HPLC analysis removes the ability to differentiate between all chemical mechanisms. This is shown by the fact that XPS collates all C-O / C=O / P-O and other groups together. This means that locating the specific reaction mechanism is not possible. HPLC does the same but with the polymeric components. This was the optimum approach for commercial cells due to the number of possible chemicals present. Improvement could be made to the study by expanding the choice of methods further to investigate whether more information is available or warranted.

Another problem is shown by an apparent dichotomy in the results. The cells subjected to high temperature showed variances in the chemical species present. Yet, the cells subjected to higher currents did not – even though temperature was the cause of the delamination at 6-C. It is possible that this is caused by the difference in cell materials. Perhaps the high current cells contained additives to stabilise at high temperature. The important thing is not the actual results, but rather the fact that it varies at all. This means that comparison of these results to other chemistries, materials or cells may not be possible. For JLR, the decision would have to be made whether or not they can make such assumptions on transfer between suppliers. Or whether post-mortem analysis becomes a critical part of cell diagnosis and selection to identify such disparities.

9.4. Next steps / future work

Firstly, the type of analysis performed in this work needs to be done on cells subjected to different % Δ SoC cycles to compensate for the erroneous results obtained with the USABC testing profile. This could also be extended to cells subjected to different discharge rates.

Building a correlation between electrical performance and internal material analysis is convoluted. The internal working of the cells is more complicated than the much simpler, sum of all parts, capacity or resistance values. However, the answers available also provide more information. The significance of this work would benefit from more post-mortem datasets, with respect to temperature and SoC.

What these results do not show is the impact of conditions when coupled together. For example, vibration may cause catastrophic cell failure if coupled with temperature or higher rates of charge. It could also have less of an impact when coupled with other, more degrading factors, such as faster rates of charging. Real-world usage profiles need to be created that amalgamate all of these and then if post-mortem analysis was performed it may be possible to make further conclusions on the mechanisms that have occurred. This would be especially interesting in determining the chemical changes in the surface film from cells subjected to high temperature and then low temperature to determine whether the surface film still contains either C-O or O-Li components or whether the product is an amalgamation of the two.

The method presented in this work to accelerate cell capacity loss and resistance increase could be tested with a vehicle test-profile. Two sets of cells could be initially characterised, one at the accelerated test profile, the other not. The electrical performance could then be compared. This type of test would be further validation of the work started here. Also, due to the error inherent within manufacturing variances that can cause the large error between similar cells under comparable conditions work involving a larger dataset could be advantageous.

10. Conclusions

The aim of this work was to investigate how post-mortem analysis can be used to detect material changes in commercial lithium-ion cells after accelerated lifetime testing.

This was de-convoluted to four main objectives which were:

1. Determine the conditions of use that impact cell lifetime and how that lifetime reduces with respect to cell capacity and resistance after an accelerated testing period
2. Determine the post-mortem methods that allows connection between electrical performance data and material changes at the negative electrode
3. Perform post-mortem analysis on the negative electrode surface film of cells at each of the lifetime affecting conditions to determine viability of the method and investigate the causes of lifetime reduction within lithium-ion cells
4. Determine whether material changes to the surface film at the negative electrode can be correlated to the cells electrical performance

Objective two contained five problems that needed addressing, these were:

1. Produce a method of opening 18650-type cylindrical cells without affecting the surface film
2. Understand the impact of rinsing electrodes on the negative electrode surface film
3. Create a process of studying the surface film composition separate from the electrolyte deposits
4. Create a process to determine the thickness of the electrode surface film
5. Create a process to stop $LiPF_6$ from affecting the chemical composition of the surface film in preparation for HPLC analysis

Objective one was investigated by identifying and then testing seven ways in which commercial lithium-ion cell capacity and resistance can be negatively affected after they have been manufactured. These were temperature, state of charge (SoC), current rate, percentage change in state of charge (% Δ SoC), pressure, orientation and vibration. Electrical characterisation showed that neither pressure nor orientation had any impact on the capacity or resistance. Therefore, post-mortem analysis was not performed on either of these. Temperature, SoC, % Δ SoC, current rate and vibration all impacted the resistance of commercial lithium-ion cells whilst SoC and temperature both also impacted the cells capacity.

Objective two was investigated by creating a method of post-mortem analysis that could be used to open, process and analyse the internal materials of the cell. This work's primary work is associated with the treatment, preparation and analysis of cell materials during post-mortem analysis. These innovations are critical to reliably connecting the electrical data to changes within cell materials.

This work found that the method (Dremel© multi-saw) used within literature to open lithium-ion cells was done in a manner that caused chemical changes to the surface film at the negative electrode. The cause of the problem was production of dust, particles and other materials during the cutting and electrode removal process. These particles contaminated the active material surface which was shown to contain small quantities of copper, manganese and iron plus higher concentrations of oxygen. It was not possible to open 18650-type cylindrical cells without contaminating the sample. These problems can be overcome by using a method that removes the top cap with a pipe cutter and then peels the cell can open instead. This new method does not create dust, particles or metal shards. It does not cut into the electrode materials, uses less resources, is less convoluted and can be performed in a similar period of time. No contaminants were found in cells that were opened using this method and therefore it should be used.

It was also established that washing electrode samples after opening to remove solvents and salts was routinely performed. However, washing is not required to remove solvents and they can be removed by subjecting samples to low pressures instead. Although washing does remove electrolyte salts it affected the surface film of the samples being studied by causing significant changes to its chemical composition. Washed samples contain less $LiPF_6$ salts but also contained no LiF; which is a known component of the surface film. Therefore, it can be concluded that washing should not be performed on delicate electrode surface films due to the chemical changes that it induces.

Another method that has been utilised more and more in the study of the lithium-ion electrode surface film is x-ray photoelectron spectroscopy (XPS). XPS is used to detect the inorganic and organic components of the electrode. This work determined a method to calculate the relative thickness of an electrodes surface film using XPS analysis coupled with sputtering. This comprehensive study determined that it was possible to sputter until the sample obtained a 'steady state' in the spectra, indicating that the sample was no longer changing. At this point, XPS spectra can be used to calculate the absolute quantity of surface film relative to graphite environments. This method reliably determines increases in surface film quantity where it does not change chemically. Indeed, it is also used to quantifiably connect electrical performance to internal material changes.

Surface films are also comprised of polymeric material, size exclusion high performance liquid chromatography (HPLC) is the primary method for studying these types of polymers. However, due to the presence of $LiPF_6$, which decomposes to form hydrofluoric (HF) acid in the presence of water, these polymeric structures could not be studied by HPLC due to sample degradation. The wet chemistry method introduced was able to selectively remove $LiPF_6$. This makes it possible to study changes in the polymeric components of the surface film under different usage

conditions. Therefore, it is now possible to use HPLC in the study of polymers within the surface film of commercially available lithium-ion cells – this was not possible before.

Objectives three and four were then investigated by using the improvements in the method of sample processing and analysis and applying them to samples subjected to different current rates, temperatures, SoC, % Δ SoC and vibration.

Vibration of lithium-ion cells introduced a previously unknown cause of resistance rise and change to the surface film at the negative electrode. This cause was removal of the film from the electrode surface and then deposition within the electrolyte. Consequently, new surface film is formed in its place. This new film does not contain additives to help produce an optimal structure and the consequence is that the resistance increases. What is most interesting is that the proposed mechanism vibration introduced is unique to it and not seen under other conditions, other than high temperatures. This means that any accelerated ageing profile should include a vibration profile within it. This is because vibration alone may only introduce a comparatively small resistance increase but when coupled with temperature, state of charge or other conditions could have significant implications.

The impact of current rate during charge was also studied. Higher charge rates increased the resistance and reduced the capacity of the cell. During post-mortem analysis with the new XPS method a relationship was established between cell resistance and thickness of the surface film. This is only true for charge rates of less than 4-C. At 6-C the chemical structure of the surface film changes. Therefore, any accelerated ageing testing of cells for this chemistry cannot utilise charge rates of 6-C but could use rates of up to 4-C without introducing additional mechanisms and only thickening the surface film. For many cells, a post-mortem characterisation of this type could identify what the specific c-rate that could be utilised was. In addition, the internal track of the electrode in 18650-type cells has a thicker surface film than the middle caused

from binder degradation causing complete delamination along this central track, further suggesting that 6 C-rates for this specific cell cannot be used for accelerated lifetime testing.

The impact that temperature and SoC have was also studied. Cells subjected to higher temperatures had a higher resistance and capacity loss. However, the capacity and resistance of these NMC / graphite cells did not increase linearly. At 45^{o}C the capacity and resistance is the highest but this was followed by low temperatures (10^{O}C) and then at 25^{O}C. For resistance, the increase can be associated with typical temperature trends, highest being worst, lowest being best. SoC showed a strong electrical relationship to both capacity and resistance with the highest SoC consistently the worst performer. Post-mortem analysis shows that the chemical composition of the film is continually changing from low to high temperatures and SoC. However, based on the two primary patterns of chemical changes seen an accelerated testing profile could contain a high SoC / low temperature study and a high temperature / high SoC condition to replicate the same chemical nature of the surface film in an accelerated period of time.

This work comprises the start of an investigation into the fundamentals of cell ageing and accelerated testing. It does this by coming from the materials and working backward to the electrical performance. It also starts a process of investigating the methods used instead of assuming that current practice is suitable. Numerous problems existed with current practice and using the methodical approach taken here it is possible to continue to add to the methods, techniques and approaches taken.

As a result of this work improvements can be made in the type of testing performed and in the type of discussion that JLR can have with suppliers over what impact operating conditions are having at a fundamental materials level. JLR now have a method to use in performing post-

mortem analysis of lithium-ion cells that provides much better consistency. This work shows that it is possible to connect electrical performance to material changes.

In an automotive context, this means that accelerated testing cannot be performed in the traditional way of increasing intensity e.g. higher temperature studies, and assume that this is the 'worst-case' scenario for the battery pack. As the lower temperature storage studies showed, for these specific cells, the lower temperature conditions have a marked impact on cell capacity. It also shows the importance of incorporating post-mortem studies and electrical performance tests to determine expected cell lifetime, especially when empirical models make assumptions with respect to surface film growth. Especially considering that such empirical models are predicting battery lifetime over a ten-year period with sometimes as little as six months of real-world performance data. A disconnect between models assumptions and real-life could result in significant warranty costs.

The actual values recorded here (e.g. 4-C charge rate) are specific to the cell chemistry and do not necessarily apply across other technologies. However, the method of analysis and validation that is required to obtain consistent and reliable post-mortem information does. And, as shown with the high variances in the electrical performance data in many instances the post-mortem results can actually be more consistent in identifying detrimental conditions from cell to cell.

In addition, the tests excluded by electrical performance data (orientation and pressure) alone are not conclusive. In this study, the results had to be pared down to those that could impact vehicle performance which in this case for these cells, during storage conditions, we saw no impact. It is likely that during charge-discharge cycling for instance that pressure will have a significant impact on battery performance and lifetime, or if cell chemistry was different.

11. References

1. European Parliament (2013) Regulation EC 443/2009 Emission performance standards for new passenger cars as part of the Community's integrated approach to reduce CO 2 emissions from light-duty vehicles.

2. Jaguar Land Rover (2013/14) Sustainability report performance update.

3. Kemp R, Blythe P, Brace C, James P, Parry-Jones R, Thielens D, Thomas M, Wenham R, Urry J (2010) Electric vehicles: charged with potential.

4. Karden E, Shinn P, Bostock P, Cunningham J, Schoultz E, Kok D (2005) Requirements for future automotive batteries–a snapshot. Journal of Power Sources 144 (2):505-512

5. Goodenough JB, Park K-S (2013) The Li-ion rechargeable battery: a perspective. Journal of the American Chemical Society 135 (4):1167-1176

6. Vetter J, Novák P, Wagner M, Veit C, Möller K-C, Besenhard J, Winter M, Wohlfahrt-Mehrens M, Vogler C, Hammouche A (2005) Ageing mechanisms in lithium-ion batteries. Journal of power sources 147 (1):269-281

7. Millner A Modeling lithium ion battery degradation in electric vehicles. In: Innovative Technologies for an Efficient and Reliable Electricity Supply (CITRES), 2010 IEEE Conference on, 2010. IEEE, pp 349-356

8. Alto P (2001) Comparing the Benefits and Impacts of Hybrid Electric Vehicle Options. Electric Power Research Institute

9. Nykvist B, Nilsson M (2015) Rapidly falling costs of battery packs for electric vehicles. Nature Climate Change 5 (4):329-332

10. Lu L, Han X, Li J, Hua J, Ouyang M (2013) A review on the key issues for lithium-ion battery management in electric vehicles. Journal of power sources 226:272-288

11. Tong H, Hung W, Cheung C (1999) Development of a driving cycle for Hong Kong. Atmospheric Environment 33 (15):2323-2335

12. Brady J, O'Mahony M (2016) Development of a driving cycle to evaluate the energy economy of electric vehicles in urban areas. Applied Energy 177:165-178

13. Han X, Ouyang M, Lu L, Li J, Zheng Y, Li Z (2014) A comparative study of commercial lithium ion battery cycle life in electrical vehicle: Aging mechanism identification. Journal of Power Sources 251:38-54

14. Marano V, Onori S, Guezennec Y, Rizzoni G, Madella N Lithium-ion batteries life estimation for plug-in hybrid electric vehicles. In: Vehicle Power and Propulsion Conference, 2009. VPPC'09. IEEE, 2009. IEEE, pp 536-543

15. Yang G Accelerated Life Tests. Life Cycle Reliability Engineering:237-331

16. Spotnitz R (2003) Simulation of capacity fade in lithium-ion batteries. Journal of Power Sources 113 (1):72-80

17. Bloom I, Cole B, Sohn J, Jones S, Polzin E, Battaglia V, Henriksen G, Motloch C, Richardson R, Unkelhaeuser T (2001) An accelerated calendar and cycle life study of Li-ion cells. Journal of Power Sources 101 (2):238-247

18. Malmgren S, Ciosek K, Lindblad R, Plogmaker S, Kühn J, Rensmo H, Edström K, Hahlin M (2013) Consequences of air exposure on the lithiated graphite SEI. Electrochimica Acta 105:83-91

19. Dedryvère R, Laruelle S, Grugeon S, Gireaud L, Tarascon J-M, Gonbeau D (2005) XPS identification of the organic and inorganic components of the electrode/electrolyte interface formed on a metallic cathode. Journal of The Electrochemical Society 152 (4):A689-A696

20. Lang M, Darma MSD, Kleiner K, Riekehr L, Mereacre L, Pérez MÁ, Liebau V, Ehrenberg H (2016) Post mortem analysis of fatigue mechanisms in LiNi 0.8 Co 0.15 Al 0.05 O 2–LiNi 0.5 Co 0.2 Mn 0.3 O 2–LiMn 2 O 4/graphite lithium ion batteries. Journal of Power Sources 326:397-409

21. Darma MSD, Lang M, Kleiner K, Mereacre L, Liebau V, Fauth F, Bergfeldt T, Ehrenberg H (2016) The influence of cycling temperature and cycling rate on the phase specific degradation of a positive electrode in lithium ion batteries: A post mortem analysis. Journal of Power Sources 327:714-725

22. Waldmann T, Wilka M, Kasper M, Fleischhammer M, Wohlfahrt-Mehrens M (2014) Temperature dependent ageing mechanisms in Lithium-ion batteries–A Post-Mortem study. Journal of Power Sources 262:129-135

23. Besenhard JO (2008) Handbook of battery materials. John Wiley & Sons,
24. Dunn JB, Gaines L, Barnes M, Wang M, Sullivan J (2012) Material and energy flows in the materials production, assembly, and end-of-life stages of the automotive lithium-ion battery life cycle. Argonne National Laboratory (ANL),

25. Nazri G-A, Pistoia G (2008) Lithium batteries: science and technology. Springer Science & Business Media,

26. Burrows A, Holman J, Parsons A, Pilling G, Price G (2013) Chemistry³: Introducing Inorganic, Organic and Physical Chemistry. Oxford University Press,

27. Venugopal G, Moore J, Howard J, Pendalwar S (1999) Characterization of microporous separators for lithium-ion batteries. Journal of Power Sources 77 (1):34-41

28. Uddin K, Perera S, Widanage WD, Somerville L, Marco J (2016) Characterising lithium-ion battery degradation through the identification and tracking of electrochemical battery model parameters. Batteries 2 (2):13

29. Liao L, Zuo P, Ma Y, Chen X, An Y, Gao Y, Yin G (2012) Effects of temperature on charge/discharge behaviors of LiFePO4 cathode for Li-ion batteries. Electrochimica Acta 60 (0):269-273. doi:10.1016/j.electacta.2011.11.041

30. Kizilel R, Lateef A, Sabbah R, Farid MM, Selman JR, Al-Hallaj S (2008) Passive control of temperature excursion and uniformity in high-energy Li-ion battery packs at high current and ambient temperature. Journal of Power Sources 183 (1):370-375. doi:10.1016/j.jpowsour.2008.04.050

31. Nakahara K, Nakajima R, Matsushima T, Majima H (2003) Preparation of particulate Li4Ti5O12 having excellent characteristics as an electrode active material for power storage cells. Journal of Power Sources 117 (1–2):131-136. doi:http://dx.doi.org/10.1016/S0378-7753(03)00169-1

32. Broussely M, Herreyre S, Biensan P, Kasztejna P, Nechev K, Staniewicz RJ (2001) Aging mechanism in Li ion cells and calendar life predictions. Journal of Power Sources 97–98 (0):13-21. doi:10.1016/S0378-7753(01)00722-4

33. Huang CK, Sakamoto J, Wolfenstine J, Surampudi S (2000) The Limits of Low-Temperature Performance of Li-Ion Cells. Journal of The Electrochemical Society 147 (8):2893-2896

34. Bourlot S, Blanchard P, Robert S (2011) Investigation of aging mechanisms of high power Li-ion cells used for hybrid electric vehicles. Journal of Power Sources 196 (16):6841-6846

35. Kassem M, Bernard J, Revel R, Pélissier S, Duclaud F, Delacourt C (2012) Calendar aging of a graphite/LiFePO4 cell. Journal of Power Sources 208 (0):296-305. doi:http://dx.doi.org/10.1016/j.jpowsour.2012.02.068

36. Renganathan S, Sikha G, Santhanagopalan S, White RE (2010) Theoretical analysis of stresses in a lithium ion cell. Journal of The Electrochemical Society 157 (2):A155-A163

37. Ramadass P, Haran B, White R, Popov BN (2003) Mathematical modeling of the capacity fade of Li-ion cells. Journal of Power Sources 123 (2):230-240. doi:10.1016/S0378-7753(03)00531-7

38. Choi SS, Lim HS (2002) Factors that affect cycle-life and possible degradation mechanisms of a Li-ion cell based on LiCoO2. Journal of Power Sources 111 (1):130-136. doi:10.1016/S0378-7753(02)00305-1

39. Jungst RG, Nagasubramanian G, Case HL, Liaw BY, Urbina A, Paez TL, Doughty DH (2003) Accelerated calendar and pulse life analysis of lithium-ion cells. Journal of Power Sources 119–121 (0):870-873. doi:http://dx.doi.org/10.1016/S0378-7753(03)00193-9

40. Bloom I, Cole BW, Sohn JJ, Jones SA, Polzin EG, Battaglia VS, Henriksen GL, Motloch C, Richardson R, Unkelhaeuser T, Ingersoll D, Case HL (2001) An accelerated calendar and cycle life study of Li-ion cells. Journal of Power Sources 101 (2):238-247. doi:http://dx.doi.org/10.1016/S0378-7753(01)00783-2

41. Wang J, Liu P, Hicks-Garner J, Sherman E, Soukiazian S, Verbrugge M, Tataria H, Musser J, Finamore P (2011) Cycle-life model for graphite-LiFePO4 cells. Journal of Power Sources 196 (8):3942-3948. doi:http://dx.doi.org/10.1016/j.jpowsour.2010.11.134

42. Broussely M, Biensan P, Bonhomme F, Blanchard P, Herreyre S, Nechev K, Staniewicz RJ (2005) Main aging mechanisms in Li ion batteries. Journal of Power Sources 146 (1–2):90-96. doi:http://dx.doi.org/10.1016/j.jpowsour.2005.03.172

43. Huang H-YS, Wang Y-X (2012) Dislocation Based Stress Developments in Lithium-Ion Batteries. Journal of The Electrochemical Society 159 (6):A815-A821

44. F. Savoy PV, M. Millet, J. Groot (2012) Impact of Periodic Current Pulses on Li-Ion Battery Performance. IEEE Transactions on industrial electronics 59 (9):3481-3488

45. Woodford WH, Chiang Y-M, Carter WC (2010) "Electrochemical Shock" of Intercalation Electrodes: A Fracture Mechanics Analysis. Journal of the Electrochemical Society 157 (10):A1052-A1059

46. Peterson SB, Apt J, Whitacre JF (2010) Lithium-ion battery cell degradation resulting from realistic vehicle and vehicle-to-grid utilization. Journal of Power Sources 195 (8):2385-2392. doi:10.1016/j.jpowsour.2009.10.010

47. Gabrisch H, Wilcox J, Doeff M (2008) TEM study of fracturing in spherical and plate-like LiFePO4 particles. Electrochemical and Solid-State Letters 11 (3):A25-A29

48. Zhang SS (2006) The effect of the charging protocol on the cycle life of a Li-ion battery. Journal of power sources 161 (2):1385-1391

49. Garcıa RE, Chiang Y-M, Carter WC, Limthongkul P, Bishop CM (2005) Microstructural modeling and design of rechargeable lithium-ion batteries. Journal of The Electrochemical Society 152 (1):A255-A263

50. Broussely M, Biensan P, Bonhomme F, Blanchard P, Herreyre S, Nechev K, Staniewicz R (2005) Main aging mechanisms in Li ion batteries. Journal of power sources 146 (1):90-96

51. Roberts SC, Aglietti GS (2010) Structural performance of a multifunctional spacecraft structure based on plastic lithium-ion batteries. Acta Astronautica 67 (3–4):424-439. doi:http://dx.doi.org/10.1016/j.actaastro.2010.03.004

52. Vetter J, Novak P, Wagner M, Veit C, Möller KC, Besenhard J, Winter M, Wohlfahrt-Mehrens M, Vogler C, Hammouche A (2005) Ageing mechanisms in lithium-ion batteries. Journal of power sources 147 (1):269-281

53. Xia J, Madec L, Ma L, Ellis L, Qiu W, Nelson K, Lu Z, Dahn J (2015) Study of triallyl phosphate as an electrolyte additive for high voltage lithium-ion cells. Journal of Power Sources 295:203-211

54. Nie M, Xia J, Dahn J (2015) Development of Pyridine-Boron Trifluoride Electrolyte Additives for Lithium-Ion Batteries. Journal of The Electrochemical Society 162 (7):A1186-A1195

55. P. Ramadass BH, P. M. Gomadam, R. White, B. N. Popov (2004) Development of First Principles Capacity Fade Model for Li-Ion Cells. Journal of the Electrochemical Society 151 (2):A196-A203. doi:10.1149/1.1634273

56. Maleki H, Howard JN (2004) Role of the cathode and anode in heat generation of Li-ion cells as a function of state of charge. Journal of power sources 137 (1):117-127

57. Hooper JM, Marco J (2014) Characterising the in-vehicle vibration inputs to the high voltage battery of an electric vehicle. Journal of Power Sources 245:510-519

58. Arora S, Shen W, Kapoor A (2016) Review of mechanical design and strategic placement technique of a robust battery pack for electric vehicles. Renewable and Sustainable Energy Reviews 60:1319-1331

59. Charkhgard M, Farrokhi M (2010) State-of-charge estimation for lithium-ion batteries using neural networks and EKF. Industrial Electronics, IEEE Transactions on 57 (12):4178-4187

60. Piller S, Perrin M, Jossen A (2001) Methods for state-of-charge determination and their applications. Journal of power sources 96 (1):113-120

61. Wright RB, Motloch CG, Belt JR, Christophersen JP, Ho CD, Richardson RA, Bloom I, Jones S, Battaglia VS, Henriksen G (2002) Calendar-and cycle-life studies of advanced technology development program generation 1 lithium-ion batteries. Journal of power sources 110 (2):445-470

62. Flynn JH (1997) The 'Temperature Integral' — Its use and abuse. Thermochimica Acta 300 (1–2):83-92. doi:http://dx.doi.org/10.1016/S0040-6031(97)00046-4

63. Hibbert DB, James AM (1987) Macmillan Dictionary of Chemistry. Chemistry. The Macmillan Press Ltd.,

64. Ratnakumar B, Smart M, Ewell R, Whitcanack L, Chin K, Surampudi S (2004) Lithium-Ion rechargeable batteries on Mars Rover. Pasadena, CA: Jet Propulsion Laboratory, National Aeronautics and Space Administration,

65. Bennett WR Considerations for estimating electrode performance in Li-Ion cells. In: Energytech, 2012 IEEE, 2012. IEEE, pp 1-5

66. Harris SJ, Timmons A, Baker DR, Monroe C (2010) Direct< i> in situ</i> measurements of Li transport in Li-ion battery negative electrodes. Chemical Physics Letters 485 (4):265-274

67. Sinha NN, Marks TH, Dahn HM, Smith AJ, Burns J, Coyle DJ, Dahn JJ, Dahn J (2012) The rate of active lithium loss from a soft carbon negative electrode as a function of temperature, time and electrode potential. Journal of The Electrochemical Society 159 (10):A1672-A1681

68. Smart M, Ratnakumar B (2011) Effects of electrolyte composition on lithium plating in lithium-ion cells. Journal of The Electrochemical Society 158 (4):A379-A389

69. Burns J, Stevens D, Dahn J (2015) In-Situ Detection of Lithium Plating Using High Precision Coulometry. Journal of The Electrochemical Society 162 (6):A959-A964

70. Klamor S, Zick K, Oerther T, Schappacher F, Winter M, Brunklaus G (2015) 7 Li in situ 1D NMR imaging of a lithium ion battery. Physical Chemistry Chemical Physics 17 (6):4458-4465

71. Agubra V, Fergus J (2013) Lithium ion battery anode aging mechanisms. Materials 6 (4):1310-1325

72. Peled E (1979) The Electrochemical Behavior of Alkali and Alkaline Earth Metals in Nonaqueous Battery Systems - The Solid Electrolyte Interphase Model Journal of the Electrochemical Society 126 (12):2047-2051. doi:10.1149/1.2128859

73. Amine K, Chen C, Liu J, Hammond M, Jansen A, Dees D, Bloom I, Vissers D, Henriksen G (2001) Factors responsible for impedance rise in high power lithium ion batteries. Journal of power sources 97:684-687

74. Zheng T, Gozdz AS, Amatucci GG (1999) Reactivity of the solid electrolyte interface on carbon electrodes at elevated temperatures. Journal of The Electrochemical Society 146 (11):4014-4018

75. Vetter J, Novák P, Wagner MR, Veit C, Möller KC, Besenhard JO, Winter M, Wohlfahrt-Mehrens M, Vogler C, Hammouche A (2005) Ageing mechanisms in lithium-ion batteries. Journal of Power Sources 147 (1–2):269-281. doi:10.1016/j.jpowsour.2005.01.006

76. Andersson AM, Edström K, Thomas JO (1999) Characterisation of the ambient and elevated temperature performance of a graphite electrode. J Power Sources 81-82:8-12

77. Aurbach D, Daroux M, Faguy P, Yeager E (1991) The electrochemistry of noble metal electrodes in aprotic organic solvents containing lithium salts. Journal of electroanalytical chemistry and interfacial electrochemistry 297 (1):225-244

78. Lin H-P, Chua D, Salomon M, Shiao H, Hendrickson M, Plichta E, Slane S (2001) Low-temperature behavior of Li-ion cells. Electrochemical and Solid-State Letters 4 (6):A71-A73

79. Suttman AK (2011) Lithium Ion Battery Aging Experiments and Algorithm Development for Life Estimation. The Ohio State University,

80. Svens P, Lindstrom J, Gelin O, Behm M, Lindbergh G (2011) Novel Field Test Equipment for Lithium-Ion Batteries in Hybrid Electrical Vehicle Applications. Energies 4 (5):741-757

81. Moon S-I, Cho I-J, Yoon D (2011) Fatigue life evaluation of mechanical components using vibration fatigue analysis technique. Journal of mechanical science and technology 25 (3):631-637

82. BATTERIES S-C, BATTERIES S-Z BATTERY CHARGING. BATTERY SEPARATORS

83. Pearson C, Thwaite C, Russel N Small-Cell Lithium-Ion Batteries: The Responsive Solution For Space Energy Storage. In: AIAA International Conference on Responsive Space, 2005.

84. Reid CM, Smart MC, Bugga RV, Manzo MA, Miller TB, Gitzendanner R Performance and Comparison of Lithium-Ion Batteries Under Low-Earth-Orbit Mission Profiles. In: Fourth International Energy Conversion Engineering Conference (IECEC), 2007.

85. Cannarella J, Arnold CB (2014) Stress evolution and capacity fade in constrained lithium-ion pouch cells. Journal of Power Sources 245 (0):745-751. doi:http://dx.doi.org/10.1016/j.jpowsour.2013.06.165

86. Aurbach D (2002) The role of surface films on electrodes in Li-ion batteries. In: Advances in Lithium-Ion Batteries. Springer, pp 7-77

87. Arora P, White RE, Doyle M (1998) Capacity fade mechanisms and side reactions in lithium-ion batteries. Journal of the Electrochemical Society 145 (10):3647-3667

88. Balbuena PB, Wang Y (2004) Lithium-ion batteries. Solid–Electrolyte Interphase

89. Cheng M, Tang W, Li Y, Zhu K (2016) Study on compositions and changes of SEI film of Li 2 MnO 3 positive material during the cycles. Catalysis Today

90. Ning G, Haran B, Popov BN (2003) Capacity fade study of lithium-ion batteries cycled at high discharge rates. Journal of Power Sources 117 (1):160-169

91. Wright RB, Motloch CG, Belt JR, Christophersen JP, Ho CD, Richardson RA, Bloom I, Jones SA, Battaglia VS, Henriksen GL, Unkelhaeuser T, Ingersoll D, Case HL, Rogers SA, Sutula RA (2002) Calendar- and cycle-life studies of advanced technology development program generation 1 lithium-ion batteries. Journal of Power Sources 110 (2):445-470. doi:http://dx.doi.org/10.1016/S0378-7753(02)00210-0

92. Tarascon J, Guyomard D (1994) New electrolyte compositions stable over the 0 to 5 V voltage range and compatible with the Li1+ xMn2O4/carbon Li-ion cells. Solid State Ionics 69 (3-4):293-305

93. Peled E (1979) The electrochemical behavior of alkali and alkaline earth metals in nonaqueous battery systems—the solid electrolyte interphase model. Journal of The Electrochemical Society 126 (12):2047-2051

94. Fong R, Von Sacken U, Dahn JR (1990) Studies of lithium intercalation into carbons using nonaqueous electrochemical cells. Journal of The Electrochemical Society 137 (7):2009-2013

95. Peled E, Golodnttsky D, Ardel G, Menachem C, Bar Tow D, Eshkenazy V The role of SEI in lithium and lithium ion batteries. In: MRS Proceedings, 1995. Cambridge Univ Press, p 209

96. Lu P, Li C, Schneider EW, Harris SJ (2014) Chemistry, impedance, and morphology evolution in solid electrolyte interphase films during formation in lithium ion batteries. The Journal of Physical Chemistry C 118 (2):896-903

97. Markervich E, Salitra G, Levi M, Aurbach D (2005) Capacity fading of lithiated graphite electrodes studied by a combination of electroanalytical methods, Raman spectroscopy and SEM. Journal of power sources 146 (1):146-150

98. Fransson L, Eriksson T, Edström K, Gustafsson T, Thomas JO (2001) Influence of carbon black and binder on Li-ion batteries. Journal of power sources 101 (1):1-9

99. Zhang SS (2006) A review on electrolyte additives for lithium-ion batteries. Journal of Power Sources 162 (2):1379-1394

100. Zhuang GV, Yang H, Blizanac B, Ross PN (2005) A study of electrochemical reduction of ethylene and propylene carbonate electrolytes on graphite using ATR-FTIR spectroscopy. Electrochemical and Solid-State Letters 8 (9):A441-A445

101. Aurbach D, Daroux M, Faguy P, Yeager E (1987) Identification of surface films formed on lithium in propylene carbonate solutions. Journal of The Electrochemical Society 134 (7):1611-1620

102. Xu K, Zhang S, Poese BA, Jow TR (2002) Lithium bis (oxalato) borate stabilizes graphite anode in propylene carbonate. Electrochemical and Solid-State Letters 5 (11):A259-A262

103. Maibach J, Lindgren F, Eriksson H, Edström K, Hahlin M (2016) Electric Potential Gradient at the Buried Interface between Lithium-Ion Battery Electrodes and the SEI Observed Using Photoelectron Spectroscopy. The journal of physical chemistry letters 7 (10):1775-1780

104. Aurbach D (2000) Review of selected electrode–solution interactions which determine the performance of Li and Li ion batteries. Journal of Power Sources 89 (2):206-218

105. Chen L, Wang K, Xie X, Xie J (2007) Effect of vinylene carbonate (VC) as electrolyte additive on electrochemical performance of Si film anode for lithium ion batteries. Journal of Power Sources 174 (2):538-543

106. Aurbach D, Gamolsky K, Markovsky B, Gofer Y, Schmidt M, Heider U (2002) On the use of vinylene carbonate (VC) as an additive to electrolyte solutions for Li-ion batteries. Electrochimica Acta 47 (9):1423-1439

107. Jeong S-K, Inaba M, Abe T, Ogumi Z (2001) Surface film formation on graphite negative electrode in lithium-ion batteries: AFM study in an ethylene carbonate-based solution. Journal of The Electrochemical Society 148 (9):A989-A993

108. Wang H, Huang H, Wunder SL (2000) Novel microporous poly (vinylidene fluoride) blend electrolytes for lithium-ion batteries. Journal of the Electrochemical Society 147 (8):2853-2861

109. Yang L, Cai M, Dai F, Xiao Q, Verbrugge MW (2016) ELECTROLYTE AND NEGATIVE ELECTRODE STRUCTURE. US Patent 20,160,172,681,

110. Kumai K, Miyashiro H, Kobayashi Y, Takei K, Ishikawa R (1999) Gas generation mechanism due to electrolyte decomposition in commercial lithium-ion cell. Journal of power sources 81:715-719

111. Leroy S, Blanchard F, Dedryvere R, Martinez H, Carré B, Lemordant D, Gonbeau D (2005) Surface film formation on a graphite electrode in Li-ion batteries: AFM and XPS study. Surface and Interface Analysis 37 (10):773-781

112. El Ouatani L, Dedryvère R, Siret C, Biensan P, Reynaud S, Iratçabal P, Gonbeau D (2009) The effect of vinylene carbonate additive on surface film formation on both electrodes in Li-ion batteries. Journal of The Electrochemical Society 156 (2):A103-A113

113. Peled E, Tow DB, Merson A, Gladkich A, Burstein L, Golodnitsky D (2001) Composition, depth profiles and lateral distribution of materials in the SEI built on HOPG-TOF SIMS and XPS studies. Journal of power sources 97:52-57

114. Gachot G, Grugeon S, Armand M, Pilard S, Guenot P, Tarascon J-M, Laruelle S (2008) Deciphering the multi-step degradation mechanisms of carbonate-based electrolyte in Li batteries. Journal of Power Sources 178 (1):409-421

115. Migge S, Sandmann G, Rahner D, Dietz H, Plieth W (2005) Studying lithium intercalation into graphite particles via in situ Raman spectroscopy and confocal microscopy. Journal of Solid State Electrochemistry 9 (3):132-137

116. Reynier Y, Yazami R, Fultz B (2007) XRD evidence of macroscopic composition inhomogeneities in the graphite–lithium electrode. Journal of power sources 165 (2):616-619

117. Grob RL, Barry EF (2004) Modern practice of gas chromatography. John Wiley & Sons,

118. Stoicheff BP (1958) High Resolution Raman Spectroscopy of Gases: XI. Spectra of CS2 and CO2. Canadian Journal of Physics 36 (2):218-230

119. Aurbach D, Gamolsky K, Markovsky B, Salitra G, Gofer Y, Heider U, Oesten R, Schmidt M (2000) The study of surface phenomena related to electrochemical lithium intercalation into Li x MO y host materials (M= Ni, Mn). Journal of The Electrochemical Society 147 (4):1322-1331

120. Van der Heide P (2011) X-ray photoelectron spectroscopy: an introduction to principles and practices. John Wiley & Sons,

121. Schechter A, Aurbach D, Cohen H (1999) X-ray photoelectron spectroscopy study of surface films formed on Li electrodes freshly prepared in alkyl carbonate solutions. Langmuir 15 (9):3334-3342

122. Madec Ln, Xia J, Petibon Rm, Nelson KJ, Sun J-P, Hill IG, Dahn JR (2014) Effect of sulfate electrolyte additives on LiNi1/3Mn1/3Co1/3O2/graphite pouch cell lifetime: correlation between XPS surface studies and electrochemical test results. The Journal of Physical Chemistry C 118 (51):29608-29622

123. Kawamura T, Okada S, Yamaki J-i (2006) Decomposition reaction of LiPF 6-based electrolytes for lithium ion cells. Journal of power sources 156 (2):547-554

124. Leroy S, Blanchard F, Dedryvere R, Martinez H, Carre B, Lemordant D, Gonbeau D (2005) Surface film formation on a graphite electrode in Li-ion batteries: AFM and XPS study. Surface and interface analysis 37 (10):773-781

125. Leroy S, Martinez H, Dedryvère R, Lemordant D, Gonbeau D (2007) Influence of the lithium salt nature over the surface film formation on a graphite electrode in Li-ion batteries: An XPS study. Applied surface science 253 (11):4895-4905

126. Blyth R, Buqa H, Netzer F, Ramsey M, Besenhard J, Golob P, Winter M (2000) XPS studies of graphite electrode materials for lithium ion batteries. Applied Surface Science 167 (1):99-106

127. Dedryvère R, Martinez H, Leroy S, Lemordant D, Bonhomme F, Biensan P, Gonbeau D (2007) Surface film formation on electrodes in a LiCoO 2/graphite cell: A step by step XPS study. Journal of Power Sources 174 (2):462-468

128. Dupin JC, Gonbeau D, Benqlilou-Moudden H, Vinatier P, Levasseur A (2001) XPS analysis of new lithium cobalt oxide thin-films before and after lithium deintercalation. Thin Solid Films 384 (1):23-32

129. Edström K, Gustafsson T, Thomas JO (2004) The cathode–electrolyte interface in the Li-ion battery. Electrochimica Acta 50 (2):397-403

130. Ensling D, Stjerndahl M, Nytén A, Gustafsson T, Thomas JO (2009) A comparative XPS surface study of Li 2 FeSiO 4/C cycled with LiTFSI-and LiPF 6-based electrolytes. Journal of Materials Chemistry 19 (1):82-88

131. Mukherjee R, Thomas AV, Datta D, Singh E, Li J, Eksik O, Shenoy VB, Koratkar N (2014) Defect-induced plating of lithium metal within porous graphene networks. Nature communications 5

132. Younesi R, Hahlin M, Björefors F, Johansson P, Edström K (2012) Li–O2 battery degradation by lithium peroxide (Li2o2): a model study. Chemistry of Materials 25 (1):77-84

133. Aurbach D, Markovsky B, Weissman I, Levi E, Ein-Eli Y (1999) On the correlation between surface chemistry and performance of graphite negative electrodes for Li ion batteries. Electrochimica acta 45 (1):67-86

134. Somerville L, Bareño J, Jennings P, McGordon A, Lyness C, Bloom I (2016) The Effect of Pre-Analysis Washing on the Surface Film of Graphite Electrodes. Electrochimica Acta 206:70-76

135. Lux S, Lucas I, Pollak E, Passerini S, Winter M, Kostecki R (2012) The mechanism of HF formation in LiPF 6 based organic carbonate electrolytes. Electrochemistry Communications 14 (1):47-50

136. Corradini D (2010) Handbook of HPLC. CRC Press,

137. Sankarasubramanian S, Krishnamurthy B (2012) A capacity fade model for lithium-ion batteries including diffusion and kinetics. Electrochimica Acta 70:248-254

138. Pinson MB, Bazant MZ (2013) Theory of SEI formation in rechargeable batteries: capacity fade, accelerated aging and lifetime prediction. Journal of the Electrochemical Society 160 (2):A243-A250

139. Lu M, Cheng H, Yang Y (2008) A comparison of solid electrolyte interphase (SEI) on the artificial graphite anode of the aged and cycled commercial lithium ion cells. Electrochimica Acta 53 (9):3539-3546

140. Ma Z, Jiang J, Shi W, Zhang W, Mi CC (2015) Investigation of path dependence in commercial lithium-ion cells for pure electric bus applications: Aging mechanism identification. Journal of Power Sources 274:29-40

141. König U, Sasse E (1983) XPS study of annealed SiO2/GaAs interfaces. Journal of The Electrochemical Society 130 (4):950-952

142. Zinner E (1983) Sputter depth profiling of microelectronic structures. Journal of the Electrochemical Society 130 (5):199C-222C

143. Briggs D (1998) Surface analysis of polymers by XPS and static SIMS. Cambridge University Press,

144. Shoji T, Masumoto S, Moriichi N, Akiyama H, Kanda T, Ohtake Y, Goda Y (2006) Apple procyanidin oligomers absorption in rats after oral administration: analysis of procyanidins in plasma using the porter method and high-performance liquid chromatography/tandem mass spectrometry. Journal of Agricultural and Food Chemistry 54 (3):884-892

145. Bertolini JC (1992) Hydrofluoric acid: a review of toxicity. The Journal of emergency medicine 10 (2):163-168

146. Petibon R, Rotermund L, Nelson K, Gozdz A, Xia J, Dahn J (2014) Study of Electrolyte Components in Li Ion Cells Using Liquid-Liquid Extraction and Gas Chromatography Coupled with Mass Spectrometry. Journal of The Electrochemical Society 161 (6):A1167-A1172

147. Williard N, Sood B, Osterman M, Pecht M (2011) Disassembly methodology for conducting failure analysis on lithium–ion batteries. Journal of Materials Science: Materials in Electronics 22 (10):1616-1630

148. Nagasubramanian G (2000) Two-and three-electrode impedance studies on 18650 Li-ion cells. Journal of power sources 87 (1):226-229

149. Aurbach D, Markovsky B, Rodkin A, Cojocaru M, Levi E, Kim H-J (2002) An analysis of rechargeable lithium-ion batteries after prolonged cycling. Electrochimica Acta 47 (12):1899-1911

150. Poe SL, Paradise CL, Muollo LR, Pal R, Warner JC, Korzenski MB (2014) METHOD FOR THE RECOVERY OF LITHIUM COBALT OXIDE FROM LITHIUM ION BATTERIES. US Patent 20,140,306,162,

151. Somerville L, Jennings P, McGordon A, Lyness C (2015) Opening, storing and processing lithium-ion cells. The university of Warwick, Coventry, England

152. Mukhopadhyay SM (2003) Sample preparation for microscopic and spectroscopic characterization of solid surfaces and films. Sample Preparation Techniques in Analytical Chemistry 162 (9):377-411

153. Abraham D, Liu J, Chen C, Hyung Y, Stoll M, Elsen N, MacLaren S, Twesten R, Haasch R, Sammann E (2003) Diagnosis of power fade mechanisms in high-power lithium-ion cells. Journal of power sources 119:511-516

154. Aurbach D, Markovsky B, Talyossef Y, Salitra G, Kim H-J, Choi S (2006) Studies of cycling behavior, ageing, and interfacial reactions of LiNi< sub> 0.5</sub> Mn< sub> 1.5</sub> O< sub> 4</sub> and carbon electrodes for lithium-ion 5-V cells. Journal of power sources 162 (2):780-789

155. Dedryvere R, Leroy S, Martinez H, Blanchard F, Lemordant D, Gonbeau D (2006) XPS valence characterization of lithium salts as a tool to study electrode/electrolyte interfaces of Li-ion batteries. The Journal of Physical Chemistry B 110 (26):12986-12992

156. Oswald S, Mikhailova D, Scheiba F, Reichel P, Fiedler A, Ehrenberg H (2011) XPS investigations of electrolyte/electrode interactions for various Li-ion battery materials. Analytical and bioanalytical chemistry 400 (3):691-696

157. Zhuang GV, Ross PN (2003) Analysis of the chemical composition of the passive film on Li-Ion battery anodes using attentuated total reflection infrared spectroscopy. Electrochemical and solid-state letters 6 (7):A136-A139

158. Orsini F, Du Pasquier A, Beaudoin B, Tarascon J, Trentin M, Langenhuizen N, De Beer E, Notten P (1998) In situ scanning electron microscopy (SEM) observation of interfaces within plastic lithium batteries. Journal of power sources 76 (1):19-29

159. Waag W, Käbitz S, Sauer DU (2013) Experimental investigation of the lithium-ion battery impedance characteristic at various conditions and aging states and its influence on the application. Applied Energy 102:885-897

160. Triola MF (2008) Essentials of statistics. Pearson Addison Wesley Boston, MA, USA:,

161. Zhang S, Zhang C, Xiong R, Zhou W (2014) Study on the Optimal Charging Strategy for Lithium-Ion Batteries Used in Electric Vehicles. Energies 7 (10):6783-6797

162. Prezas PD, Somerville L, Jennings P, McGordon A, Basco J, Duong T, Bloom I (2016) Effect of Fast Charging of Lithium-Ion Cells: Performance and Post-Test Results. SAE Technical Paper,

163. Goebel F, Morgan C (1981) Electrochemical cell insensitive to physical orientation. Google Patents,

164. Barai A (2015) Improvement of consistency, accuracy and interpretation of characterisation test techniques for Li-ion battery cells for automotive application. University of Warwick,

165. Eddahech A, Briat O, Vinassa J-M (2015) Performance comparison of four lithium–ion battery technologies under calendar aging. Energy 84:542-550

166. Guo Z, Liaw BY, Qiu X, Gao L, Zhang C (2015) Optimal charging method for lithium ion batteries using a universal voltage protocol accommodating aging. Journal of Power Sources 274:957-964

167. Barai A, Chouchelamane GH, Guo Y, McGordon A, Jennings P (2015) A study on the impact of lithium-ion cell relaxation on electrochemical impedance spectroscopy. Journal of Power Sources 280:74-80

168. Orazem ME, Tribollet B (2011) Electrochemical impedance spectroscopy, vol 48. John Wiley & Sons,

169. Petzl M, Kasper M, Danzer MA (2015) Lithium plating in a commercial lithium-ion battery–A low-temperature aging study. Journal of Power Sources 275:799-807

170. Bernard P, Martinez H, Tessier C, Garitte E, Franger S, Dedryvere R (2015) Role of Negative Electrode Porosity in Long-Term Aging of NMC//Graphite Li-Ion Batteries. Journal of The Electrochemical Society 162 (13):A7096-A7103

171. Song G (2000) Equivalent circuit model for AC electrochemical impedance spectroscopy of concrete. Cement and Concrete Research 30 (11):1723-1730

172. Song J, Lee H, Wang Y, Wan C (2002) Two-and three-electrode impedance spectroscopy of lithium-ion batteries. Journal of Power Sources 111 (2):255-267

173. Barrett HA, Ferraro A, Burnette C, Meyer A, Krekeler MP (2012) An investigation of heavy metal content from disposable batteries of non-US origin from Butler County, Ohio: An environmental assessment of a segment of a waste stream. Journal of Power Sources 206:414-420

174. Epstein S (1944) Steel. Google Patents,

175. Chaboche J, Dang Van K, Cordier G (1979) Modelization of the strain memory effect on the cyclic hardening of 316 stainless steel. In: Structural mechanics in reactor technology. Transactions. Vol. L.

176. Abukhshim N, Mativenga P, Sheikh M (2006) Heat generation and temperature prediction in metal cutting: A review and implications for high speed machining. International Journal of Machine Tools and Manufacture 46 (7):782-800

177. Burns J, Petibon R, Nelson K, Sinha N, Kassam A, Way B, Dahn J (2013) Studies of the effect of varying vinylene carbonate (VC) content in lithium ion cells on cycling performance and cell impedance. Journal of The Electrochemical Society 160 (10):A1668-A1674

178. Cross AD (1969) Introduction to practical infrared spectroscopy.

179. Kang L-Q, Cai Y-Q, Peng Y-Q, Ying X-L, Song G-H (2011) Silica-supported sulfonic acid-functionalized ionic liquid coated with [bmim][PF6] as a scavenger for the synthesis of amides. Molecular diversity 15 (1):109-113

180. Chernyak Y, Clements JH (2004) Vapor pressure and liquid heat capacity of alkylene carbonates. Journal of Chemical & Engineering Data 49 (5):1180-1184

181. Tasaki K, Goldberg A, Lian J-J, Walker M, Timmons A, Harris SJ (2009) Solubility of lithium salts formed on the lithium-ion battery negative electrode surface in organic solvents. Journal of The Electrochemical Society 156 (12):A1019-A1027

182. Saikia D, Wang T-H, Chou C-J, Fang J, Tsai L-D, Kao H-M (2015) A comparative study of ordered mesoporous carbons with different pore structures as anode materials for lithium-ion batteries. RSC Advances 5 (53):42922-42930

183. Steinberger R, Walter J, Greunz T, Duchoslav J, Arndt M, Molodtsov S, Meyer D, Stifter D (2015) XPS study of the effects of long-term Ar+ ion and Ar cluster sputtering on the chemical degradation of hydrozincite and iron oxide. Corrosion Science 99:66-75

184. Weis J (2008) Ion chromatography. John Wiley & Sons,

185. McCann HG, Bullock FA (1955) Reactions of fluoride ion with powdered enamel and dentin. Journal of dental research 34 (1):59-67

186. Yasui S, Shojo T, Inoue G, Koike K, Takeuchi A, Iwasa Y (2012) Gas-Solid Reaction Properties of Fluorine Compounds and Solid Adsorbents for Off-Gas Treatment from Semiconductor Facility. International Journal of Chemical Engineering 2012

187. Sloop SE, Kerr JB, Kinoshita K (2003) The role of Li-ion battery electrolyte reactivity in performance decline and self-discharge. Journal of power sources 119:330-337

188. Wood DL, Li J, Daniel C (2015) Prospects for reducing the processing cost of lithium ion batteries. Journal of Power Sources 275:234-242

189. Reeves S, Morris RS (2004) Improved MCMB anodes by surface modification with self-assembling nonionic surfactants. Electrochemical and solid-state letters 7 (8):B29-B30

190. Liu J, Kunz M, Chen K, Tamura N, Richardson TJ (2010) Visualization of charge distribution in a lithium battery electrode. The Journal of Physical Chemistry Letters 1 (14):2120-2123

191. Braithwaite JW, Gonzales A, Nagasubramanian G, Lucero SJ, Peebles DE, Ohlhausen JA, Cieslak WR (1999) Corrosion of Lithium-Ion Battery Current Collectors. Journal of The Electrochemical Society 146 (2):448-456

192. Frankel G (1998) Pitting corrosion of metals a review of the critical factors. Journal of the Electrochemical Society 145 (6):2186-2198

193. Bloom I, Jansen AN, Abraham DP, Knuth J, Jones SA, Battaglia VS, Henriksen GL (2005) Differential voltage analyses of high-power, lithium-ion cells: 1. Technique and application. Journal of Power Sources 139 (1):295-303

194. Burns J, Krause L, Le D-B, Jensen L, Smith A, Xiong D, Dahn J (2011) Introducing symmetric Li-ion cells as a tool to study cell degradation mechanisms. Journal of The Electrochemical Society 158 (12):A1417-A1422

195. USABC (2001) Electric Vehicle Battery Test Procedures manual, Revision 2.

196. Hooper JM, Marco J, Chouchelamane GH, Lyness C (2016) Vibration durability testing of nickel manganese cobalt oxide (NMC) lithium-Ion 18,650 battery cells. Energies 9 (1):52

197. Hu Y, Kong W, Li H, Huang X, Chen L (2004) Experimental and theoretical studies on reduction mechanism of vinyl ethylene carbonate on graphite anode for lithium ion batteries. Electrochemistry communications 6 (2):126-131

198. Wagner CD, Naumkin AV, Kraut-Vass A, Allison JW, Powell CJ, Rumble Jr JR (2003) NIST Standard Reference Database 20. NIST XPS Database Version 3:251-252

199. Etacheri V, Marom R, Elazari R, Salitra G, Aurbach D (2011) Challenges in the development of advanced Li-ion batteries: a review. Energy & Environmental Science 4 (9):3243-3262

200. Sato T, Maruo T, Marukane S, Takagi K (2004) Ionic liquids containing carbonate solvent as electrolytes for lithium ion cells. Journal of Power Sources 138 (1):253-261

201. Dupin J-C, Gonbeau D, Vinatier P, Levasseur A (2000) Systematic XPS studies of metal oxides, hydroxides and peroxides. Physical Chemistry Chemical Physics 2 (6):1319-1324

202. Aurbach D, Daroux M, Faguy P, Yeager E (1988) Identification of surface films formed on lithium in dimethoxyethane and tetrahydrofuran solutions. Journal of the Electrochemical Society 135 (8):1863-1871

203. Ely DR, García RE (2013) Heterogeneous nucleation and growth of lithium electrodeposits on negative electrodes. Journal of the Electrochemical Society 160 (4):A662-A668

204. Guan T, Zuo P, Sun S, Du C, Zhang L, Cui Y, Yang L, Gao Y, Yin G, Wang F (2014) Degradation mechanism of LiCoO 2/mesocarbon microbeads battery based on accelerated aging tests. Journal of Power Sources 268:816-823

205. Ecker M, Gerschler JB, Vogel J, Käbitz S, Hust F, Dechent P, Sauer DU (2012) Development of a lifetime prediction model for lithium-ion batteries based on extended accelerated aging test data. Journal of Power Sources 215:248-257

206. Klett M, Eriksson R, Groot J, Svens P, Högström KC, Lindström RW, Berg H, Gustafson T, Lindbergh G, Edström K (2014) Non-uniform aging of cycled commercial LiFePO 4//graphite cylindrical cells revealed by post-mortem analysis. Journal of Power Sources 257:126-137

207. Xiong D, Petibon R, Nie M, Ma L, Xia J, Dahn J (2016) Interactions between Positive and Negative Electrodes in Li-Ion Cells Operated at High Temperature and High Voltage. Journal of The Electrochemical Society 163 (3):A546-A551

208. Abraham D, Reynolds E, Sammann E, Jansen A, Dees D (2005) Aging characteristics of high-power lithium-ion cells with LiNi 0.8 Co 0.15 Al 0.05 O 2 and Li 4/3 Ti 5/3 O 4 electrodes. Electrochimica Acta 51 (3):502-510

209. Kumaresan K, Guo Q, Ramadass P, White RE (2006) Cycle life performance of lithium-ion pouch cells. Journal of power sources 158 (1):679-688

210. Kerlau M, Marcinek M, Srinivasan V, Kostecki RM (2007) Studies of local degradation phenomena in composite cathodes for lithium-ion batteries. Electrochimica acta 52 (17):5422-5429

211. Jungst RG, Nagasubramanian G, Crafts CC, Ingersoll D, Doughty DH Analysis of Lithium-Ion Battery Degradation During Thermal Aging. In: 198th Meeting of the Electrochemical Society, Phoenix, AZ (US), 2000. pp 23-27

212. Sherwood PM (2013) Paul van der Heide: X-ray photoelectron spectroscopy: An introduction to principles and practices. Analytical and Bioanalytical Chemistry 405 (8):2415-2416

213. Single F, Horstmann B, Latz A (2016) Dynamics and morphology of solid electrolyte interphase (SEI). Physical Chemistry Chemical Physics 18 (27):17810-17814

214. Keil P, Jossen A (2016) Charging protocols for lithium-ion batteries and their impact on cycle life—An experimental study with different 18650 high-power cells. Journal of Energy Storage 6:125-141

215. Anseán D, Dubarry M, Devie A, Liaw B, García V, Viera J, González M (2016) Fast charging technique for high power LiFePO 4 batteries: A mechanistic analysis of aging. Journal of Power Sources 321:201-209

216. Li J, Murphy E, Winnick J, Kohl P (2001) Studies on the cycle life of commercial lithium ion batteries during rapid charge–discharge cycling. Journal of Power Sources 102 (1):294-301

217. Zhang Q, White RE (2008) Capacity fade analysis of a lithium ion cell. Journal of Power Sources 179 (2):793-798

218. Zheng Y, Han X, Lu L, Li J, Ouyang M (2013) Lithium ion battery pack power fade fault identification based on Shannon entropy in electric vehicles. Journal of Power Sources 223:136-146

219. Spotnitz R, Franklin J (2003) Abuse behavior of high-power, lithium-ion cells. Journal of Power Sources 113 (1):81-100